Chapter 1: Introduction

The motivation of this work is to achieve of laser emission at 1.3μm with the active region of InAs/GaAs quantum dots and InGaAsN/GaAs quantum well. More specifically, the goal of this study was to reach 1.3μm emitting wavelength of vertical surface emitting laser (VCSELs). This study was done in parallel with the development of Molecular Beam Epitaxy (MBE) growth technology on GaAs based substrate. In this report, we will study the electrical and optical properties on InAs/GaAs QDs and InGaAsN/GaAs quantum well are characterized.

With the development of telecommunication infrastructure, the need for high data transmission rates has increased. To reach higher data transmission rates, the frequency of the electromagnetic radiation must correspondingly increase. The modern fiber-optic communication must rely on high performance semiconductor lasers, so as to transmit high volume and low-loss optical signal to further distance without repeaters. And high performance semiconductor lasers are essential for the establishment of high-speed internet infra-structure. Optical glass fibers is cheap around three wavelengths 850nm, 1300nm and 1500nm with minimum light dispersion around 1300nm. In order to reach high transmission rate and narrow beam divergence lasers are needed. Only the GaAs based devices technology can satisfy the low cost and high performance characteristics.

The laser technology has also developed in time. At the beginning, bulk homo-junction was used. Now quantum well lasers are used in general, especially the low dimensional InAs quantum dot active media used for optical communication. There is very important to study the quantum dot lasers, which theoretically have better characteristics than the quantum well lasers.

In this thesis, we demonstrate the high performance 1.3μm VCSELs with InAs

QDs and InGaAsN QWs active region. In the fully doped QDs VCSELs can produce a single transverse mode and its RT-CW threshold current can be achieved below 1 mA for 5.5 μm aperture which equivalent to a threshold current density of 1.9KA/cm^2.

We demonstrate intra-cavity contact VCSELs with low threshold current of 3.8mA (with 18μm aperture size the threshold current density of 1.9KA/cm^2) and output power longer than 1mW at 1304nm emitting wavelength under continuous wave operation. A RT-CW single mode output power of 0.75 mW with an initial slope efficiency of 0.17 W/A was obtained and a side mode suppression ratio of 40 dB was achieved at 7 μ m aperture for the size current conferment layer.

1.1 Motivation

Data transmission by optical fiber has several irrefutable advantages over use of conventional high frequency coaxial cables, including higher transmission rates, long distance, and low cost etc. Laser devices with the emission wavelengths between 1.3 and 1.6 μm are of primary importance in optical local (LAN) and metro (MAN) area networks, due to zero dispersion zero at 1.3 μm and minimum loss at 1.55 μm in optical silica fiber. Figure 1.1 shows the estimated of the bitrate-distance relation for laser emitters of different wavelength. It is seen that the lowest attenuation at 1550nm makes of this windows most suitable for long distance optical communication. The requirements for standard optical communication lasers in these applications are a broad, stable operating temperature range, emission spectra between 1.3-1.6 μm, and moderate power. For commercial light sources of 1550nm radiation, this wavelength range involves InP-based lasers with active regions such as GaInAsP. However the cost of InP lasers is high because of a complicated post–growth process, temperature stability and high substrate cost .As the result, the use of optical fiber communication

in local networks is cost-ineffective.

Diode lasers provide cost efficient solution for short distance data communication in optical fiber system, currently operating at 850 and 1310nm. An alternative solution to InP epitaxy would be to use materials grown on GaAs. However, using alloys which are nearly lattice-matched to GaAs or by adding indium to GaAs would increase the emitting wavelength beyond 1.1μm. The main approaches suggested to achieve 1.3-1.55μm emission from the structure grown on GaAs substrates, are by using InGaAs and GaAsSb, InGaAsN quantum wells and InAs/GaAs quantum dots [1-5]. In Figure 1.2 shows the lattice parameters and band gap energies of some selected III-V binary and their alloys, which can be potentially used for the active region of 1.3μm laser diode.

However the most important issue of 1.3μm GaAs technology is to create a defect free active region emitting at 1.3μm range.

Why InAs QDs ?

A research of the GaAs based material system was pioneered by Kondow by introducing the InGaAsN material in 1996[5]. Quantum dot structures demonstrates much longer emission wavelength as compared with quantum well structure of the same amount of In(Ga)As. This is owning to the transformation of the thin two dimensional quantum well into three dimensional islands, whose average size in growth direction is much higher. QD structures are very attractive due to the advantages of deep localization of the active region, narrow spectral lines and extremely low threshold current density, high quantum efficiency and temperature induced transition to the excited state lasing.

Why Nitrogen ?

For the low-cost high performance VCSELs at the telecommunication wavelengths, several requirements must be satisfied. (1) The active region needs to be grown on GaAs in order to take advantage of AlGaAs/GaAs semiconductor DBRs. (2) Adding N to InGaAs/GaAs quantum well reduces the lattice constant, increasing the amount of indium possible, and have a band gap smaller than 1eV and lattice match to GaAs. (3) The InGaAsN/GaAs quantum wells are of type I, with favorite band offset for IR range semiconductor. A great deal of experimental and theoretical observations suggest the valence band offset between dilute nitride GaNAs and GaAs is very small and the majority of the bandgap offset comes from conduction band lowering [5,6,7]. Due to the band offset between InGaAsN QW and GaAs barrier layer, the band offset provides the high value of T_0 in the device characteristics. Conventional AlGaAs lasers usually have T_0 values above 120 degrees, while T_0 values for InGaAsP lasers are only 60-80 K. InGaAsN/GaAs quantum wells with GaAs barriers have been estimated to have T_0 as high as 180 K [5] and values between 100 and 215 K have been experimentally observed [8].

1.2 PIN laser

In general, a laser is made up of three components: a pump, gain medium, and resonant cavity. In semiconductor lasers, the pump is a source of both electrons and holes. This generation of carriers can occur either optically, such as exciting carriers by absorbing light with energies greater than the bandgap, or electrically, such as in a forward biased *p*-*n* junction. For example, in *p*-*n* junction, electrons are injected from the *n*-type doped region and holes injected from the *p*-type doped region, resulting in the electron and hole were interaction and recombination in the intrinsic region with excess energy given off as either lattice vibrations or light. In a double

heterostructure *p*-*i*-*n* diode, an intrinsic material of smaller bandgap and is placed between *n* and *p*-type doped semiconductors as the gain medium. Indirect gap semiconductors such as Si and Ge are very inefficient at light emission and give off most of this energy in the form of heat, while direct gap semiconductors, such as GaAs, InP and their alloys, are highly efficient at emitting photons.

As a Fabry–Perot laser, cavity is produced by a pair of cleavage planes and shown in Fig 1.3. In Fabry-Perot lasers, the mirrors are simply cleaved facets perpendicular to the active region. Initially the light is spontaneously emitted from the active region as in the case of LED device. But under high current densities, the number of electrons in an excited state or the conduction band, is greater than the number of electrons in the ground state or the valence band, a condition known as population inversion. Above this inversion limit, light absorption is no longer the dominant mechanism and stimulated emission takes place. Light travels along the active region, being amplified in the entire device at a distance which, for the in-plane laser case, is typically hundreds of microns [9].

1.3 History of Vertical Cavity Surface Emitting Laser (VCSEL)

The first VCSEL structure was reported in 1965 by Melngailis [10,11] consisting of an *n*+-*p*-*p*+ junction of InSb. IR range VCSEL was first proposed and fabricated by K.Iga and his colleagues at Tokyo Institute of Technology, Japan, in 1970[12-14]. These early VCSEL devices utilized metallic mirrors which resulted in high threshold current. They indicated that in order to realize low threshold current, VCSELs should have (1) extremely small cavity volume, (2) high optical gain and (3) mirrors with extremely high reflectivity [15]. Figure 1.4 shows a VCSEL structure, in which the mirrors are parallel to the active region, and light travels perpendicular through the

thin active region. In this configuration, the light travels a very small distance through the gain medium on each pass so the mirrors must be highly reflective and active region must be highly efficient. If layers of alternating semiconductor or dielectric are monolithic grown in one direction, each layer with an optical thickness of $\lambda/4n$, the reflections from each of the boundaries would add in phase to produce a large reflection coefficient. The number of layers required to produce a highly reflective mirror at a particular wavelength is determined by the difference in the refractive index of the contrasting materials. These structures are known as Distributed Bragg reflecting (DBR) mirrors. High quality semiconductor DBRs need to reduce loses coming from misfit dislocations and emission light must be transparent to the lasing wavelength of the active region. For example one of a commercially available 980nm VCSEL design is an InGaAs/GaAs quantum well laser has be used nearly lattice-matched GsAs/AlGaAs DBRs and selective oxide configuration which showed a very low threshold current of 8.5μA[16]

The unique characteristics of VCSELs have stimulated a wide range of research, from basic studies of microcavity physics and sophisticated compound semiconductor heterostructures to advances in epitaxial growth and device-fabrication technologies.

1.4 Outline of the Dissertation

In this section an outline of this thesis will be presented. Chapter 1 provides a motivation for this work, including current competing alternatives to using both InAs quantum dot and InGaAsN active region on a GaAs substrate for long wavelength lasers.

Chapter 2 focuses on MBE growth of InAs QDs materials, such as the growth parameters of the InAs QDs and the behaviors of InGaAs, InAlAs combination alloy systems. We present electrical and optical properties of the epi layers which we grown.

Details of the experiences and difficulties encountered while growing this new material are discussed. In Chapter 3 we develop the growth technology and demonstrate the laser characteristics in edge emitting laser and VCSELs. In this section, we present the laser results and discuss different ridge size of the edge emitting lasers and the structure design of the fully doped QDs VCSELs. Chapter 4 presents optical characterization techniques used to study the dilute nitride-arsenide alloys. First, the unique mechanism by which N reduces the bandgap of GaAs by band anticrossing is discussed. The InGaAsN material properties are measured to understand incorporation of the alloy components. Also, we analyze the structural changes that can affect luminescent properties after thermal annealing. The material quality was identifyied by optical and electrical measurements. Optical measurement which detect, luminescence in materials performed in order to help better understand the effects of thermal annealing on luminescence, the dependence of the bandgap on temperature, and the compositional uniformity of this new material.

Chapter 5 presents results of several lasers such as edge emitting lasers and intra-cavity contacted VCSELs with the GaInNAs and GaInNAsSb active regions. Finally, chapter 6 concludes the thesis with suggestions for future work.

References

[1] A. F. Phillips, S. J. Sweeney, A. R. Adams, and P. J. A. Thijs, "The temperature dependence of 1.3 and 1.55μm compressively strained InGaAs(P) MQW semiconductor lasers," IEEE J. Select. Topics Quantum Electron., vol. 5, pp. 301-352, 1999.

[2] C. W. Coldren, M. C. Larson, S. G. Spruytte, and J. S. Harris Jr., "1200nm GaAs based vertical cavity lasers employing GaInNAs multiple quantum well active region," Electron. Lett., vol. 36, no. 11, pp. 951-952, May 25, 2000.

[3] S. Sato, Y. Osawa, T. Saitoh, and I. Fujimura, "Room-temperature pulsed operation of 1.3μm GaInNAs/GaAs laser diode," Electron. Lett., vol. 33, no. 16, pp. 1386-1387, July, 1997.

[4] M. R. Gokhale, P. V. Studentkov, J. Wei, and S. R. Forrest, "Low threshold current, high efficiency 1.3μm wavelength aluminum-free InGaAsN-based quantum-well lasers," IEEE Photon. Tech. Lett., vol. 12, pp. 131-133, 2000.

[5] M. Kondow, K. Uomi, A. Niwa, T. Kitantai, S. Watahiki, and Y. Yazawa, "GaInNAs: A Novel Material for Long-Wavelength-Range Laser Diodes with Excellent High-Temperature Performance," Jpn. J. Appl. Phys., vol. 35, no. 2B, pp. 1273-1275, Feb., 1996.

[6] T. Kitatani, M. Kondow, T. Kikawa, Y. Yazawa, M. Okai, and K. Uomi, "Analysis of Band Offset in GaNAs/GaAs by X-Ray Photoelectron Spectroscopy," Jpn. J. Appl. Phys., vol. 38, pp. 5003-5006, 1999.

[7] P. Krispin, S. Spruytte, J. S. Harris, and K. Ploog, "Electrical depth profile of ptype GaAs/Ga(As,N) heterostructures determined by capacitance-voltage measurements," J. Appl. Phys., vol. 88, pp. 4153, 2000.

[8] T. Kitatani, K. Nakahara, M. Kondow, K. Uomi, and T. Tanaka, "A 1.3-μm GaInNAs/GaAs Single-Quantum-Well Laser Diode with a High Characteristic

Temperature over 200 K," Jpn. J. Appl. Phys., vol. 39, pp. 86-87, 2000.

[9] “Liquid-phase epitaxy growth of III-V compound semiconductor material and their device application,” M.G. Astles. IOP publish Ltd 1990.

[10] I. Melngailis, "Longitudinal injection-plasma laser of InSb," Appl. Phys. Lett., vol. 6, no. 3, pp. 59-60, 1965.

[11] Potter, R., "Surface Emitting Lasers." MPhil Dissertation, University of Essex, 1998.

[12] H. Soda, K. Iga, C. Kitahara, and Y. Suematus, “GaInAsP/InP surface emitting injection lasers,” Jpn. J. Appl. Phys., vol. 18, pp. 2329-2330, 1979.

[13] K. Iga, “Surface-Emitting Laser—Its Birth and Generation of New Optoelectronics Field,” IEEE J. Select. Topics Quantum Electron., vol. 6, pp. 1201-1215, 2000.

[14] E. Towe, R. F. Leheny, and A. Yang, “A Historical Perspective of the Development of the Vertical-Cavity Surface-Emitting Laser,” IEEE J. Select. Topics Quantum Electron., vol. 6, pp. 1458-1464, 2000.

[15] J. S. Harris Jr., “GaInNAs long-wavelength lasers: progress and challenges,” Semicon. Sci. Technol. vol.17, pp. 880-891, 2002.

[16] G. M. Yang, M. MacDougal and P. D. Dupkus, ”Utlalow threshold current vertical cavity surface emitting laser obtain with selective oxidation,” electron. Lett, Vol. 31. pp886-888, 1995.

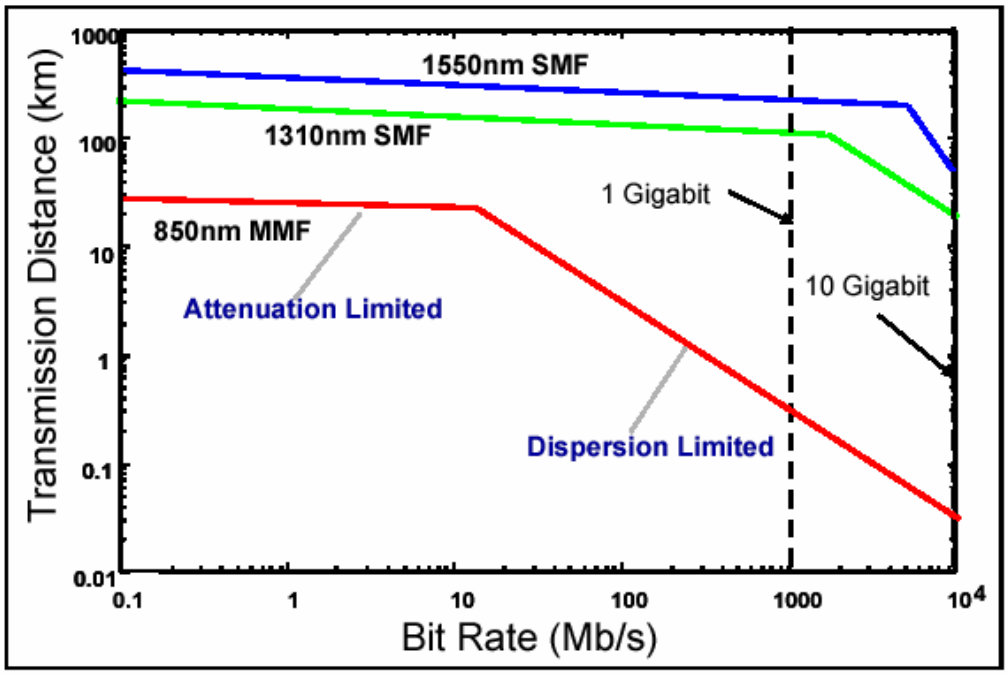

Fig 1.1 Transmission distance in silica fiber versus transmission speed for different wavelengths of available lasers [15].

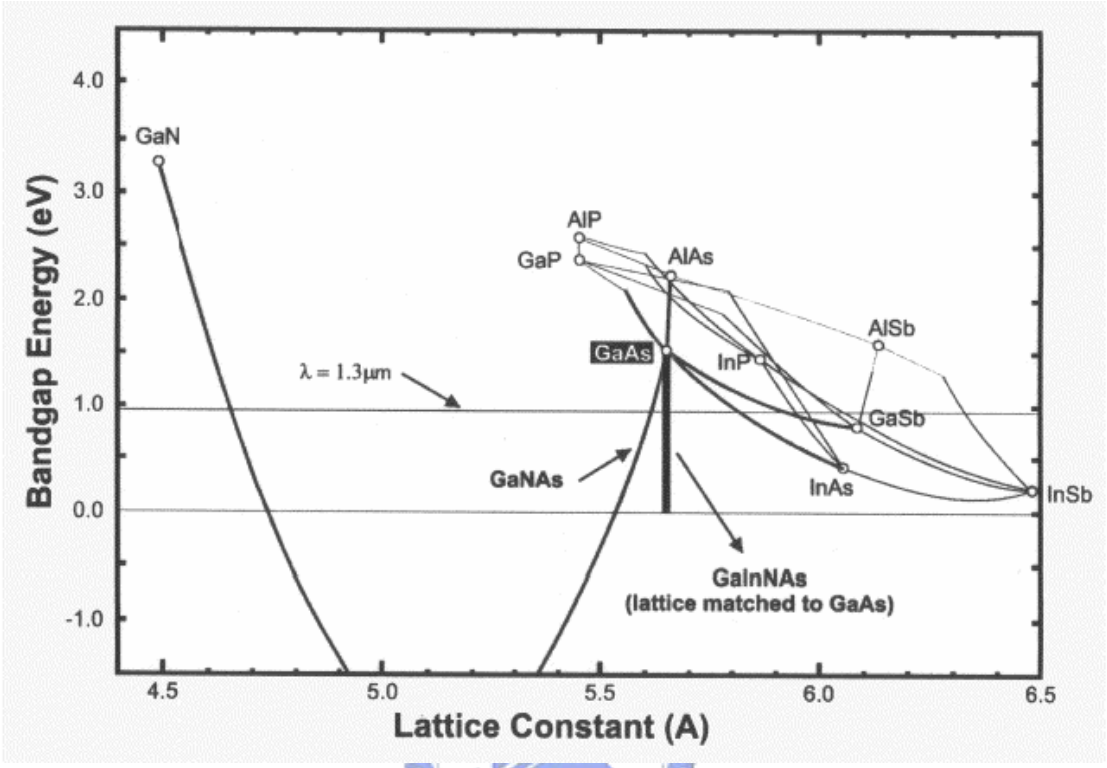

Fig 1.2 The lattice parameters and band gap energies of the selected III-V binary and their alloys.

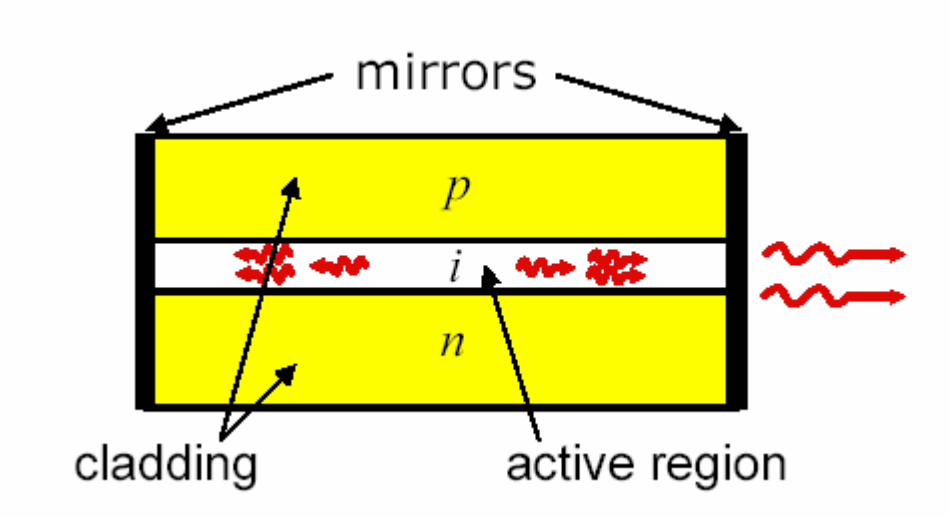

Fig 1.3 The schematic of a Fabry –Perot cavity laser.

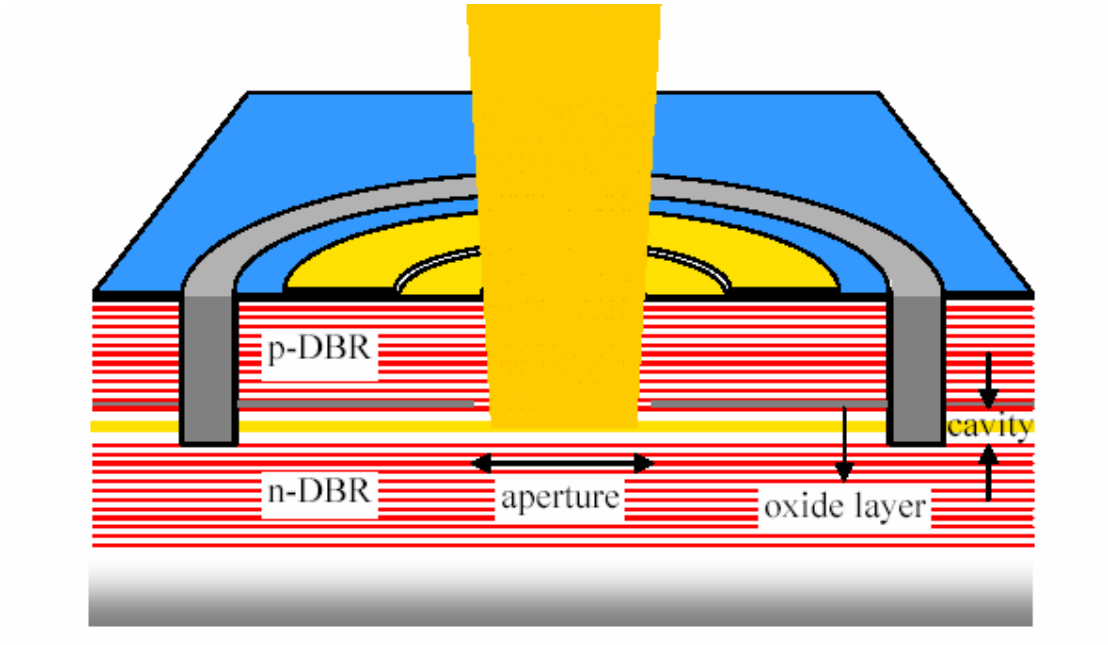

Fig 1.4 A VCSEL structure with the DBR mirrors with active region, and light travels perpendicular through the thin active region [17].

Chapter 2: Molecular Beam Epitaxy Growth of InAs Quantum dot

The growth of InAs QDs on GaAs substrates has been a subject of intense studies over the recently years, due to important device applications of such layers in optoelectronics. Molecular Beam Epitaxy (MBE) techniques allow the epitaxial growth of different compounds. GaAs and related compounds were the model materials for optoelectronics of III-V semiconductors. The controlled growth of single crystalline layers on an atomic scale makes and it is possible to design new materials with optimized electrical and optical characteristics.

All MBE machines are equipped with means for obtaining and maintaining ultrahigh vacuum at a level no worse than $1x10^{-10}$ torr which is caused by the necessity for minimizing flows of uncontrollable impurities onto the surface. With reference to the growth on GaAs of the 7% lattice-mismatched InAs layer, during the initial stage of deposition, InAs grows following the layer-by-layer 2D mechanism with the in-plane lattice parameter matched to that of the underlying GaAs substrate. While we increase the thickness of InAs layer, the strain increasing. The growth mode of InAs thin film switched from 2D growth to 3D growth mode. This evidence can be in suit monitored by Reflection high-energy electron diffraction (RHEED). The growth of self-assembled 3D islands on top of a 2D wetting layer precise and physically grown on the underlying epilayer, is usually referred to as Stranskie-Krastanow (SK) growth.

MBE growth technology requires ultra-high vacuum conditions and MBE is naturally compatible with many surface science techniques. Of particular importance are those techniques which can be operated in situ as growth proceeds.

2.1 MBE introduction

Molecular Beam Epitaxy (MBE) is a method of laying down layers of materials with atomic thicknesses on to substrates. MBE was developed in the early 1970`s as a technology to grow high purity epitaxy layers of compound semiconductors [1,2]. This is done by creating a 'molecular beam' of a material which impinges on to the substrate. The resulting 'superlattices' have a number of technologically method using in quantum well lasers included for semiconductor systems and Giant Magneto-Resistance for metallic systems. In essential, MBE is more than an UHV-based evaporation method. MBE involves the generation of fluxes of constitutions matrix and doping species and their reaction at the substrate to form an epitaxy layer. Figure 2.1 shows a schematic of the process chamber and its components. Elemental or compound constituents are heated to cause mass transfer from the flux generators to the substrate, via the vapor phase. To maintain the high purity and integrity of the deposit, stringent vacuum conditions are required. MBE is basically a line-of-sight technique from source to substrate, and the fluxes of constituents can be temporally modulated either by altering the evaporation or by physically interrupting the beam using rapid action mechanical shutters as show in Fig 2.2.

A key attribute of MBE is the precision with which the composition and doping of a structure can be tailored; such as that atomically abrupt features can be produced. To achieve this level of control within realistic time, deposition rates around a monolayer per second are used. This technology constraints on the operational temperatures of sources and the speeds with which shutters are required to operate.

For the above, key feathers to be addressed in a discussion of technology associated with the MBE process are

1. Vacuum requirements (ion, cryo, turbo pumps)

2. MBE components (Source, shutters, heating cells)

3. Manipulation: Combined motion feed-throughs and Manipulator.

4. MBE diagnostic and analytical facilities

5. Vacuum measurement

    Primary vacuum T.C. gauges

    Secondary vacuum ion gauges

    Residual gas analysis

6. Valves

    Viton sealed right angle valves

    Gate valves

    All metal valves

    Leak valves

7. RHEED and Screen

8. Introduction and preparation load-locks

9. Automation: Process control software

10. IR meter

2.2 SK mode growth of InA/GaAs quantum dots by MBE

InAs quantum dot is the most promising material for the application of long wavelength optical communication. The experimental challenge is to prepare the semiconductor structures typically 10nm in size, in an efficient and reproducible way. As known they are three kinds of approaches to fabricate the InAs QDs by growth technology, which are Frank-van der Merwe (FM), Stranski-Krastanow (SK) and Volmer Weber (VW) modes. The schematic diagrams of the growth mode show in figure 2.3. The characteristics of each growth modes are used the different kinds of mechanism. For example, FM mode uses layer-by layer growth. SK mode is based on

the stain of lattice mismatch. Stranski-Krastanow growth is observed for several material combinations [3]. The size of the islands can be adjusted within a certain range shift of emitted light. The change in size corresponding to an energy shift of the emitted light, is due to the carrier state in the different level.

In the Stranski-Krastanow (SK) growth mode, a smooth strained InAs layer can be produced in the beginning of a few monolayers (ML), until the inAs layer partially by spontaneous formation of islands on the top of the wetting layer showing in Fig 2.3. The island size can be adjusted by the growth parameters which are the substrate temperature and the composition of InAs binary compound material deposited [4].

The most important benefits of this growth technology are (1) a giant number of nanostructures (Dots) formed by one simple step processing (2) The nanostructure (Dots) can reveal a high uniformity in size and composition. (3)By using the SK growth mode may be covered epitaxy by host material without any crystal or interface defects.

2.3 The effect of InAs growth rate

The InAs quantum dot can be grown by using SK mode based on the strain effect between InAs and GaAs. The lattice mismatch of these two materials is more than 7 %. The QD growth is controlled by the substrate temperature, V/III ratio [5,6], growth interruption and indium deposition rate[5]. In this section, we present the indium deposition rate effect on the optical properties of emitting wavelength and PL intensity. The indium growth rate is one of the most important parameters in the formation of the InAs quantum dots in this report. The structure design was described as below, InAs QDs active region were sandwiched between the 60nm-thick GaAs barrier layer and 30nm-thick AlAs carrier confirm layer. An InAs QDs active layer was deposited on the GaAs surface for surface morphology studying. The substrate temperature is

set at 600^{0}C for GaAs buffer layer and ramp down to 485^{0}C for deposition the InAs QDs active layer. The thickness of InAs QDs will be kept as the same thickness as 2.8ML in order to reach longer wavelength for 1.3μm applications. All growth conditions such as substrate temperature, V/III ratio maintain the same value for all samples. Various the indium growth rates in our study, they are 0.04, 0.05, 0.06, 0.08, 0.11, 0.17, 0.26 and 0.53A/s are used. The optical properties were measured by RT-PL and the surface characteristics of InAs QDs layer will be ascertained by Atomic Force Microscopy measurement (AFM).

Figure 2.4 shows the RT-PL spectra of all samples with different indium deposition rates. It is observed red shift of emission wavelength in samples with lower indium grow rate. The RT-PL spectrum shows that the peak intensity becomes stronger versus the lower indium growth rate. The emission wavelength red shifts due to lower indium growth rate to allow for longer migration time on the GaAs surface, resulting in larger InAs QDs. The dots density of different indium growth rates were revealed by Atomic Force microscope (AFM). Table 2-1 shows the relation between indium growth rate and the dots density. The higher indium growth rate provides the higher dot density which can be observed in the AFM images. As known, a laser is made up of three components: a pump, gain medium, and resonant cavity. The main problem of QDs lasers is low material gain; it is due to the lower dot density. The dot density must be higher than 5x10^{10}/cm^2 in order to have enough gain for the devices [7]. Our results show that the indium growth rate should be higher than 0.26A/s in order to yield, a dot density of higher than 5x10^{10}/cm^2. As compared with the dot density and PL intensity, it is trade off between the indium growth rate and peak intensity. Increasing the indium growth rate reduces the surface migration time of InAs QDs, but increases the dot density and makes the QDs size become small.

In this study, we optimum the indium growth rate for growing InAs quantum

dots with high dot density for the use of devices. Based on this growth condition, we achieved the high density InAs quantum dots without decreasing the material quality of the epi layer. This growth conditions will be useful fabricated the optical electronics devices.

2.4 The V/III ratio of InAs/InGaAs QDs

We present the effects of arsenic (As_4) beam flux influence on the MBE growth parameters in the optical properties of self-assembled InAs/GaAs QDs. The growth temperature of InAs QDs affects the size and the density of QDs significantly. It can be easily proved it by optical properties measurements. In this study, we kept a constant growth temperature for the growth of the active layer. In order to investigate InAs QDs by optical properties under different kinds of arsenic beam pressures. As known the As_4 beam flux plays an important role for the quantum efficiency of the QDs [8]. The diffusion length of the In atoms is found to be responsible for the changes in the optical properties of the QDs beside the amount of deposited island material [4]. To achieve more precise information single active layer was used in this study.

Four samples were grown at 480 °C with different arsenic beam pressures while InAs/InGaAs QDs are deposited. We measure RT-PL around the center of the wafers,on which an 2.8 ML InAs QDs and covered by InGaAs quantum well is deposited. The influences of arsenic pressure and growth interruptions on the optical properties of the InAs QDs grown at 480 °C are showed in Fig 2.5. The quantum efficiency of the QDs at room temperature can obviously be enhanced by decreasing As_4 pressure from $1x10^{-6}$ to $3x10^{-7}$ torr. To optimize the arsenic beam flux for growing the InAs QDs layer, four values of As_4 beam flux were used. It is observed that RT-PL intensity increasing of the samples while decrease the As_4 beam flux. The

pressure of As_4 beam flux was $3x10^{-10}$torr, it is three times higher than the previous sample may cause the large amount of big InAs clusters with dislocations. While the As_4 beam flux is $1E^{-7}$ torr, the PL intensity is lower than the samples grown with As_4 pressure of $3x10^{-7}$torr. The low PL intensity may be, the result of three–dimensional islands formed in the system. One sample with the As_4 beam flux of $3x10^{-7}$ torr and the thickness of InAs QDs of 2.6ML shows the highest PL intensity of all samples. A small redshift of the PL spectra can also be determined by decreasing arsenic pressure despite the same amount of deposited InAs. The As_4 beam pressure is lowered to enlarge the diffusion length of the adsorbed In atoms. This verifies the increase in the diffusion length of the adatoms, since the diffusion length is found to influence the size and density of the QDs.

Samples with As_4 beam flux of $1x10^{-6}$ torr show only one PL peak at 1.3μm at room temperature as compared with other samples. A broad shoulder on the high energy side of the PL peak appears in the spectrum when the As_4 beam flux is reduced. It indicates the result of growing InAs QDs layer under higher As_4 beam flux demonstrated high dot density.

In this study we show that the As_4 beam flux significant affects the InAs QDs. The As_4 beam flux can be used as a parameter to improve the QDs material quality.

2.5 Quantum Dot cover by Quantum Well (Dot inWell) structure

Quantum dot (QD) lasers on GaAs substrates emitting at 1300 nm have been demonstrated in the recent years.Since emission at 1300 nm is important for communication, recent work has focused on obtaining InAs quantum dots on GaAs substrates. In order to extend the PL emission wavelength up to 1.3 μm, researchers usually keep high substrate temperature and low growth rate during the growth of QDs [8,9], but due to the surface migration enhancement of the In atom, it leads to a

considerable In segregation and lower QD density. Suppressing the indium segregation and intermixing requires us to utilize another method to accomplish this purpose because it is inefficient by InGaAs or by GaAs overgrowth. The InAs QDs island overgrown by InGaAs strain-reducing layer (SRL) [10] or InAs QDs inserted in the InGaAs well [11] have been successfully used to extend the InAs/GaAs QD emission wavelength to 1.3 μm. However, InGaAs SRL and InGaAs double quantum well would lead to a decrease of the confirmed potential barrier, leading to a decreased separation between discrete energy levels of InAs QDs.

2.6 InAs QDs cover by the InGaAs QW

When pure InAs QDs is grown on GaAs surface, the lattice mismatch is about 7 percent. Since the lattice constant in the $In_xGa_{1-x}As$ alloys varies only slightly versus x, the process of QD formation is supposed to be the same as GaAs material. This dots in a well" (DWELL) design not only improves carrier capture by the dots, but also increases the density of quantum dots (to $6x10^{10}$ cm^{-2}) over growth on GaAs directly as shown in Fig 2.6. The structural and optical properties of GaAs-based 1.3 μm InAs/InGaAs/GaAs dots-in-a-well (DWELL) structures have been optimized in terms of different InGaAs composition by GaAs growth rates, the amount of InAs QDs deposited is set as 2.8ML [12]. In this study we keep the total thickness of InGaAs quantum well as 48A and vary the indium composition, they are 14.8%, 16% and 17% as shown in Table 2.2. It shows an improvement of the optical efficiency by increasing the Ga growth rate and decreasing the indium composition. The RT-PL spectra demonstrate the highest PL intensity which was the 2.8ML InAs QDs covered with 14.8% InGaAs quantum well in Fig 2.7. The RT-PL spectrum shows emitting wavelength at 1310nm with narrow full half width maximum (FHWM). The line-shape becomes more and narrower while the emitting wavelength remains around

1.3μm. It means that more uniform QDs size distribution occurs at a few. The PL spectrum shows that the growth condition is suitable and the InAs thickness is under the critical thickness. The total strain of the sample in the structure of InAs QDs coved by InGaAs quantum well on the GaAs substrate, was under controlling by these growth parameters. The emission wavelength of PL spectra were founded that red emitting shift of the samples with coverage 16% and 17% InGaAs quantum well. The higher indium composition in the QWs, the PL emission wavelength shows the more red shift of the wavelength and decreases the PL intensity. The red shift of the PL wavelength probably due to the large QDs size in the active region or the large band offset between the GaAs barrier. The lower PL intensity is due to much strain in the QDs and some related defects decrease the PL intensity. Too high indium composition in the active region makes large strain between the interface of layer to layer and degrades the material quality.

In this study we obtain the optimal indium composition and total thickness in the InGaAs QW for the growth condition for the reference parameters. The InGaAs QW of 60A with 14.8% indium content is also grown in this study. It shows the shortest emission wavelength at 1.28 μm of all samples in Fig 2.7. The emitting wavelength of this sample shows a blue shift compared with reference sample, which is quite unusual behavior in our experiments. From the RT-PL spectrum, the lower PL intensity with broad FHWM is obtained in this sample. Compared with all samples in this study, the higher In composition in the QW results in a red shift in the wavelength and may contain some relative defects. These results suggest that the optimum QW composition for 1.3 μm applications is ~15%. Our optimum structure exhibits a room temperature emission at 1.32 μm with a narrow linewidth of 27 meV.

2.7 Optical emission range of InAs/InGaA/GaAs quantum dots active region

Theoretical modeling of optical transition in the self-organized InAs/GaAs quantum dot predicts an increase in the emission wavelength with increasing the island base size [13]. We present the systematic experiment study of the emission wavelength of the InAs/InGaAs QDs ensemble as a function of effective thickness of deposited InAs QDs. This information is necessary for designing the growth of InAs QDs devices and helpful for growth of defect free samples [14].

The emitting wavelength of InAs QDs covered GaAs barrier layer is around 1150nm, this wavelength is too short for the optical communication. Figure 2.8 shows the RT-PL spectrum of single active layer with InAs/GaAs QDs and InAs/InGaAs/GaAs QDs structures. In order to approach longer emitting wavelength, InAs QDs covering InGaAs quantum well structure was used. An InGaAs quantum well is the most common idea to reach the emitting wavelength at 1.3μm.

Structure of samples was grown on N-type GaAs substrate by covering 60nm GaAs barrier layer and the active region with InAs QDs coverage by InGaAs quantum well in the center of the structure. The thickness of InAs deposition is varied from 2.2 to 3.33 monolayers (ML). The transition from two to three dimensional InAs growth is monitoring by RHEED pattern during deposition. The boundary thickness from two and three dimensional growth is found equal to 1.7ML. After the InAs thickness more than 1.7ML, the RHEED pattern is switched from streaky to spotty. The RHEED patterns become streaky after the GaAs cover layer which deposited on the InAs QDs.

In this chapter we will modify some growth parameters and demonstrate the excellent optical properties. It will be continuously discussed in the below sections. The room-temperature optical properties also improve with decreasing InAs coverage. A strong dependence of the QD density and emission wavelength on the In

composition of InGaAs quantum well has been observed. In our assumed that increases additional material from wetting layer and InGaAs layer into dots and decreases repulsive strain field between neighboring islands. Substrates responsible for improved QD density with increasing indium composition in InGaAs strain buffer layer (SBL). The optical efficiency is sharply degraded when the InGaAs QW In composition is increased from15% to 17%.

It shows a red shift of the peak spectrum while increases the thickness of InAs quantum dots. The line-shape becomes more and more narrowing when the emitting wavelength is still around 1.3μm. The narrow line shape means more uniform QD size distribution occurred. While the total thickness is more than 2.8ML, the emitting wavelength appears a blue shift. The blue shift is due to inhomogeneous broadening of the dot size. The emission wavelength comes from the small size InAs QDs. In our suggestion there are a few groups of QDs deposition at the same time. The blue shift emission appears from the smaller QDs, while the larger QDs are over the critical thickness and contain defects and no emission wavelength appear from the larger QDs.

2.8 InAs QDs cover with InAlAs strain reduce layer

Typically, InAs QD lasers show poor temperature sensitivity of the threshold current density at a low temperature compared with the quantum well active layers. However, experimental results provide evidence of a much weaker characteristic temperature T0 above 200K [13, 14, 15]. Theoretical investigation on multilevel QD lasers indicates that carriers in the higher energy levels have a higher nonradiative recombination rate, even if the population of these higher energy levels is relatively low [16]. Therefore, the current issues for further improvements of the temperature characteristics is increasing the energy separation between the ground state and first

excited state [17, 18] Increasing to isolate the QD ground state from other energy levels. Usually the peak separation between the ground and first excited state are relatively small, ranging from 66nm to 88nm.

Recently, many groups have reported approaches to attain self-assembled InAs QDs with a favorable energy separation and emission wavelengths by using InAlAs/InGaAs as the strain-reduced layers (SRLs) [18-20]. In these works, self-assembled InAs QDs with SRLs were grown at high temperatures. In-segregation and interface intermixing can be effectively suppressed by inserting the InAlAs layer. InAs QDs emitting at long wavelengths and have a large energy separation have since then been successfully fabricated [20].

The strain reduce layer structure were designed for investigating the carrier confinement effects. Four structures inserting with InAlAs strain reduce layer were designed. The confinement effects on the carriers were investigated, along with the associated optoelectronic characteristics of InAs QDs. A 0.3 μm-thick buffer GaAs layer was first grown onto the (100) GaAs substrate at 600 ℃. The samples were ramp down the substrate temperature to 480 ℃ to grow a nominally 2.6 monolayer (ML)-thick InAs QDs layer at a growth rate of 0.26 Å/s, as determined by reflection high-energy electron diffraction (RHEED). The self-assembled InAs QDs were then covered with composite $In_{0.14}Al_{0.86}As/In_{0.14}Ga_{0.86}As$ SRLs. Each sample had a total thickness of 54 Å strain reduce layers. Samples were named as A, B, C and D. The thicknesses of the $In_{0.14}Al_{0.86}As$ layers in samples A, B, C and D, respectively were 0, 10, 14 and 20 Å, respectively. The samples were finally heated to 600 ℃ to grow a 0.3 μm-thick GaAs cap layer. In order to examine the QDs behaviors by atomic force microscopy (AFM), samples were grown under the same conditions but without a GaAs cap layer on the surface of the wafers. The band diagram in fig 2.9 depicts the structure of the samples.

Figure 2.10 presents the RT-PL spectra of the samples with InAs/$In_{0.14}Al_{0.86}As$/$In_{0.14}Ga_{0.86}As$ QDs active region. All samples have two main peaks in the PL spectrum. Figure 2.11 shows the AFM images, in which high dot density was observed for the sample with 10A $In_{0.14}Al_{0.86}As$ strain reduce layer. The low-energy PL feature is related to the ground states of InAs QDs. The high-energy PL feature may result from the wetting layer or small InAs QDs with carriers in the ground states and the originally sized InAs QDs with carriers in the excited states. The smooth form of the high-energy PL feature excludes the possibility of emission from the thin wetting layer, which would yield a zigzag-like PL feature associated with the variation in the thickness of the monolayer. The PL intensity as a function of the excitation power indicated that the ratio of the intensity of the excited state peak to that of the ground peak declined as the pumping power was increased at a low pumping power, but increased with pumping power at high pumping power as shown in Fig 2.12. This dependence of the intensity ratio on the pumping power, determined by the distribution of excess carriers over various energy levels in a quantum-confined structure [8], reveals that the excited-state transition of carriers in InAs QDs is responsible for the high-energy PL feature.

Figures 2.10 indicate that the ground-state and the first excited-state transitions in sample D are blueshifted by 16 and 22 meV from those in sample A, respectively. Figure 2.13 shows that the energy separation between the first excited state and the ground state is increased from 78 meV in sample A, which has a low confining InGaAs barrier, to 103 meV in sample D, which has a 2nm high confining $In_{0.14}Al_{0.86}As$ barrier. The line-width of ground state increases from 36 to 40 meV and the value of excited state reduce from 80 to 72meV as shown in Fig 2.14. It means that the dots size is quite uniform after inserting the $In_{0.14}Al_{0.86}As$ strain reduce layer. Although sample D has a large energy separation, its optoelectronic properties,

including emission wavelength and intensity, are poorest of all samples. The optical characteristics of sample D will be less the potential application to optoelectronic devices. The efficiency of luminescence and the optoelectronic properties can be improved by incorporating the composite InAlAs/InGaAs SRLs into the InAs QDs. The ground-state energy and the energy separation of sample B were 0.965 eV and 101 meV, respectively. As the thickness of the InAlAs layer was increased to 20 Å, as for sample C, the ground-state transition energy and the energy separation are increased to 0.971 eV and 103 meV, respectively [21].

This study investigated the optoelectronic characteristics of InAs QDs with a high potential InAlAs/InGaAs SRL barrier by PL spectroscopy. The carrier transition and optical characteristics of InAs QDs depend strongly on the thickness and composition of the SRLs. The sample of QDs with 10 Å $In_{0.14}Al_{0.86}As$ /44 Å $In_{0.14}Ga_{0.86}As$ SRLs showed the greatest PL intensity and a large energy separation of 103 meV. The low-temperature growth of SRLs reduces the segregation of indium and interface intermixing during epitaxial process. Moreover, introducing a high potential SRL barrier into the QD structures enhances the effects of carrier confinement and the size uniformity of QDs, as verified by the PL spectra and AFM images of the samples. Hence, an InAs QD laser operated at a wavelength of 1.3 μm with a high characteristic temperature may be realized.

Reference

[1] A. Cho, “Film Deposition by Molecular Beam Techniques,” J. Vac. Sci. Tech., vol. 8, pp. S31-S38, 1971.

[2] A. Cho and J. Arthur, ”Molecular Beam Epitaxy,“ Prog. Solid-State Chem., vol. 10, pp. 157-192, 1975.

[3] T. R. Ramachandran, A. Madhukar, I. Mukhametzhanov, R. Heitz, A. Kalburge, Q. Xie, and P. Chen, “Nature of Stranski–Krastanow growth of InAs on GaAs(001),” J. V. S. T B :Microelectronics and Nanometer Structures, vol. 16, I 3, pp1330-1333, 1998.

[4] Victor M. Ustinov, Alexey E. Zhukov, Anton Yu. Egorov, and Niolai A. Maleev, “Quantum Dot lasers,” OXFORD.

[5] G. S. Solomon, J. A. Trezza, J. S. Harris Jr., “Substrate temperature and monolayer coverage effects on epitaxial ordering of InAs and InGaAs islands on GaAs,” Appl. Phys. Lett., vol. 66, 991, 1995.

[6] G. S. Solomon, J. A. Trezza, and J. S. Harris Jr., “Effects of monolayer coverage, flux ratio, and growth rate on the island density of InAs islands on GaAs,” Appl. Phys. Lett, vol. 66, 3161, 1995.

[7] F. Y. Chang, C. C. Wu, and H. H. Lin, “Effect of InGaAs capping layer on the properties of InAs/InGaAs quantum dots and lasers,” Appl. Phy. Lett. vol 82, No 25 .23, 2003.

[8] G. S. Solomon, J. A. Trezza, and J. S. Harris Jr., “Substrate temperature and monolayer coverage effects on epitaxial ordering of InAs and InGaAs islands on GaAs, “Appl. Phys. Lett., Vol. 66, No. 8, pp20, 1995.

[9] H. Kitabayashi, T. Wako, “Atomic force microscope observation of the initial stage of InAs growth on GaAs substrates,” J. Crystal Growth, 150 .152, 1995.

[10] T. Yamachi, Y. Matsuba, L. Bolov, M. Y. Tabuchi, and A. Nakamura, “Correlation

between the gap energy and size of single InAs quantum dot on GaAs(001) studied by scanning spectroscopy," Appl .Phys.Lett., 77, 4368, 2000.

[11] P. Rotella, G. von Winckel, S. Raghavan, A. Stintz, Y. Jiang, and S. Krishna, "Study of structural and optical properties of quantum dots-in-a-well heterostructures," J. Vac. Sci. Technol. B, 22, No3, 2004.

[12] J. S. Wang, R. S. Hsiao, G. Lin, L. Wei, Y. T. Wu, A. R. Kovsh, N. A. Maleev, A. V. Sakharov, D. A. Livshits, J. F. Chen, and J. Y. Chi, "Ridge waveguide 1310 nm lasers based on multiple stacks of InAs/GaAs quantum dots," Phys. Stat. Sol. C, Vol. 0, No. 4, pp. 1339–1342, 2003.

[13] L. V. Asryan, M. Grundmann, N. N. Ledentsov, O. Stier, R. A. Suris, and D. Bimberg, "Maximum modal gain of a self-assembled InAs/GaAs quantum-dot laser," J. Appl. Phys. 90, 1666, 2001.

[14] K. Nishi, H. Saito, S. Sugou, and J-S. Lee, "A narrow photoluminescence linewidth of 21 meV at 1.35 μm from strain-reduced InAs quantum dots covered by $In_{0.2}Ga_{0.8}As$ grown on GaAs substrates," Appl. Phys. Lett., 74, 1111, 1999.

[15] G. Park, O. B. Shchekin, S. Csutak, and D. G. Deppe, "Room-temperature continuous-wave operation of a single-layered 1.3 μm quantum dot laser," Appl. Phys. Lett., 75, 3267, 1999.

[16] X. Huang, A. Stintz, C. P. Hains, G. T. Liu, J. Chen, and K. J. Malloy, "Very low threshold current density room temperature continuous-wave lasing from a single-layer InAs quantum-dot laser," IEEE Photonics Technol. Lett., 12, 227, 2000.

[17] G. Park, O. B. Shchekin, and D. G. Deppe, "Temperature Dependence of Gain Saturation in Multilevel Quantum Dot Lasers," IEEE J. Quantum Electron., 36, 1065, 2000.

[18] R. Jia, D. S. Jiang, H. Y. Liu, Y. Q. Wei, B. Xu, and Z. G. Wang, "Influence of

combined InAlAs and InGaAs strain-reducing laser on luminescence properties of InAs/GaAs quantum dots," J. Crystal Growth, 234, 354-358, 2002.

[19] Z. Y. Zhang, B. Xu, P. Jin, X. Q. Meng, Ch. M. Li, X. L. Ye, and Z. G. Wang, "Photoluminescence study of self-assembled InAs/GaAs quantum dots covered by an InAlAs and InGaAs combination layer," J. Appl. Phys., 92, 511, 2002.

[20] Z. D. Fang, Z. Gong, Z. H. Miao, L. M. Kong, X. H. Xu, H. Q. Ni and Z. C. Niu, "Effect of the InAlAs and InGaAs combination strain-reducing layer on 1.3 μm emission self-assembled InAs/GaAs quantum dots," J. Phys. Appl. Phys., 37 1012-1016, 2004.

[21] H. Y. Liu, and I. R. Sellers et al, "Engineering carrier confinement potentials in 1.3-μm InAs/GaAs quantum dots with InAlAs layers: Enhancement of the high-temperature photoluminescence intensity," Appl. Phys. Lett., 83, 3716, 2003.

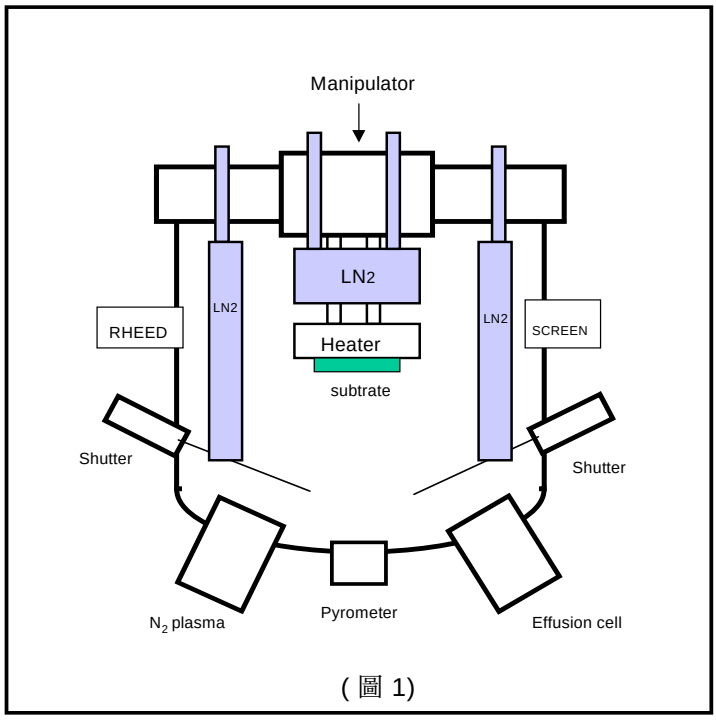

Fig 2.1 The schematic of the process chamber and it`s components.

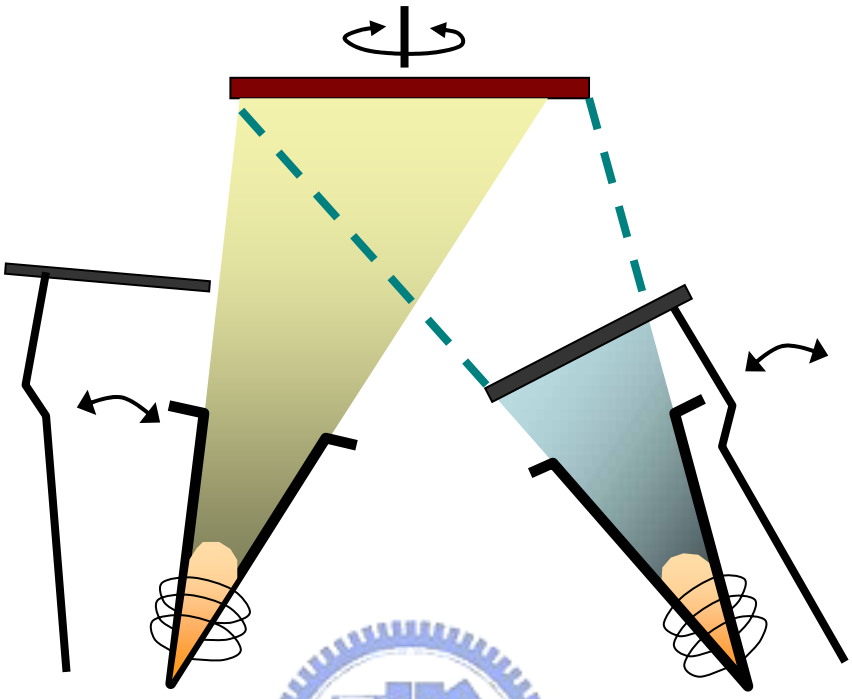

Fig 2.2 Schematic of sources shutters and substrate position in the MBE chamber.

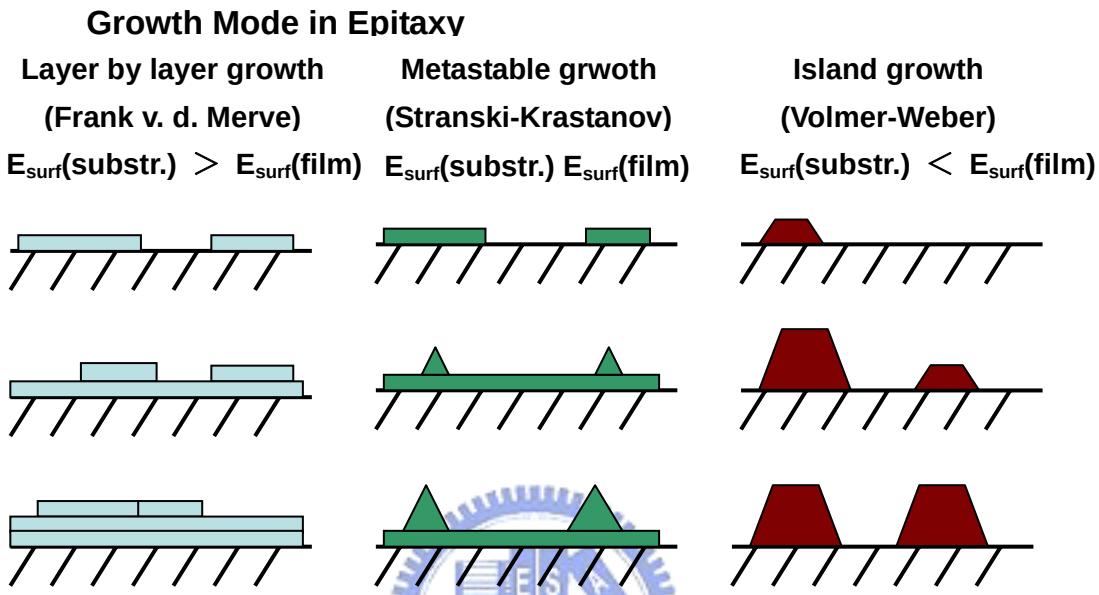

Fig 2.3 Schematic digrams of the growth modes for semiconductor system (a) Frank-van der merwe (FM, layaer by layer);(b) Stranski-Krastanow (SK, island with the wetting layer);(c) Volmer-Weber (VW, island)

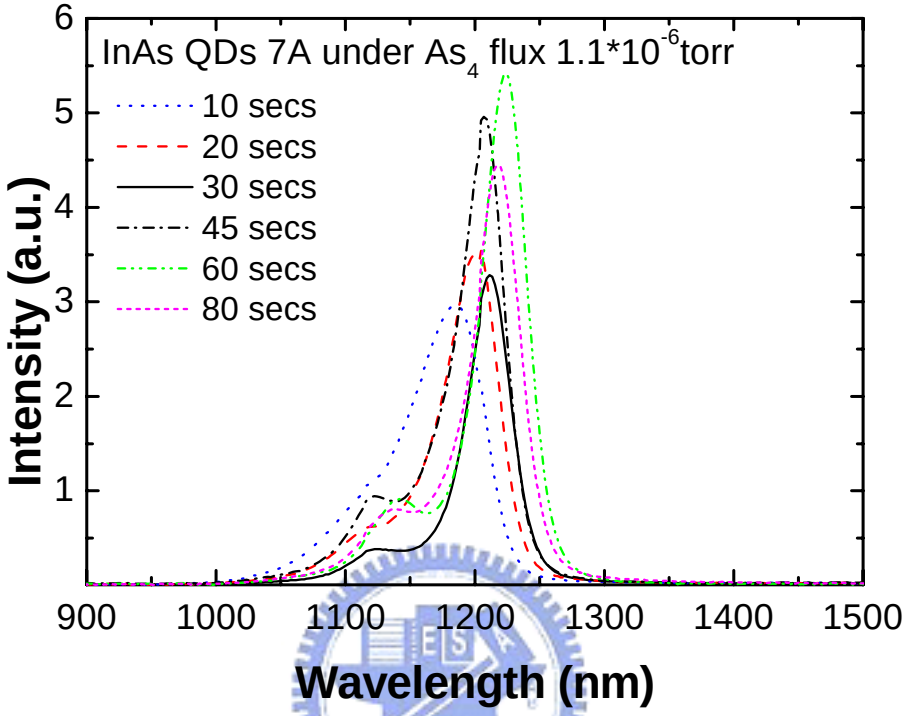

Fig 2.4 The RT-PL spectrum of all samples with different indium growth rate.

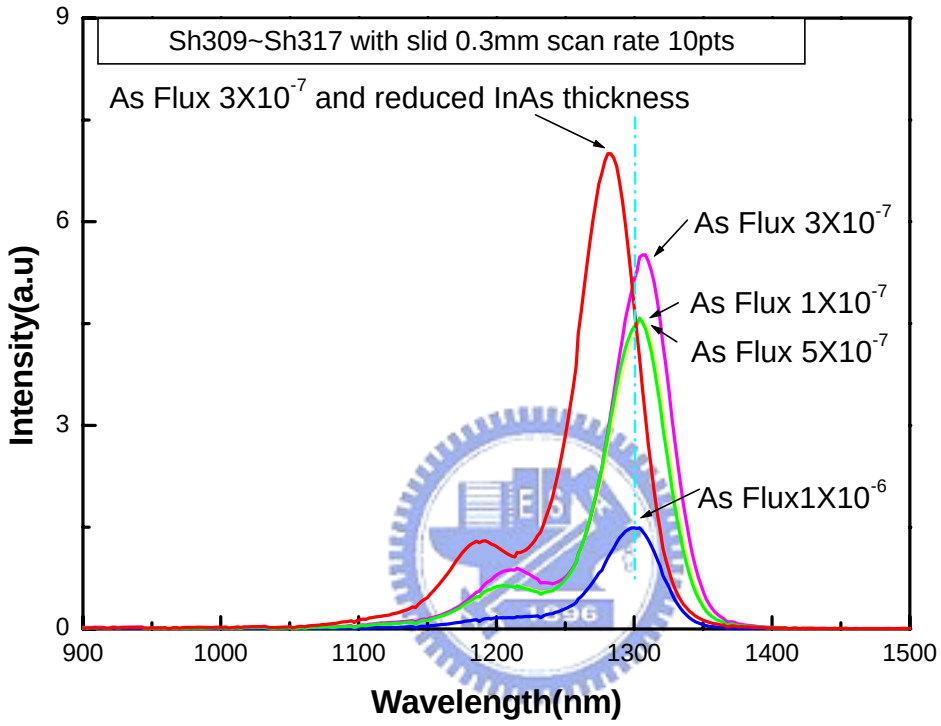

Fig 2.5 RT-PL spectra of InAs/InGaAs/GaAs QDs under difference As beam flux

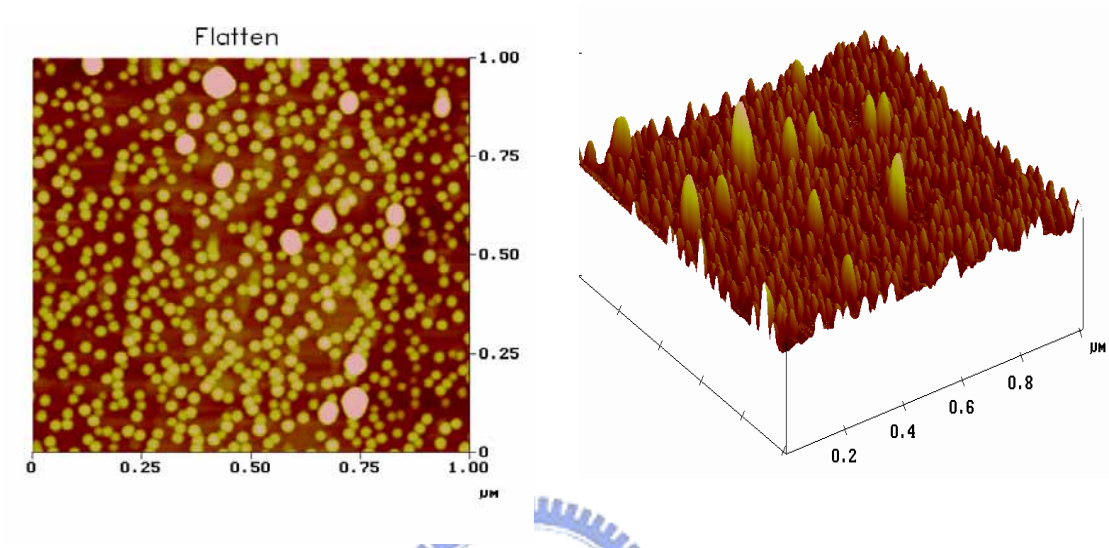

Fig 2.6 The AFM images of InAs/InGaAs/GaAs Dot in Well structure. ($6x10^{10}/cm^2$)

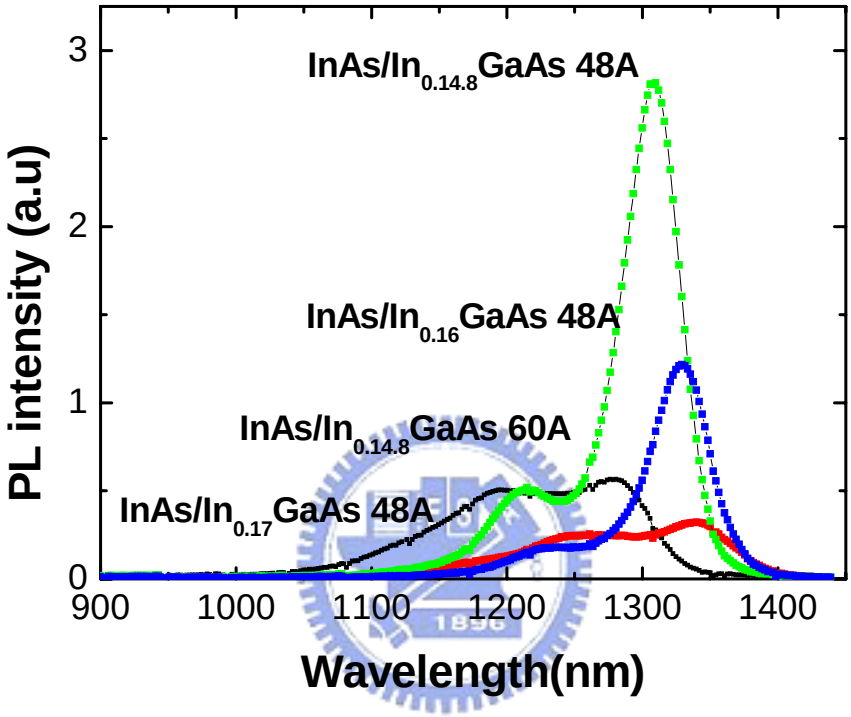

Fig 2.7 RT-PL spectra of InAs Dot in well structure varied indium composition in the quantum well.

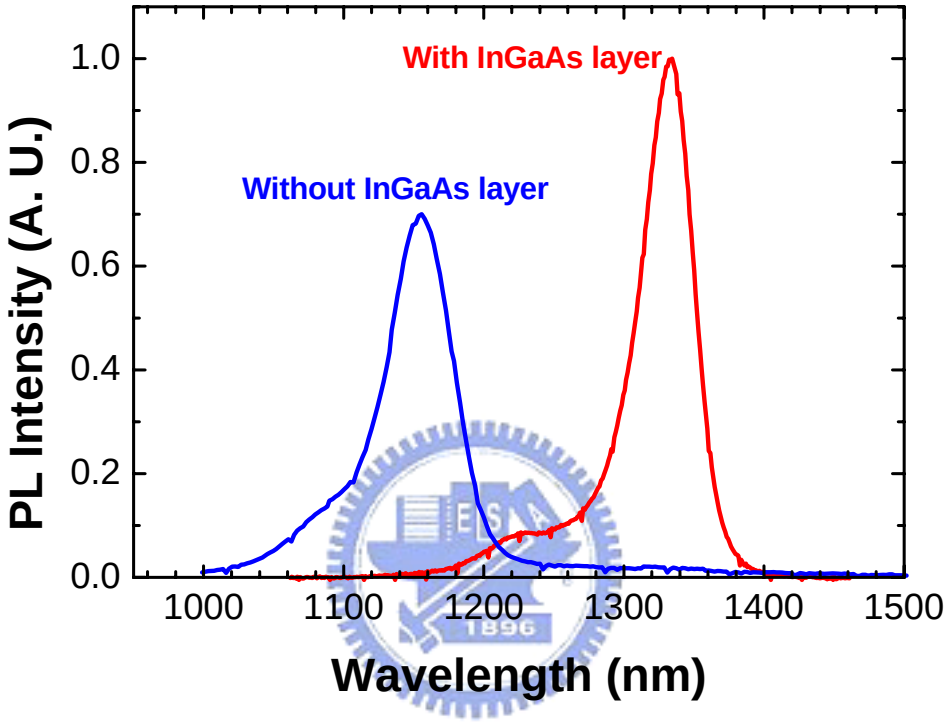

Fig 2.8 RT-PL spectra of InAs/GaAs QDs and with covered InGaAsQW.

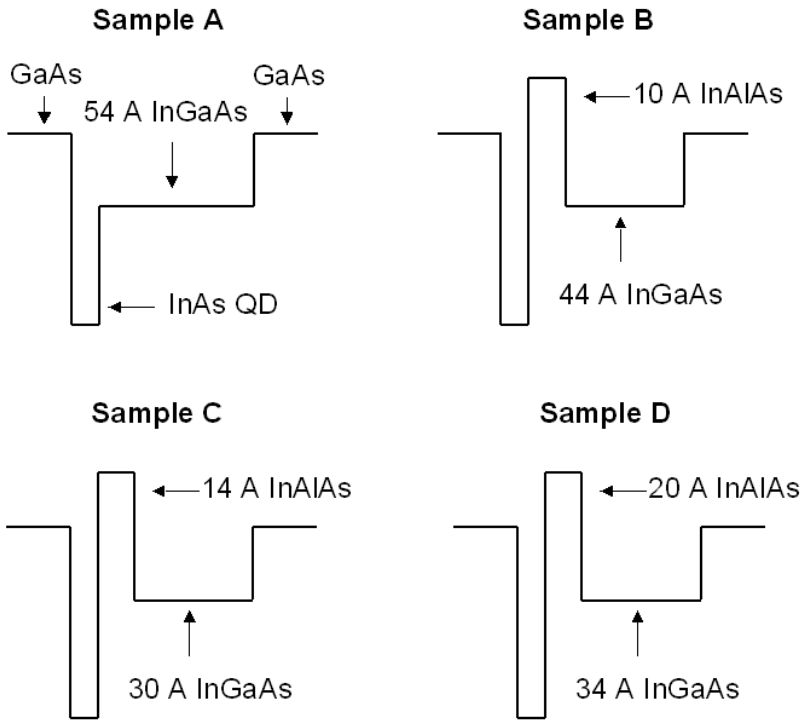

Fig 2.9 The schematic depicts the structure of the samples in band diagram from A to D

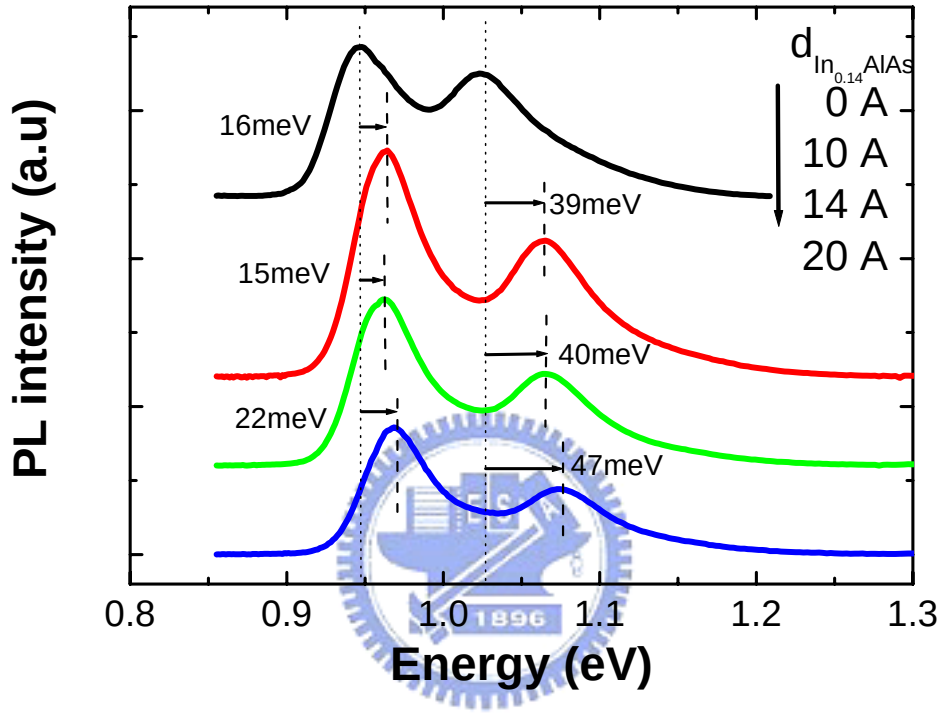

Fig 2.10 The RT-PL spectra of the samples (A to D) with InAs/InAlAs/InGaAs/GaAs QDs active region.

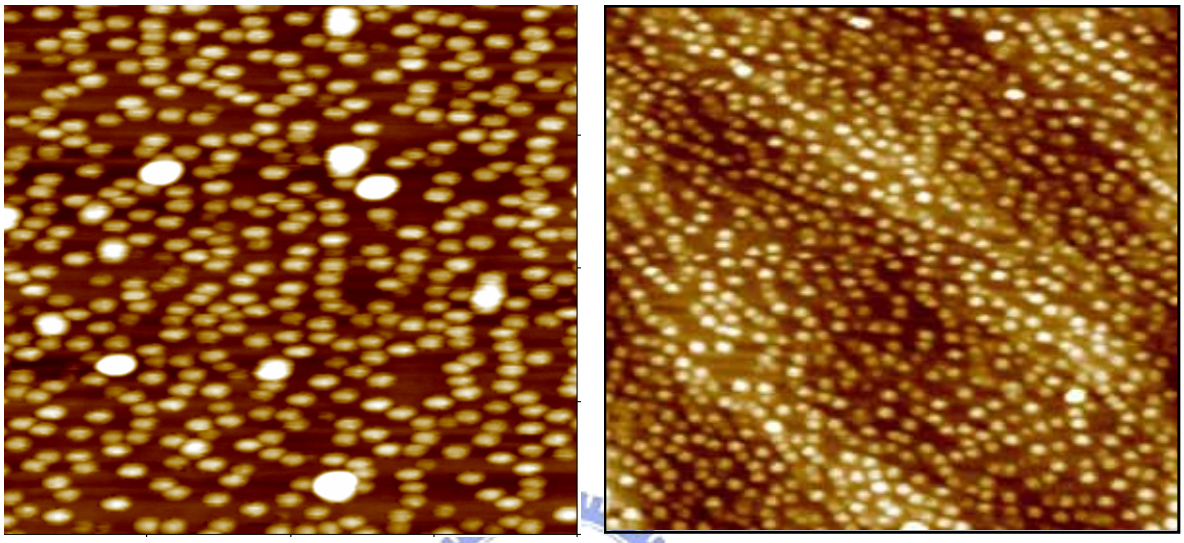

Dot density : $3x10^{10}$ cm^{-3} **Dot density : $9x10^{10}$ cm^{-3}**

Fig 2.11 1.0 x 1.0 μm^2 atomic force microscopic image of a sample with 2.6 ML InAs QDs covered with 10 Å InAlAs/44 Å InGaAs strain reduce layer.

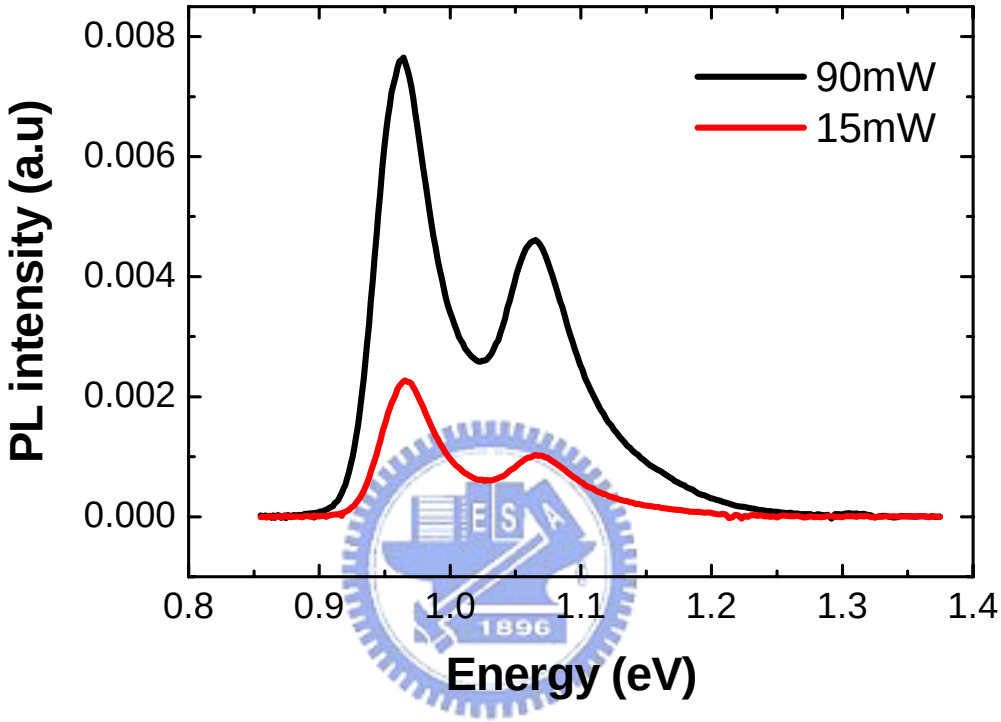

Fig 2.12 RT-PL spectra of InAs/InAlAs/InGaAs/GaAs structure under 15 and 90mW excited power.

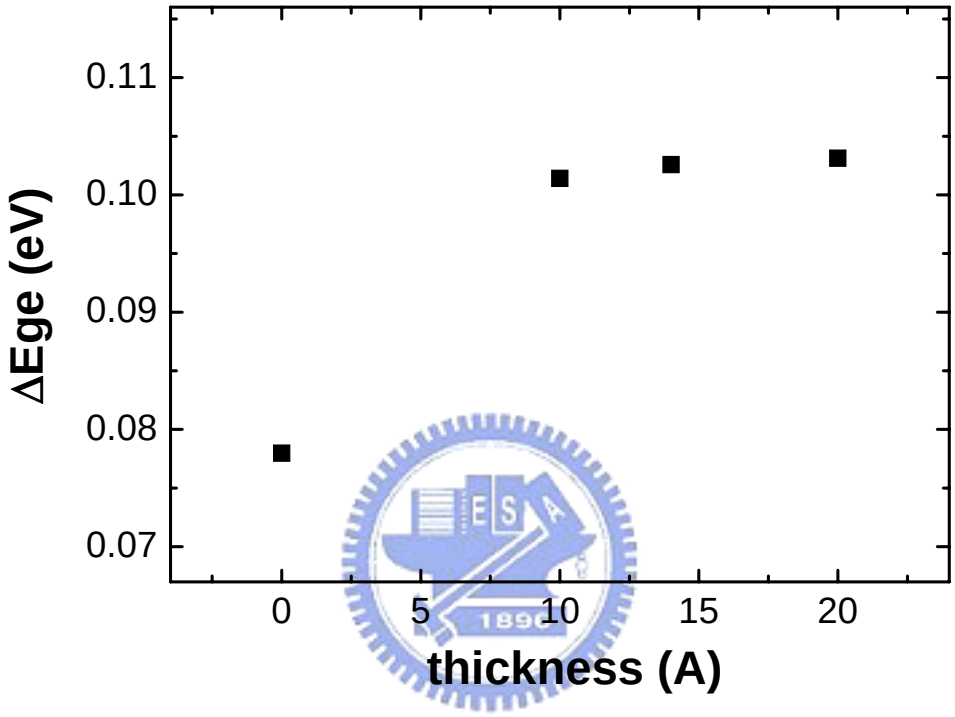

Fig 2.13 Energy separations of InAs QDs covered with InAlAs strain reduce layer between ground state and first excited state.

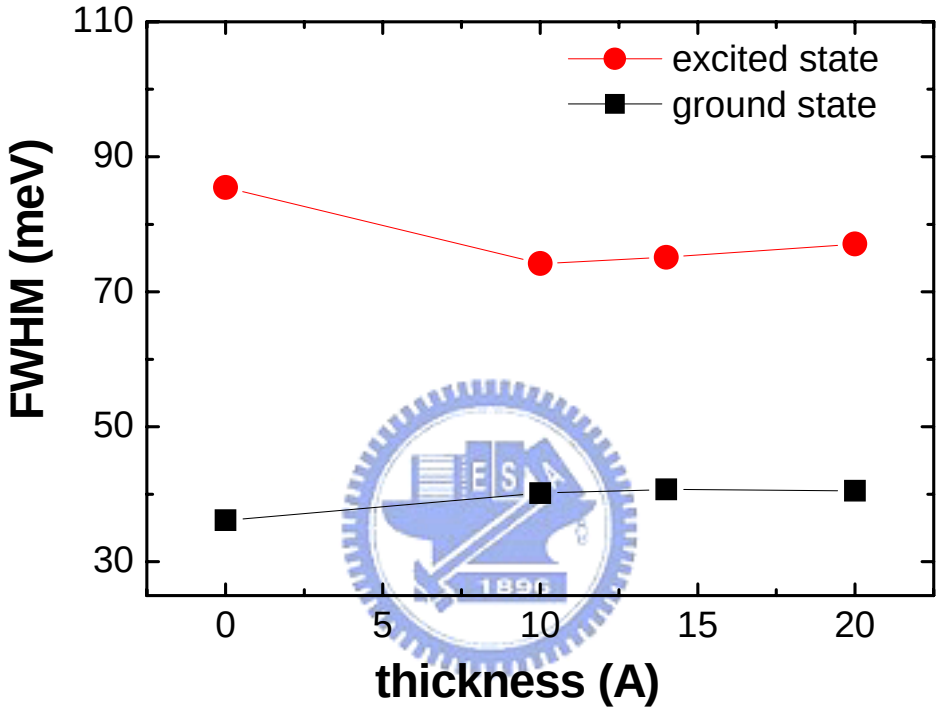

Fig 2.14 The line-width of ground state and excited state of InAs / InAlAs / InGaAs / GaAs active region.

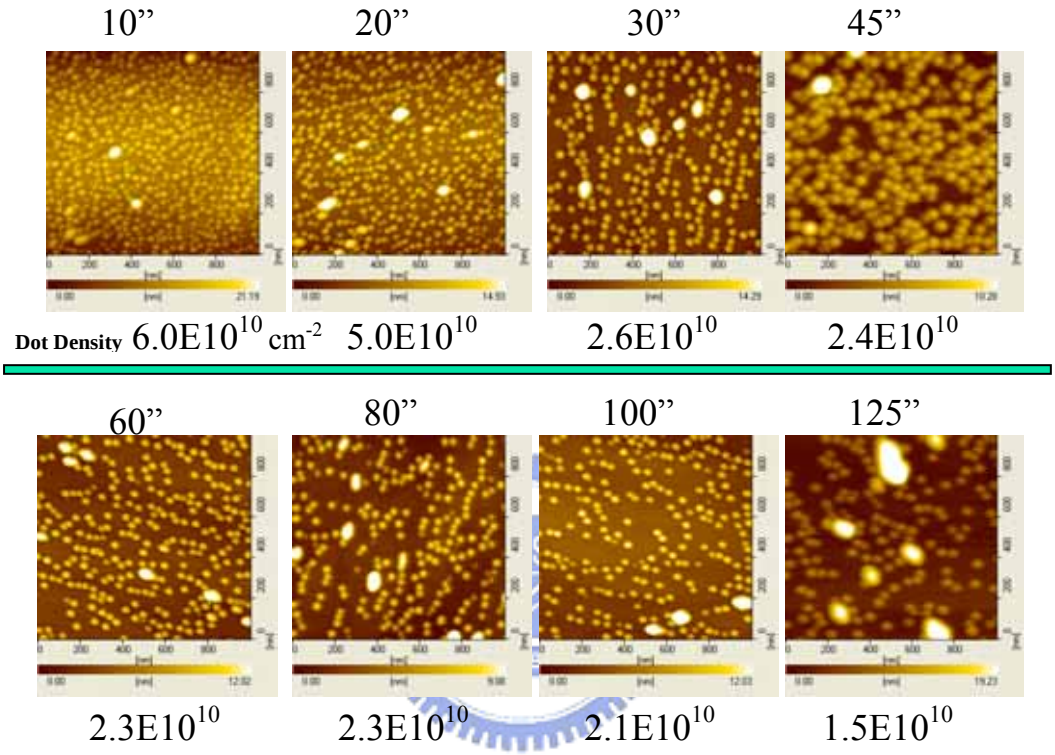

QD formation (secs)	**10**	**20**	**30**	**45**	**60**	**80**	**100**	**120**
G. R (A/sec)	**0.53**	**0.26**	**0.17**	**0.11**	**0.08**	**0.06**	**0.05**	**0.04**
Dot Density (cm^{-3})	**$6E10^{10}$**	**$5E10^{10}$**	**$2.6E10^{10}$**	**$2.4E10^{10}$**	**$2.3E10^{10}$**	**$2.3E10^{10}$**	**$2.1E10^{10}$**	**$1.5E10^{10}$**

Table 2.1 Indium growth rate influence the InAs QDs density on GaAs surface.

InGaAs QW	14.8 %	16 %	17 %
Wavelength (nm)	1308	1329	1340

Table 2.2 The emission wavelengths of InAs/InGaAs/GaAs QDs structure, indium composition in the InGaAs were 14.8%, 16% and 17%.

Chapter 3: QDs lasers

Currently the quest for 1.3 μm GaAs-based lasers is a powerful driving force in the development of low cost lasers for optical communications. InAs quantum dots (QDs) buried in InGaAs quantum well (QW) is one of the promising candidates [1-3] among other approaches utilizing either InGaAsN or GaAsSb [4] QW structures. The possibility to avoid non-radiative recombination in structures emitting at 1.3 μm is one of the main advantages of QDs. Efficient light emission and relatively low density of QDs may result in low threshold current density. For example, a threshold current density of 16A/cm^2, which is the lowest ever reported for any kind of diode lasers, has been achieved using InAs QDs in InGaAs QW [5]. However, because of the non-uniformity of the QD array size distribution, the low surface density also causes a low maximum optical gain achievable at the ground state. Stacking of QD layers with multiple layers was shown to be an effective tool to enhance the optical gain. Very recently a significant improvement in the performance of QD lasers was achieved by this technique. Differential efficiency of 88% was achieved in the 1.28 μm laser with ten pair QD stacks [6] and characteristic temperature of 232 K was achieved in the 1.29 μm laser with five QD stacks placed in p-type doped waveguide [7]. However, in most of the published results, high-contrast waveguide design with cladding layers of high Al content (>0.7) was used to improve overlap between optical field and electron waves (*Γ-factor*) in order to achieve 1.3 μm lasing in QD lasers. Such a design causes a large vertical beam divergence of almost 70 degree, not in accordance with the demand of low beam divergence for efficient coupling of laser light to optical fiber.

Chapter 3.1 InAs QDs lasers

Here we will discuss the normally broad low-contrast $Al_{0.3}Ga_{0.7}As$/GaAs waveguide structure design of InAs/InGaAs dots in well active region with 5 pairs of QDs layers. The advantages of low Al content AlGaAs cladding layer not only improves beam divergence also offers lower resistance, which is important for high speed and high power applications. Based on the growth technology in our development, the vertically coupled QDs laser also has been discussed in the next section.

Structures in this study were grown by solid source molecular beam epitaxy (SS MBE) in a Riber Epineat machine on n^+-GaAs (100) substrates. In the beginning of fabrication of QDs lasers, a set of single active layer with InAs/InGaAs QDs active region was preparing for the optical properties measurement. InAs QDs were formed in Stranski-Krastanow growth mode by a successive deposition of 2.8 monolayers (ML) of InAs at substrate temperature of 490^0C central of the laser structure. QD formation was controlled in situ by monitoring the diffraction pattern of high energy electrons. Then they were covered with $In_{0.15}Ga_{0.85}As$ layer of 5 nm thickness and flanged with 5nm GaAs barrier at the same temperature.

Figure 3.1 shows the RT-PL spectrum of three samples. One of them is single InAs/GaAs QDs with thickness of 2.8ML. Two of them are InAs Dots with 2.6ML and 2.8ML, which are covered by 5nm $In_{0.15}$GaAs quantum well. Sample geometry and all other parameters were the same for all three samples. As shown in Fig 3.1, increasing amount of deposited material for QD formation leads to the gradual red shift of PL spectra position. Spectrum of single InAs QDs shows the emission wavelength at 1.19μm. Starting at 1.19 μm for the smallest QDs, it reaches 1.3 μm for the biggest QDs. PL intensity is at about the same level for the InAs QDs and InAs/InGaAs samples. The brightest PL intensity was observed in the 2.8ML

InAs/InGaAs QDs. At low excitation intensity of 40 W/cm^2, room-temperature PL intensity is very sensitive to the presence of non-radiative recombination. Under our growth condition the wavelength of InAs QDs can be tuned in a wide range without the formation of non-radiative recombination centers. This situation is different from the case of InGaAsN QW, where the extension to longer wavelength is typically followed by steep degradation of the optical quality. However, there is a short wavelength shoulder in PL spectra which shifts along with the PL maximum position. This emission corresponds to the radiative recombination via excited state of QDs. This fact shows that the population of excited state is noticable even under low excitation.

Active region of the lasers consisted of five stacks of QDs emitting at 1.31 μm, was formed as described above. From SEM image, they were separated with 30-nm-thick GaAs spacer layers as shown in Fig 3.2. The total thickness of GaAs waveguide was 0.6 μm. *N*-type and *p*-type $Al_{0.3}Ga_{0.7}As$ cladding layers of 1.5 μm thickness were heavily doped to the level of 1×10^{18} cm^{-3} with Si and Be, respectively. The growth temperature of the bottom cladding layer was 700^{0}C whereas it was chosen to be 600^{0}C for the top one and for the waveguide region to avoid indium atom out-diffusion from the QDs. After growth, lasers were processed into stripes of different widths and cavity lengths. A 10 μm-wide shallow-mesa structure was formed by wet etching for preliminary study of laser performance. 5-μm-wide stripes were formed by double-channel ridge-waveguide self-aligned process using reactive ion etching. Laser characteristics were measured in pulsed operation and continuous wave (*cw*) operation at room temperature. The pulse operation condition was 1 μs duration time and 100 kHz period. Figure 3.3 shows the dependence of the threshold current density on the cavity length measured in pulsed regime for 10-μm-width stripe lasers with as-cleaved facets. Depending on the cavity length (*L*)

laser diodes operate either via ground state (L>1.5 mm) at 1.31 μm or via excited state (L<1.5 mm) at around 1.2 μm. Lasing spectra typical for these two cases are also shown in inserts of Fig 3.3. The reason of this effect is the gain saturation of the ground state. When mirror loss exceeds the value of maximum modal gain ground state lasing becomes impossible. However, due to the additional degeneracy, the excited state provides higher value of the optical gain and higher value of transparency current. In this case lasing switches to the excited state and it is followed by a jump of emission wavelength to the shorter value and by steep increase in the threshold current density.

Figure 3.4 shows the L-I-V curve of QDs lasers under pulse operation at room temperature, the threshold current density is about 350 A/cm^2 for L longer than 3 mm and it increases to about 700 A/cm^2 for the diodes with about 2-mm cavity length. The dependences of total output power under CW operation for both facets on drive current is shown in Fig 3.5 for the ridge waveguide diode of 5-μm-width with 3-mm-length in as-cleaved facets. The lasing spectrum at a current close to the threshold current is presented in the insert. Lasing wavelength is 1.31 μm. The far field pattern recorded in direction perpendicular to the *p-n* junction plane is shown in the insert. Its Gaussian shape with full width at half maximum of 45^0 proves the single lateral mode (SM) operation. This diode shows a threshold current of 26 mA which is equal to 173 A/cm^2 and external differential efficiency of 45% (0.43 W/A). Lower value of the threshold current density than that of 10-μm-wide shallow-mesa devices shows that current spreading is significant in the latter case. The temperature stability of threshold current of this diode is described by characteristic temperature of 85 K within 20-60^{0}C temperature range in Fig 3.6. Turn-on voltage is as low as 1.0 V and resistance is as low as 1.0Ω, (1.5×10^{-4} Ω-cm^2) as presented in Fig.3.4. Such combination of parameters is achieved for the first time for 1.3-μm QD lasers diode

with reasonable vertical beam divergence of 45^0.

In the summary, we realize continuous wave single mode operation at 1.31 μm in lasers with low *Γ-factor,* which shows perspectives of QDs to be used as an active region of GaAs-based edge-emitting and vertical cavity surface emitting lasers for optical communication [8].

Chapter 3.2 The vertical coupled InAs/GaAs quantum dot lasers

Applications using InAs/GaAs quantum dots as the active region in a semiconductor laser are expected to have ultra low threshold current and temperature stability, because of the delta function density of state [9]. Long wavelength lasers based on self-organized InAs quantum dots embedded in InGaAs quantum well (QWs) have been demonstrated to have very low threshold current density ($16A/cm^2$) [10-13]. J. lott et al. [14] fabricated 1.3 μm vertical cavity surface emitting lasers (VCSELs) using multi-stacks InAs/GaAs QDs in the active region. Because InGaAsN/GaAs quantum well can overcome the high surface state problem of the materials and can be grown monolithically on GaAs substrates, it has interesting application to the 1.3 μm single-mode Fabry-Perot lasers for high-power applications. [13,15]

Growth and characterization of the epitaxial layers for InAs QDs lasers have been one of the major ongoing research areas. By using thinner electronic vertically coupled quantum dots active region, the optical model gain can be increased due to the improved optical-electrical overlap factor. Shi and Xie [22] have predicted that the electronic vertical coupling QD (EVCQD) lasers would reveal a higher single-mode output power compared with the uncoupled case through solving coupled rate equations, especially when there is a large fluctuation in dot size. Ustinov et al [18] have demonstrated the vertically electronic coupled QD lasers with lasing wavelength around 1.0 μm. Moreover, combining the inhomogeneous broadening due to size

fluctuation with the mini-band formation due to electronic couple enables EVCQD media to yield "a continuous large-broad gain spectrum", which is very useful for many applications, such as VCSELs, tunable lasers, semiconductor optical amplifiers (SOA) and others. In this section we will study multi stack InAs/GaAs vertically coupled quantum dots lasers.

The laser structures were grown by solid source molecular beam epitaxy on Riber epineat machine. Indium and gallium were supplied from conventional Knudsen effusion cells, and arsenic was supplied from a cracker source. The QDs employed herein as an active medium in the lasers, were grown in the Stranski-Krastanow growth mode by the deposition of InAs 2.6 monolayers (MLs) with a growth rate of 0.085 ML/s and a substrate temperature of 485 ^{0}C, and then covering these layers with a 10 nm thick GaAs layer at the same temperature; the growth temperature of the remaining layers was at 600 ^{0}C. The formation of QDs was controlled *in situ* by monitoring the diffraction pattern of high-energy electrons (RHEED). The dot density estimated from atomic force microscopic (AFM) images, was around $5x10^{10}cm^{-2}$.

The structure was grown on a n^{+}-GaAs (100) substrate, consisting of a 0.3 μm thick n-type GaAs buffer layer, a n-type 1.5 μm thick $Al_{0.3}Ga_{0.7}As$ bottom cladding layer, a GaAs waveguide layer, a p-type 1.5 μm thick $Al_{0.3}Ga_{0.7}As$ upper cladding layer and a p^{+}-doped 0.4 μm thick GaAs contact layer as shown in Fig 3.7. Ten stacks of InAs QDs as the active region were symmetrically placed in the center of the waveguide region, separated only by 17 nm thick GaAs spacer layers [16].

From the TEM image, the lateral and vertical dimensions of the strain field of the QD islands are around 22 and 6.7 nm, respectively as shown in Fig 3.7. The n-type and *p*-type cladding layers were heavily doped with Si and Be, respectively, to 1×10^{18} cm^{-3}. The lasers were processed into stripes of different widths and cavity lengths. 50 μm wide shallow-mesa structures were formed by wet etching in order to identify the

material quality. To obtain the single lateral-mode devices, 3 μm wide stripes were formed by double-channel ridge-waveguide self-alignment, by reactive ion etching. Laser characteristics with as-cleave facets were measured in pulsed (1 μs, 100 kHz) operation at room temperature.

Figure 3.8 shows the L-I curve of 50um broad area lasers with 17 nm spacer. Threshold current density and the transparency current density per QD layer as low as 12 A/cm^2 and 6.3 A/cm^2 were obtained, respectively in Fig 3.9. Figure 3.10 plots the dependence of the reciprocal external differential quantum efficiency on the cavity length for the 50 μm-wide devices under pulsed operation. The internal differential quantum efficiency as high as 90 % and a maximum measured external differential efficiency of 73 % was achieved for a stripe-length of L = 1 mm indicates high crystal quality, although an as many as ten layers in the highly strained EVCQD active region were used.

Figure 3.11 (a) shows the EL spectra of a 3 μm-wide, 500 μm-long device at different injection current densities under pulsed operation. The EL spectra exhibit a strong overlap between ground state emission and excited states emission, maybe because of inhomogeneous broadening due to a fluctuation in the QD size and the formation of a mini-band, which is caused by vertical coupling of the electronic wave function. The spectra-bandwidth increases with the injection current to around 230 nm at 40 KA/cm^2. Such a large-broad continuous EL spectrum differs markedly from that obtained in the uncoupled case, in which the continuous EL spectrum is less than 80 nm [17-20]. Figure 3.11 (b) displays the lasing spectra of 3 μm-wide, 2 mm-long devices at an injection current of 1 A under CW operation. For comparison, a similar ten stacks 1.3 μm QD laser with a conventional uncoupled InAs/InGaAs/GaAs QDs active region is also represented as a dashed line. The spectral bandwidth of the EVCQD lasers is almost half of that in the uncoupled case in which the carriers

occupy the excited states at high injection current. That such a narrow lasing spectrum differs markedly from that obtained in the uncoupled case probably follows from the fact that the carriers tunnel in the vertical direction within the EVCQD active region [21,22]. The results indicate that the EVCQD active region has great potential for single mode laser applications.

Chapter 3.3 InAs/InGaAs QDs fully doping VCSELs

The main purpose of this chapter is to present the current status of quantum dot vertical cavity surface emitting lasers(VCSEL). We will discuss the some specific feathers of QD microcavity structures of the device applications. One of the key advances in photonic technology in recent years is the development of vertical microcavity devices such as VCSELs, semiconductor optical amplifiers. VCSELs are high performance lasers that can be produced much like low-cost LED. The advantages of VCSELs are low beam divergence and very stable performance characteristics over temperature. They can be modulated at high data rates, and with low threshold currents. VCSELs also offer the manufacturing of wafer fabrication and test, otherwise easily to produce either small or large arrays.

The first VCSELs were reported by Professor Iga's group at Tokyo Institute of technology in 1979 year [23,25]. Only recent technology developments changed the scale from little laboratory to high performance commercially devices. The potential advantage of using the QDs as active medium in VCSEL is intentionally reduced lateral carrier diffusion [24,25]. An oxide-confined structure represented a major breakthrough in the evolution of VCSEL`s design, they can provide preciously control both optical and electrical confinement, leading to remarkable improvements of the threshold current and efficiency. The first paper on the GaAs-based 1.3 μm QD

VCSEL is published in year of 2000 [26]. Three layers of QDs were centered in a 1λ-thick GaAs optical microcavity, spaced by the doped GaAs intra-cavity contacted layer, and cladded by the oxidized DBR. The oxidized DBRs with alternating AlAs/GaAs layers of 5.5 and 7 pairs for the top and bottom DBRs, respectively are used to obtain high reflectivity. The CW operated power for the best devices approach 1.2 mW for 8 μm aperture size and the maximum wall-plug efficiencies approach 15%.

It is not until 2002 that QDs VCSEL with true semiconductor AlGaAs/GaA DBR [27], i.e. without oxidation, is first grown under the Ioffe-ITRI joint scientific program. Undoped DBRs with alternating $Al_{0.9}Ga_{0.1}As$/GaAs layers of 29 and 35 pairs are used for the top and bottom distributed bragg reflectors (DBRs), respectively. Three groups of 3-layer QDs are periodically positioned in the anti-node of the optical field in Fig 3.12(a),(b). The modal gain is expected to be higher by incorporating this periodic gain structure. At room temperature under continuous wave operation, the maximum optical output exceeds over 2 mW with 12 μm aperture size.

In conventional 850-nm VCSELs p and n-doped AlGaAs DBRs are usually exploited. The design provides easy device fabrication, which is completely planar structure. Fully doped QD VCSELs are promising for simple fabrication, as their fabrication is fully compatible with the well-developed technology of 850 nm QW VCSELs[23]. However, some studies show that one of the main cavity loss mechanisms is related to free carrier absorption inside of DBRs especially due to p-doping [24.25]. While the undoped DBRs bring the advantage of low optical losses to the VCSEL designer, they also bring the disadvantage of insulating electrical properties. It is important to point here that the reasonable electrical conductivity in real DBRs requires a relativity high doping around more than $5x10^{18}$ at the interfaces.

In order to achieve a current spreading layer with a low resistance, desirable for low device heating and high modulation speeds, the doping levels of the n-contact and p-contact layers should be higher. In contrast, to obtain low optical losses, the doping level should be low. This is quite critical for low gain active media VCSELS. In our QDs VCSELs, the p-type DBR is grown by incorporation of CBr4 as the donor source and the doping level of $Al_{0.9}Ga_{0.1}As$ and GaAs as $2x10^{17}cm^{-3}$. The detailed structure of fully doped QDs VCSELs with 23 pains $Al_{0.9}Ga_{0.1}As$/ GaAs p-type top DBRs and 33 pairs n-type bottom DBRs is shown in Fig 3.13. There are 5 groups of QDs region centered the cavity, each group included 3 pairs InAs/InGaAs/GaAs QDs layers. Single 12nm AlAs layer was used for the current confined layer. The single transverse mode and RT-CW threshold current below 1 mA are achieved for 5.5 μm aperture conducted in Fig. 3.14(a). The lasing spectrum of QDs VCSELs under different driving current at CW operation is shown in Fig 3.14(b). However, the optical output is below 1 mW and the series resistance is rather high. Further optimization is anticipated for high performance QD VCSELs of 1.3 μm range.

Finally, we think that the design with oxidized DBRs and fully doped QDs VCSELs seems to be suitable choice for fabrication of QDs VCSELs. However successful realization of process VCSELs requires much advantaged fabrication technology. The most critical components of such technology include epitaxy growth, precise etching of multiple layers semiconductor structures, stable and reproducible oxidation of AlGaAs and AlAs alloys, and low resistively contacts.

Reference

[1] K. Nishi, H. Saito, S. Sugou, and J. S. Lee, “A rarrow photoluminescence linewodth of 21meV at 1.35meV from strain-reduced InAs quantum dots covered by $In_{0.2}GaAs$ grown on GaAs substrates,” Appl. Phys. Lett., 74, 1111, 1999.

[2] L. F. Lester, A. Stintz, H. Li, T. C. Newell, E. A. Pease, B. A. Fuchs, and K. J. Malloy, “Optical characteristics of 1.24um InAs quantum dot laser diodes,” IEEE Photon. Technol. Lett., 11, 931, 1999.

[3] V. M. Ustinov, N. A. Maleev, A. E. Zhukov, A. R. Kovsh, A. Yu. Egorov, A. V. Lunev, B. V. Volovik, I. L. Krestnikov, Yu. G. Musikhin, N. A. Bert, P. S. Kop'ev, Zh. I. Alferov, N. N. Ledentsov, and D. Bimberg, “InAs/InGaAs quantum dot structures on GaAs substrates emitting at 1.3um,” Appl. Phys. Lett., 74, 2815, 1999.

[4] For a review, see D.W. Kisker and J.E. Bisberg, MRS bulletin, 27, 512, 2002.

[5] G. T. Liu, A. Stintz, H. Li, T. C. Newell, A. L. Gray, P. M. Varangis, K. J. Malloy, and L. F. Lester, “ The influence of quantum well composition on the performance of quantum dot lasers using InAs/GaAs dots in well (DWELL) structure,” IEEE Journal of Quantum Electronics, 36, 1272, 2000.

[6] A. R. Kovsh, N. A. Maleev, A. E. Zhukov, S. S. Mikhrin, A. P. Vasil'ev, Yu. M. Shemyakov, M. V. Maximov, D. A. Livshits, V. M. Ustinov, Zh. I. Alferov, N. N. Ledentsov, and D. Bimberg, “InAs/InGaAs/GaAs quantum dot lasers of 1.3um range with high 88% differential efficiency,” Electron Lett, 38, 1104, 2002.

[7] O. B. Shchekin, J. Ahn, and D. G. Deppe, ”The role of p-type doping and the density of states on the modulation response pf quantum dot lasers,” Electron Lett 38, 712 2002.

[8] J. S. Wang, R. S. Hsiao, G. Lin, L. Wei, Y. T. Wu, A. R. Kovsh, N. A. Maleev, A. V. Sakharov, D. A. Livshits, J. F. Chen, and J. Y. Chi, “Ridge waveguide 1310 nm

lasers based on multiple stacks of InAs/GaAs quantum dots," phys. stat. sol. C Vol. 0, No. 4, pp. 1339–1342, 2003.

[9] Y. Arakawa and H. Sakaki, "Multidimensional quantum well laser and temperature dependence of its threshold current," Appl. Phys. Lett., vol. 40, pp. 939-941, 1982.

[10] G. T. Liu, A. Stinz, H. Li, T. C. Newell, A. L. Gray, P. M. Varangis, K. J. Malloy, and L. F. Lester, "The influence of quantum-well composition on the performance of quantum dot lasers using InAs-InGaAs dots-in-a-well (DWELL) structures," IEEE J. Quantum Electron., vol. 36, pp. 1272-1279, 2000.

[11] A. Markus, J. X. Chen, C. Paranthoën, A. Fiore, C. Platz, and O. Gauthier-Lafaye, "Simultaneous two-state lasing in quantum-dot lasers," Appl. Phys. Lett., vol. 82, pp. 1818-1820, 2003.

[12] A. E. Zhukov, A. R. Kovsh, D. A. Livshits, V. M. Ustinov, and Zh. I. Alferov, "Output power and its limitation in ridge-waveguide 1.3 μm wavelength quantum-dot lasers," Semicond. Sci. Technol., vol. 18, pp. 774-781, 2003.

[13] A. R. Kovsh, N. A. Maleev, A. E. Zhukov, S. S. Mikhrin, A. P. Vasil'ev, Yu. M. Shernyakov, M. V. Maximov, D. A. Livshits, V. M. Ustinov, Zh. I. Alferov, N. N. Ledentsov, and D. Bimberg, "InAs/InGaAs/GaAs quantum dot lasers of 1.3 μm range with high (88%) differential efficiency," Electron. Lett., vol. 38, pp. 1104-1106, 2002.

[14] J. A. Lott, N. N. Ledentsov, A. R. Kovsh, V. M. Ustinov, and D. Bimberg, "Multiple stacks of InAs/InGaAs quantum dots for GaAs-based 1.3 μm vertical cavity surface emitting lasers," The 16th Annual Meeting of the IEEE LEOS, vol. 2, pp. 499-500, 2003.

[15] L. F. Lester, A. Stintz, H. Li, T. C. Newell, E. A. Pease, B. A. Fuchs, and K. J. Malloy, "Optical characteristics of 1.24-μm InAs quantum-dot laser diodes," IEEE Photonics Technol. Lett., vol. 11, pp. 931-933, 1999.

[16] Jyh-Shyang Wang, Ru-Shang Hsiao, Jenn-Fang Chen, Chu-Shou Yang, Gray Lin, Chiu-Yueh Liang, Chih-Ming Lai, Hui-Yu Liu, Tung-Wei Chi, and Jim-Y. Chi, "Engineering Laser Gain Spectrum Using Electronic Vertically Coupled InAs–GaAs Quantum Dots," IEEE Photonics Technology Letters, vol. 17, NO. 8, 2005.

[17] P. M. Varangis, H. Li, G. T. Liu, T. C. Newell, A. Stintz, B. Fuchs, K. J. Malloy, and L. F. Lester, "Low-threshold quantum dot lasers with 201 nm tuning range," Electron. Lett., vol. 36, pp. 1544-1545, 2000.

[18] V. M. Ustinov, A. Yu. Egorov, A. R. Kovsh, A. E. Zhukov, M. V. Maximov, A. F. Tsatsul'nikov, N. Yu. Gordeev, S. V. Zaitsev, Yu. M. Shernyakov, N. A. Bert, P. S. Kop'ev, Zh. I. Alferov, N. N. Ledensov, J. Böhrer, D. Bimberg, A. O. Kosogov, P. Werner, and U. Gösele, "Low-threshold injection lasers based on vertically coupled quantum dots," J. Cryst. Growth, vol. 175/176, pp. 689-695, 1997.

[19] M. V. Maximov, L. V. Asryan, Yu. M. Shernyakov, A. F. Tsatsul'nikov, I. N. Kaiander, V. V. Nikolaev, A. R. Kovsh, S. S. Mikhrin, V. M. Ustinov, A. E. Zhukov, Zh. I. Alferov, N. N. Ledenstov, and D. Bimberg, "Gain and threshold characteristics of long wavelength lasers based on InAs/GaAs quantum dots formed by activated alloy phase separation," IEEE J. Quantum Electron., vol. 37, pp. 676-683, 2001.

[20] S. L. Chuang, Physics of Optoelectronic Devices, New York: John Wiley & Sons, Inc., 1995, pp. 432-437.

[21] P. M. Smowton and P. Blood, "The differential efficiency of quantum-well lasers," IEEE J. Select. Topics Quantum Electron., vol. 3, pp. 491-498, 1997.

[22] B. Shi and Y. H. Xie, "Influence of coupling effect in the operation of vertically coupled quantum-dot lasers," Appl. Phys. Lett., vol. 82, pp. 4788-4790, 2003.

[23] Haruhisa Soda, Ken-ichi Iga, Chiyuki Kitahara, and Yasuharu Suematsu,

"Surface emitting injection lasers," Jpn. J. Appl. Phys., vol. 18, 2329-2330, 1979.

[24] J. M. Gerard, O. Cabrol, and B. Sermage, "InAs quantum box: highly efficient radiative traps for light emitting devices on Si," Appl. Phs. Lett., 68, 3123-3125 1996.

[25] Ustinov, V.M.; Zhukov, A.E.; Maleev, N.A.; Kovsh, A.R.; Mikhrin, S.S.; Volovik, B.V.; Musikhin, Yu.G.; Shernyakov, Yu.M.; Maximov, M.V.; Tsatsul'nikov, A.F.; Ledentsov, N.N.; Alferov, Zh.I.; Lott, J.A.; and Bimberg, D., "1.3μm InAs/GaAs quantum dot lasers and VCSELs grown by molecular beam epitaxy," J. Cryst. Growth, 227-228, 1155-1161, 2001.

[26] Lott, .A, Ledentsov, N. N, Ustinov, V. M, Maleev, N. A, Zoukov, A. E, Kovsh, A. R, Maximov, M. V. Volovik, B. V, Alferov, Zh. I and Bimberg. D, "InAs-InGaAs quantum dot VCSELs on GaAs substrate emitting at 1.3um," Electron.Lett., 36, 1384-1385, 2000.

[27] Yang, G. M, MachDougal, M. H and Dapkus, P. D, "Ultralow threshold current vertical cavity surface emitting lasers obtained with selective oxidation," Electron .lett., 31, 886-888, 2000.

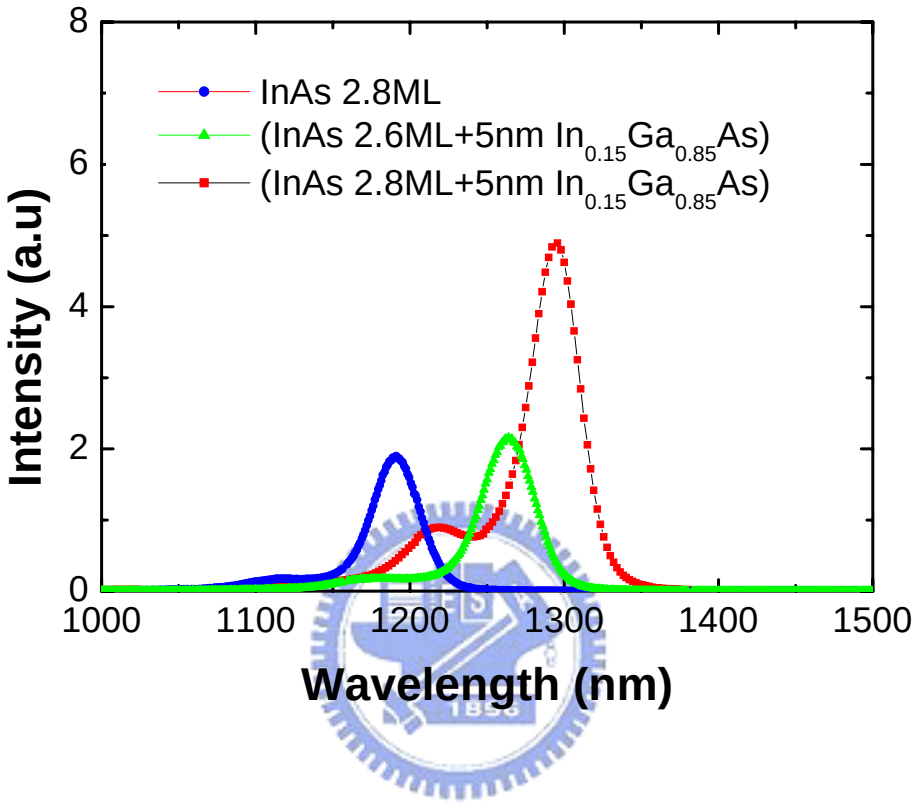

Fig 3.1 RT-PL spectra for samples with one QD layer formed by depositing different amount of single InAs (2.8 ML) QDs and InAs (2.6~2.8ML), covered with 5-nm-thick $In_{0.15}Ga_{0.85}As$ layer. Excited state (ES) and ground state (GS) peak position shifts toward longer wavelength when the thickness of InAs is increasing.

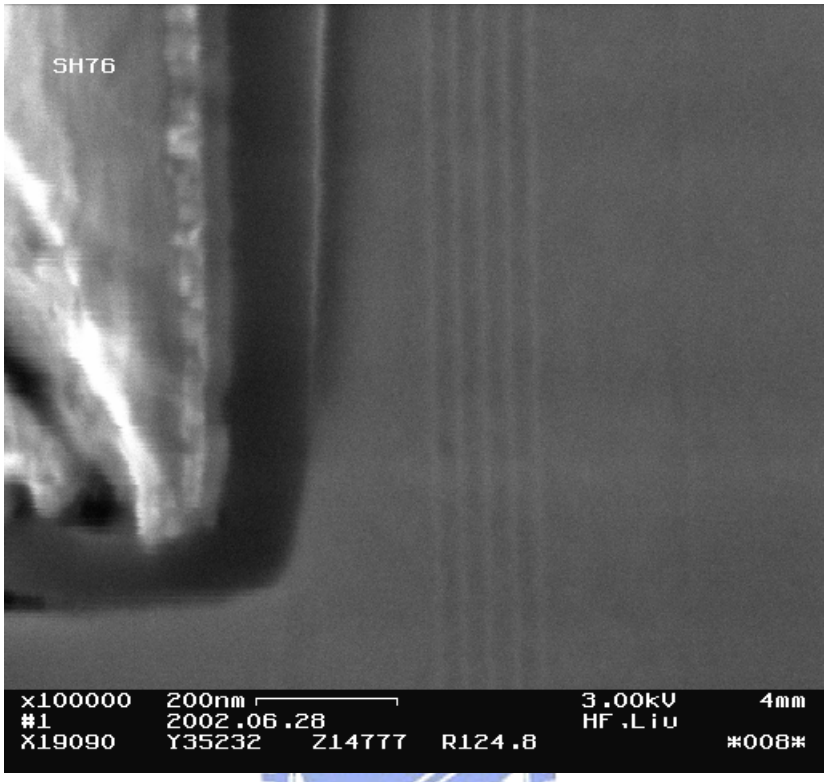

Fig 3.2 SEM image of 5 pairs InAs/InGaAs/GaAs QDs layers with the 30nm GaAs spacer layer.

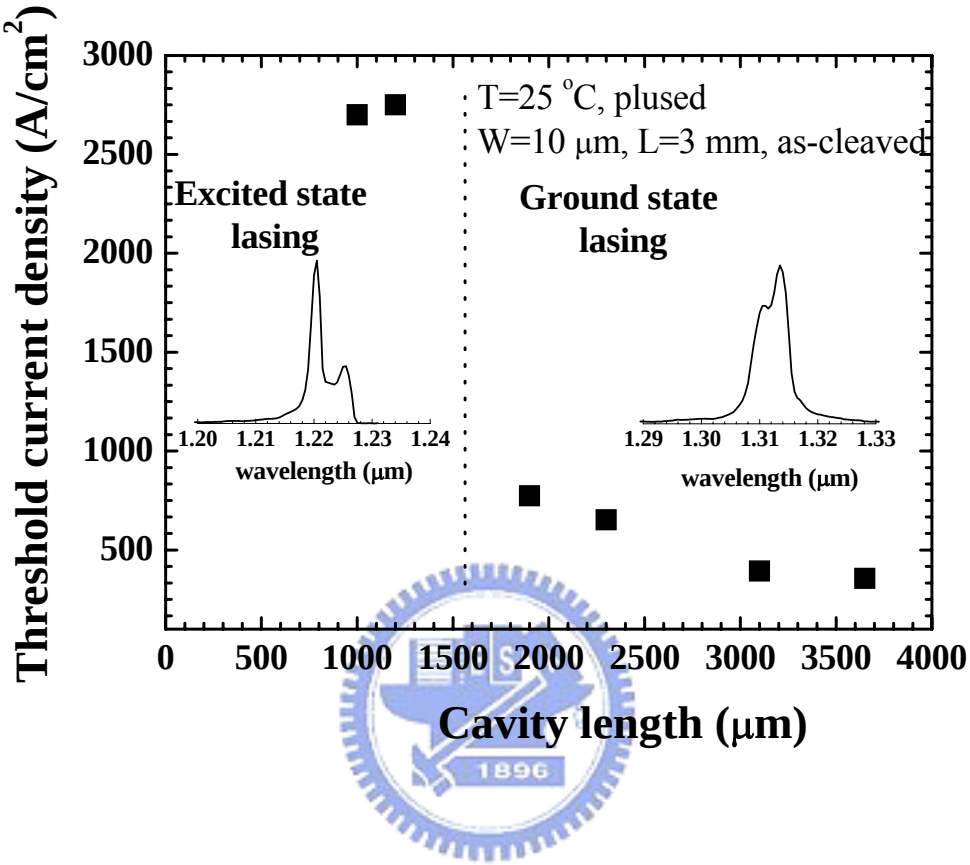

Fig 3.3 Dependence of the threshold current density on the cavity length for 10-μm-width stripe lasers with as-cleaved facets. The emitting wavelength at 1.22 μm with the excited lasing.

.

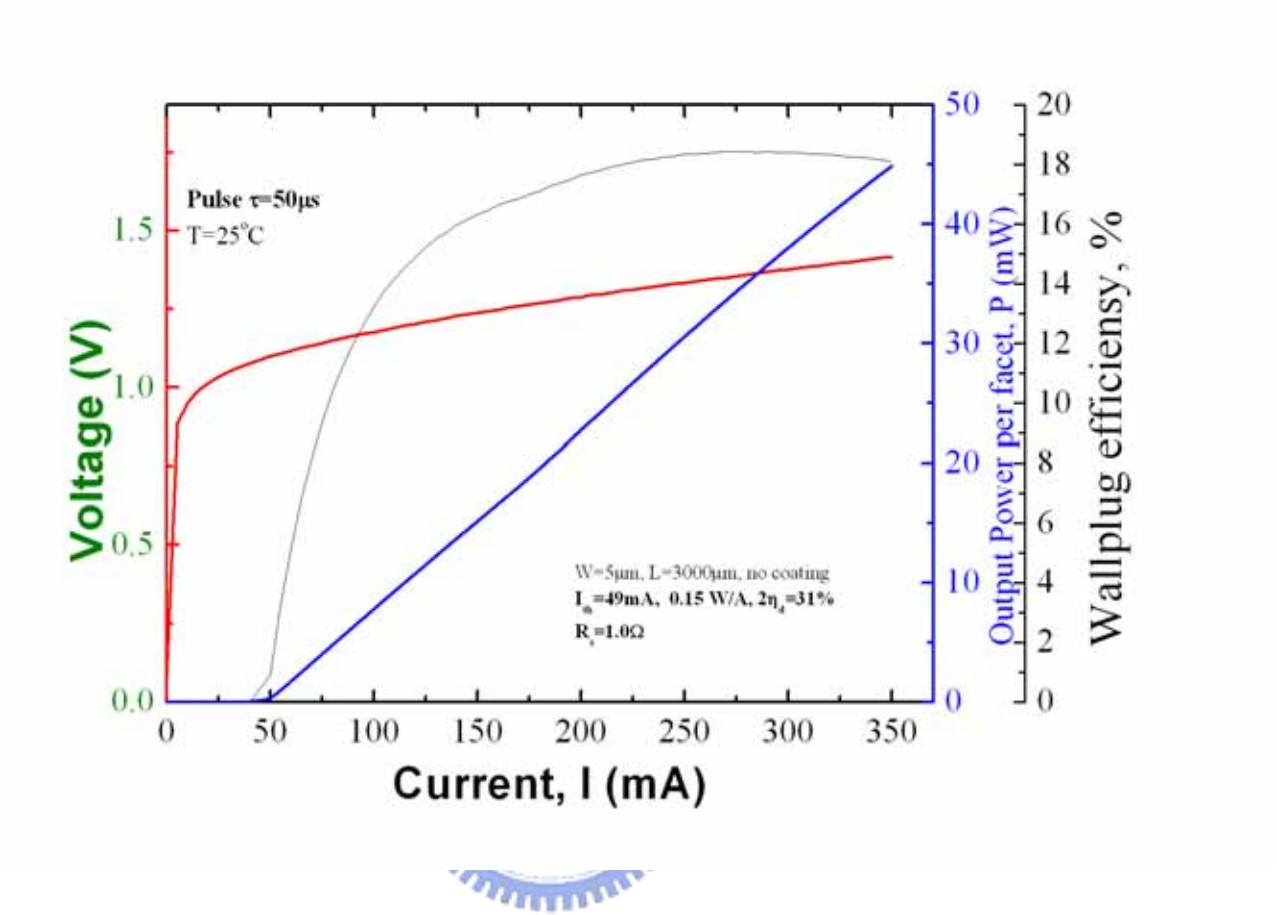

Fig 3.4 The L-I-V curve of QDs edge emitting lasers in 5μm ridge with 3mm cavity length under pulsed operation at room temperature.

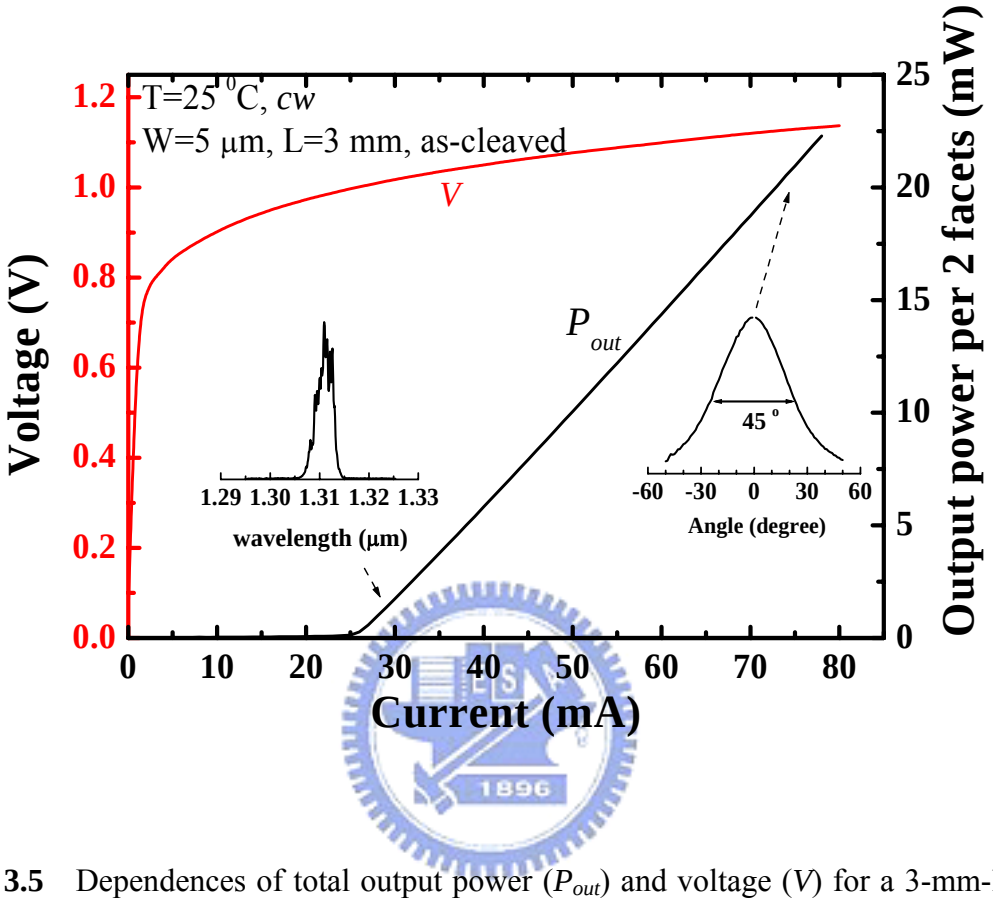

Fig. 3.5 Dependences of total output power (P_{out}) and voltage (V) for a 3-mm-long and 5-μm-wide ridge waveguide diode, with as-cleaved facets. Lasing spectrum above the threshold and far-field pattern in vertical direction are shown in the inserts.

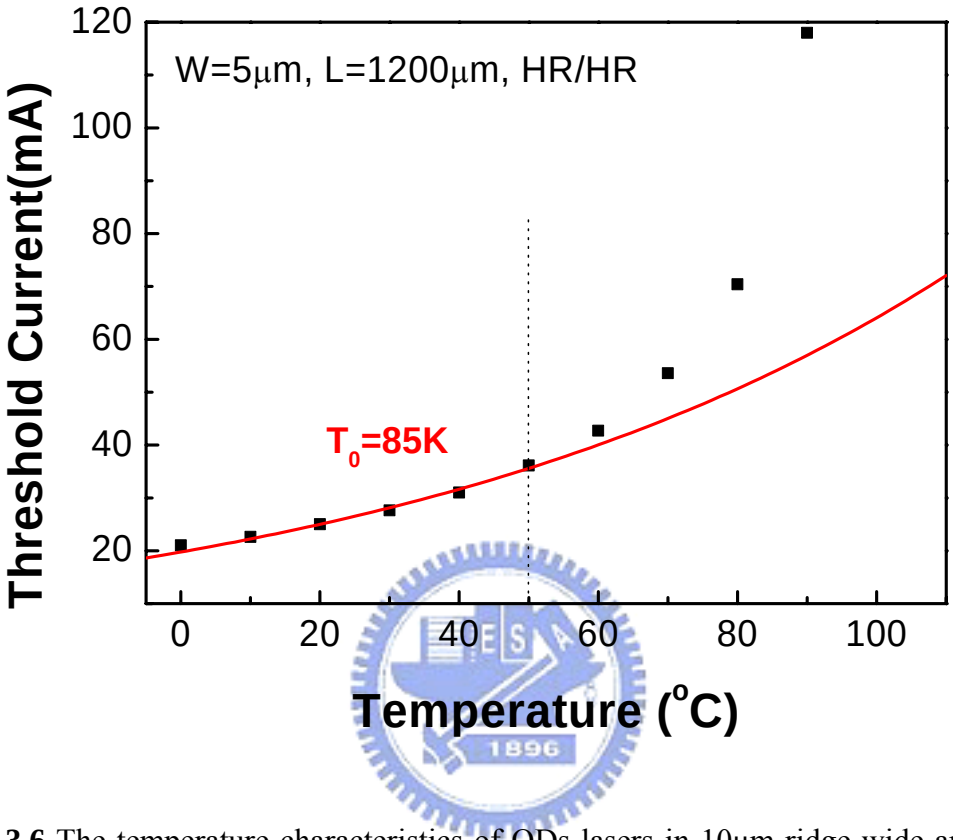

Fig 3.6 The temperature characteristics of QDs lasers in 10μm ridge wide and 5mm cavity length.

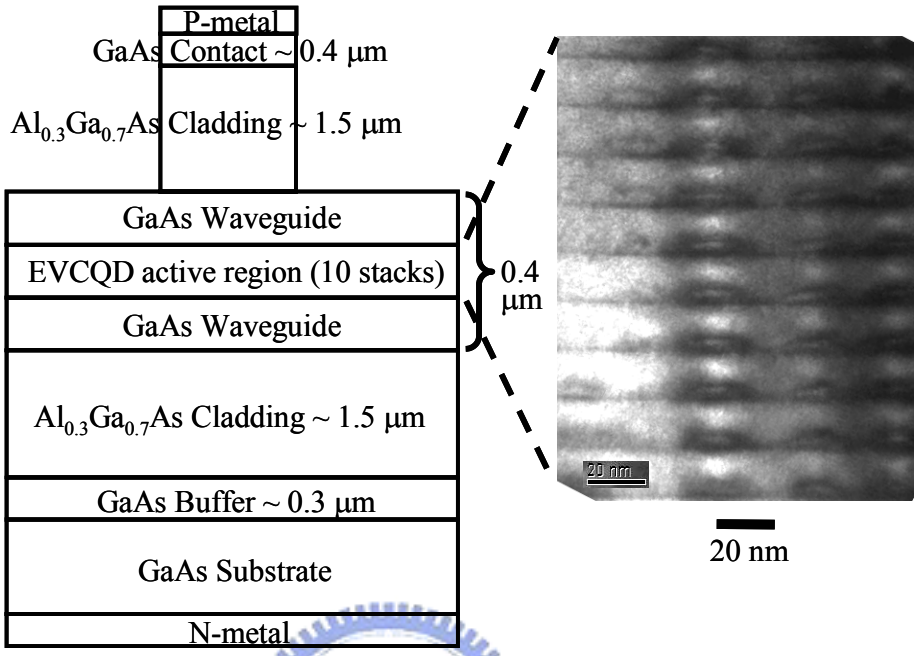

Fig 3.7 Schematic diagram of QD laser structure with narrow ridge waveguide, and cross-sectional TEM image of ECVQD active region.

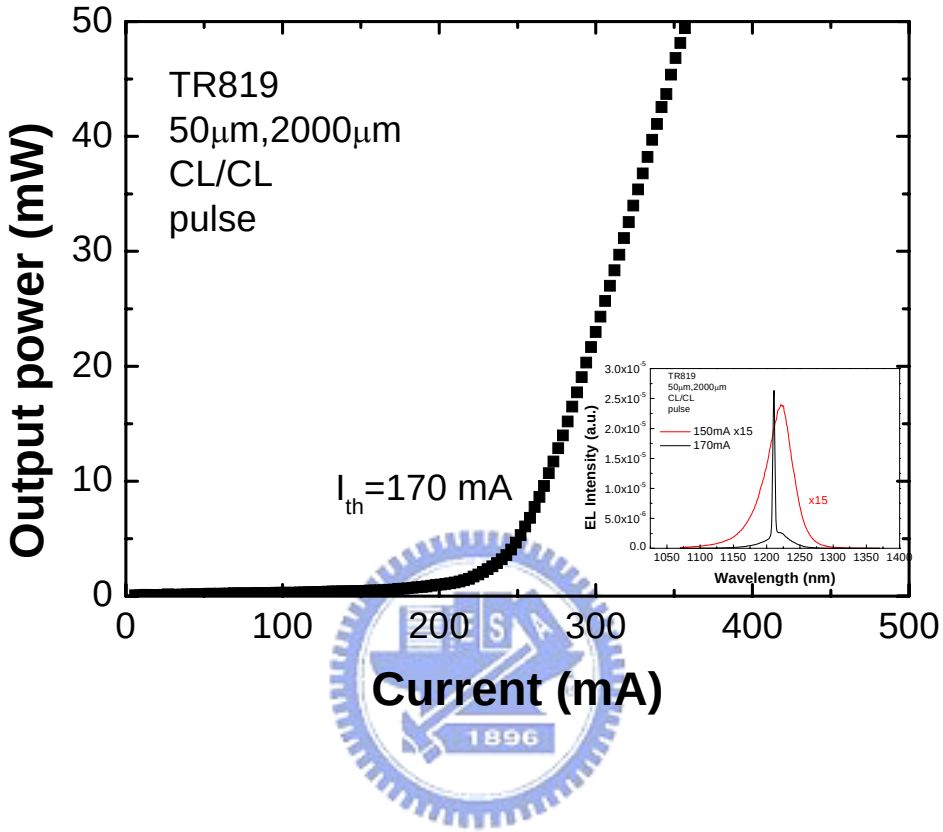

Fig 3.8 The L-I curve of a 10-pair vertical coupled InAs/GaAs QDs laser with a 17nm GaAs space layer. The laser dimensions are 50μm wide ridge and 2mm in length. The insert shows the lasing spectrum.

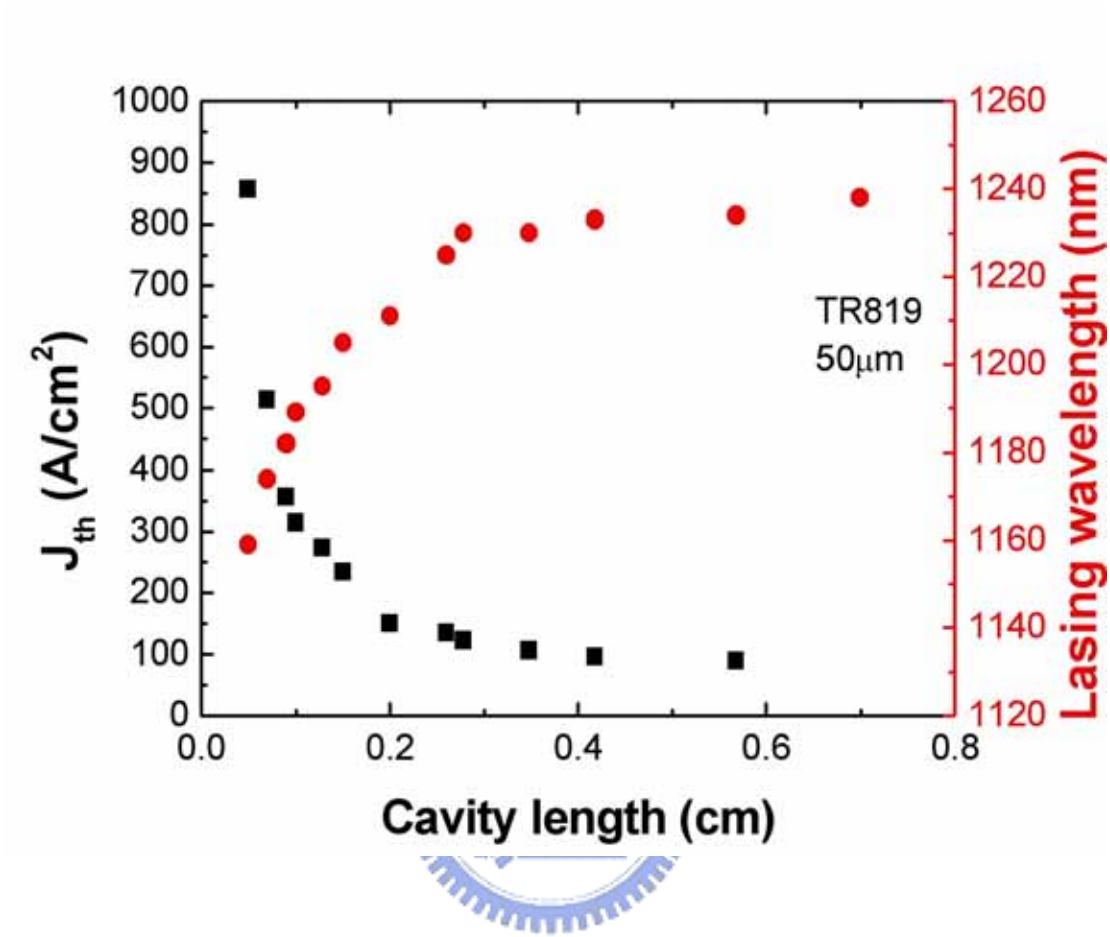

Fig 3.9 Dependence of threshold current density of the lasers on the cavity length, with a 50μm ridge width.

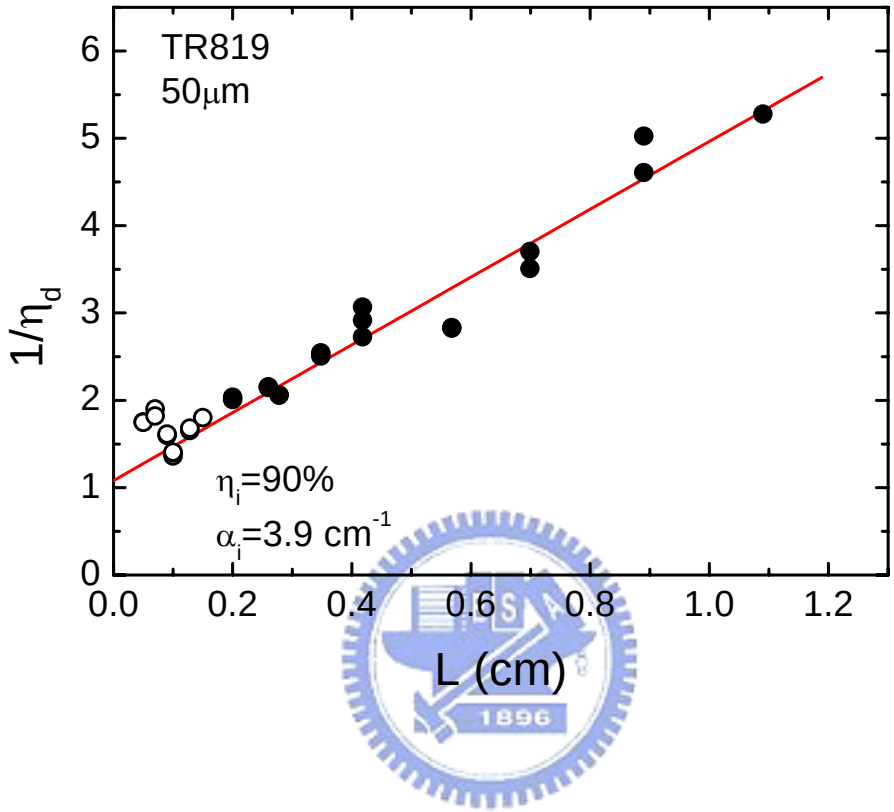

Fig 3.10 The dependence of the reciprocal external differential quantum efficiency on the cavity length for the 50 μm-wide devices under pulsed operation at room temperature.

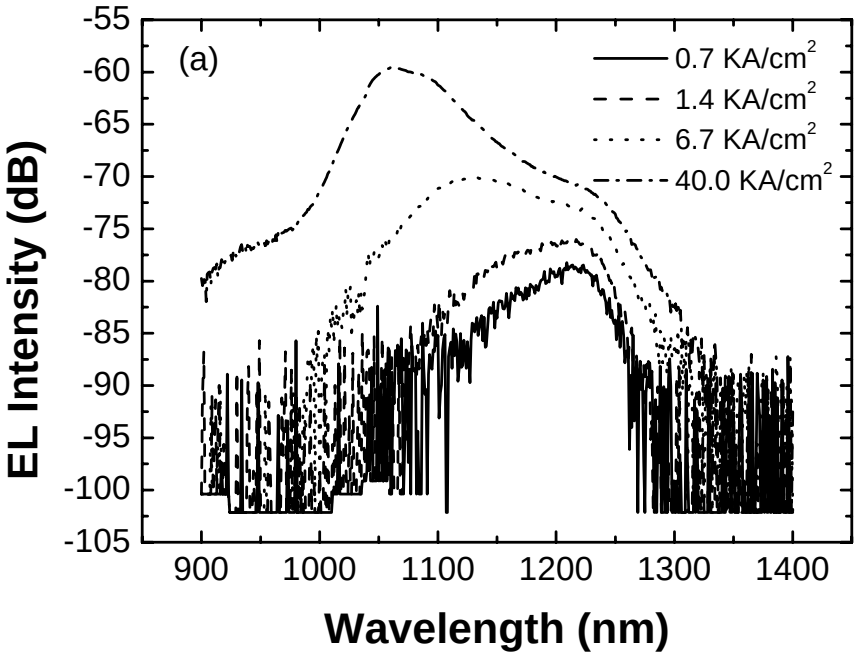

Fig. 3.11 (a) EL spectra of a 3 μm-wide, 500 μm-long device at different injection current densities under pulsed operation.

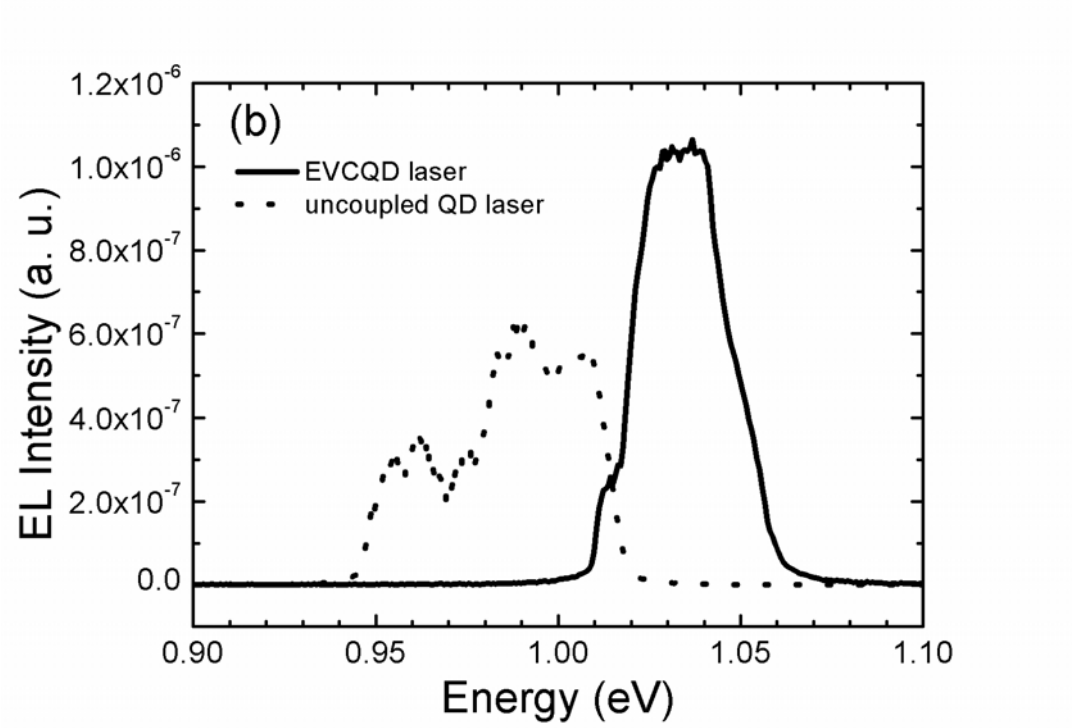

Fig. 3.11 (b) Lasing spectra of 3 μm-wide, 2 mm-long cavity devices at an injection current of 1 A under CW operation. The dashed line shows a lasing spectrum for a similar ten stacks 1.3 μm QD laser with a conventional uncoupled InAs/InGaAs/GaAs QD active region.

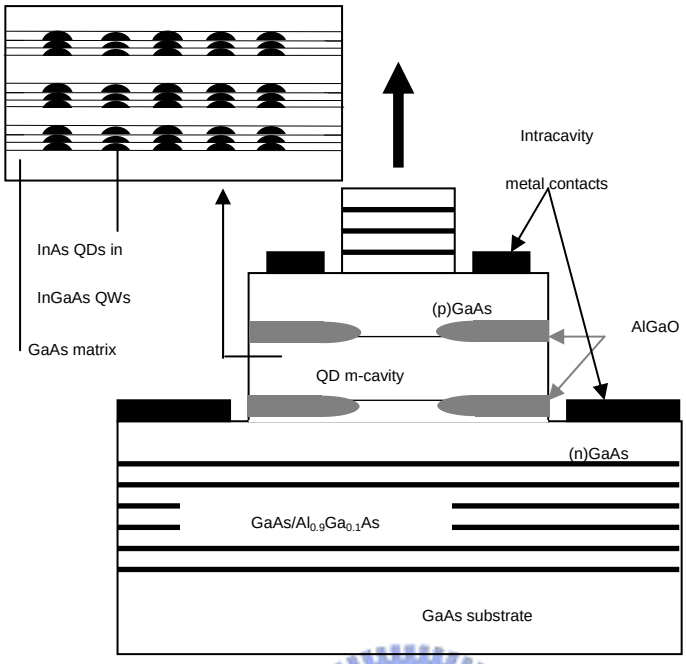

Fig 3.12 (a) The structure design of three groups of 3-layer QDs in the active region.

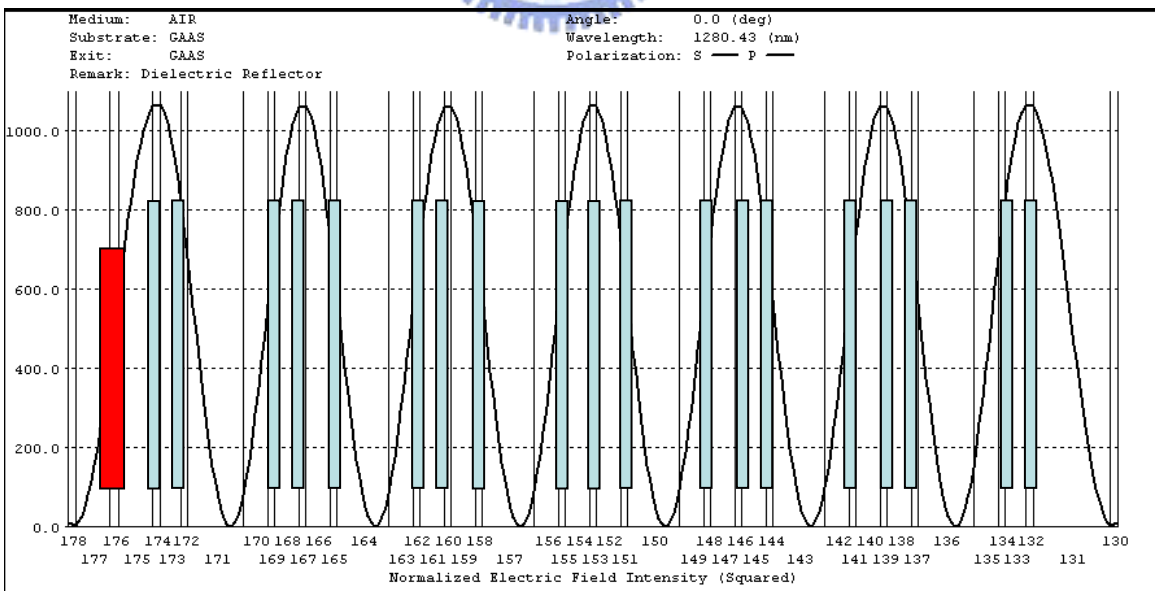

Fig 3.12 (b) InAs/InGaAs/GaAs QDs are periodically positioned in the anti-node of the optical field.

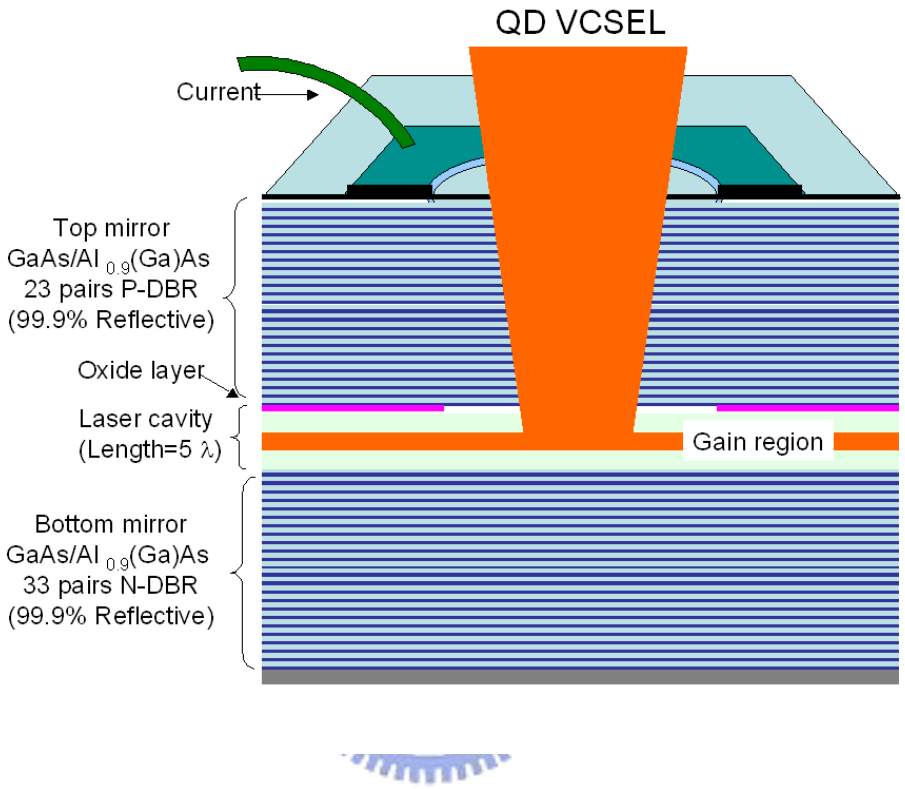

Fig 3.13 The schematic of fully doped VCSELs with InAs/InGaAs/GaAs QDs active media.

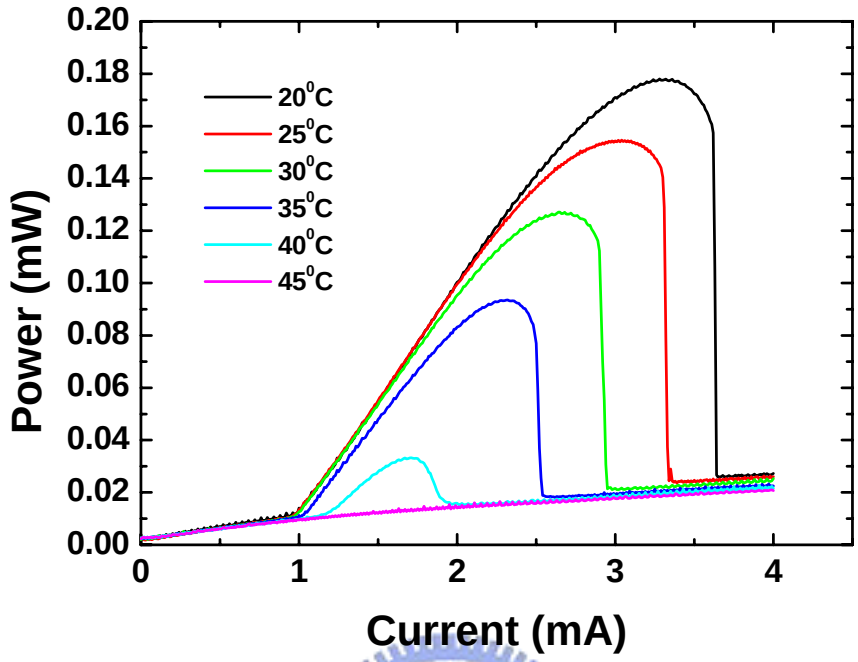

Fig 3.14 (a) Room temperature CW single mode lasing at threshold current below 1 mA with 5.5 μm aperture size.

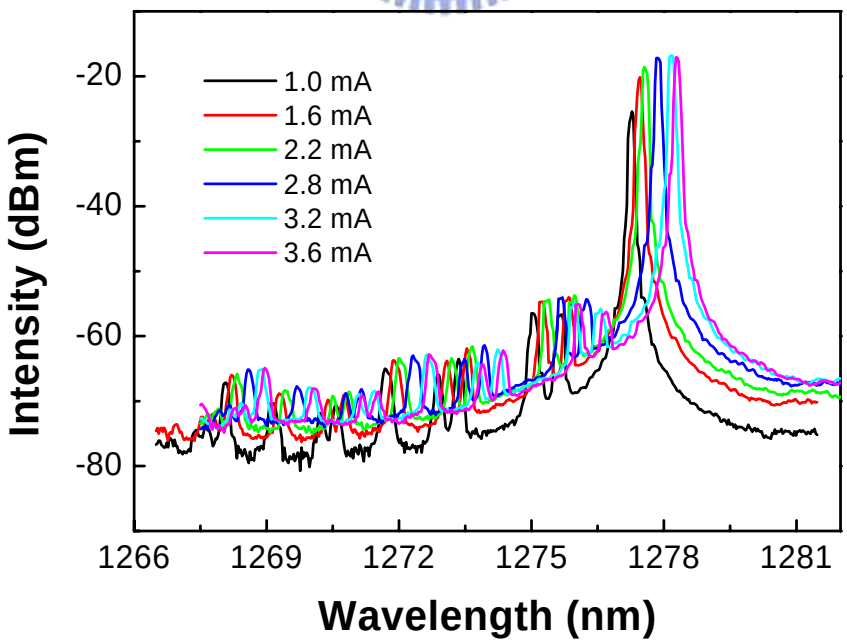

Fig 3.14 (b) Single mode CW lasing spectrum of QDs VCSELs under different

driving current.

Chapter 4: Molecular Beam Epitaxy Growth of InGaAs(N)(Sb) alloys

In this chapter, molecular beam epitaxy (MBE) growth of GaInNAsSb and its alloys is discussed. By MBE growth technologies and techniques were chosen for the highest quality and most flexible growth. Growth techniques used to optimize the growth condition of GaNAs bulk and InGaAsN(Sb)/GaAs quantum well such as RF plasma parameters, growth temperature and post thermal annealing proceed. To avoid the phase separation during growth of GaAsN related alloys; low substrate growth temperature was considering. Since the growth of GaNAs is different than other traditional III-V semiconductors, the series of growths we used to calibrate and optimize the nitride arsenide alloy will also be presented.

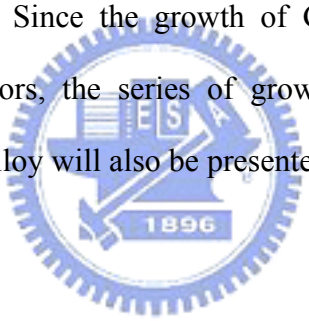

4.1 Nitrogen RF plasma

There are many approaches to deposit nitrogen by MBE, the highest quality material grown thus has been using an RF plasma source. The nitrogen RF plasma source MBE (RFMBE) has proved to be a state-of-the-art method for the epitaxial growth of III-nitride quantum well heterostructures provided that high quality epi layers are available. The gas plasma is an effective tool for conversion of highly stable source gases such as N_2 to more active atomic and molecular species suitable for MBE growth. There are many different parameters which can control the plasma such as the forward RF power, reflected RF power, injected N flow rate, mixed As/N materials, ion deflection plate and the size, holes of the aperture in the front plate. In our study, we design a separation pumping system in order to improve the batter

material quality of nitrogen based thin films. Figure 4.1 shows the schematic of the nitrogen plasma system. The design of exit holes minimizes ion content in the beam, while the active neutral species are directed toward the substrate as shown in Fig 4.2.

Dilute nitride GaAsN, InGaAsN are relatively new compounds in the III-V semiconductor and RF plasma was often used to grow the high growth rate GaN. The normal growth rate of GaN epitaxy was around 1~2μm/hr, in order to obtain the low growth rate for the diluted nitrogen we used the few numbers of holds and reduce the power and N flow rate. For optimized growth condition of the RF plasma with the GaAsN and InGaAsN compound will be discussed in the fellow sections.

The unique properties of III-nitride semiconductors make them suitable for a broad range of applications in electronics, optoelectronics and sensing. They can be used for optoelectronic devices from UV to IR wavelengths, solid-state lighting, high power high frequency transistors, high temperature electronics, radiation hard and space electronics, as well as a wide range of sensors.

4.2 Nitrogen`s effect on the bandgap of GaAs

By adding nitrogen to GaAs the band gap doesn't follow a linear dependence between the binary compounds as the Vegards law .There is an extremely large bandgap bowing towards lower energies [1], as shown in Fig 4.3. Actully the bandgap drops sharper in dilute nitride regime than by adding indium into the GaAs material. There were a lot of theories explaining for this bandgap bowing. One theory states that nitrogen instead of alloying with GaAs contributes an impurity-like level to the band structure of GaAs similar to a dopant level. However, it is not like the typical dopant, nitrogen doesn't provide charge since it is isoelectronic with the crystal. In this theory the N level exists about the conduction band not lying within the bandgap

of GaAs. It is strong interaction between conduction band and narrow resonant band formed by nitrogen states [1-9]. They are another theory has been suggested that bandgap bowing effect. The nitrogen distorts the GaAs lattice cause the indirect L valley in the band structure of GaAs mixed causing the conduction band lower[9-14] are proposed in this theory.

Both theories predict the correct behavior of bandgap effect when Nitrogen into GaAs, in the experiments observed N resonant level closed in energy to the L vally in GaAs. No matter what kind of theory we believe, they predicted the effect of GaAs bandgap will remain the same.

4.3 RF plasma optimization on GaAsN material

The most outstanding results for edge emitting lasers were achieved by MBE growth of InGaAsN QWs using RF (radio-frequency) plasma nitrogen source [15-17]. So far the same team has presented the best characteristics of 1.3 μm VCSEL [18-20]. In the present work we have carefully optimized the operation of plasma source and the growth parameters of GaAsN layers. It`s important to obtain the growth window for adding the nitrogen material into the GaAs layer without degrading the PL quality. By studying of the effect of plasma condition on (In)GaAsN quality in order to understand the real effecting with nitrogen materials. Defects related to ion damage, the plasma source, probably the reason to explain the decreasing efficiency of the radiative recombination even in the case when nitrogen content is less than 1–2%. However, we have achieved highly efficient radiative recombination in GaAsN layers by optimizing operation conditions in the RF plasma nitrogen source, growth regimes, and post-growth annealing. UNI Bulb RF Plasma Source produced by Applied EPI was used to generate active species of nitrogen. Samples under investigation were

grown on N type (100) GaAs substrates. An GaAsN film was sandwiched between GaAs barrier layer and $Al_{0.3}GaAs$ cladding layer used for PL properties studies. We varied the growth temperature and growth rate of the GaAsN layer whereas substrate temperature of the rest of the structure was set at 600^0C. The crystal quality of the samples was evaluated by x-ray diffraction with incident beam in the [004] and [511] azimuths. RT-PL measurements were carried out using a doubled frequency YAG: Nd solid state laser and CCD and InGaAs spectrometer as shown in Fig 4.4.

The first set of GaAsN layers was grown at 470^0C using different aperture design. Thus, the quality of the layer is expected to be dependent on plasma composition, which can be affected by the aperture layout. Three apertures with different conductance (ø 200 μm, number of holes, $h = 25,\ 50,\ 66$) were used. Figure 4.5(a) shows the dependence of nitrogen content, y, in $GaAs_{1-y}N_y$ layers on plasma light intensity measured by a photodetector, V_{OPT}. In Figure 4.5(b) we showed the N content versus parameter C_{SOURCE}, which is definite as $h \times V_{OPT} / R_{GaAs}$, where R_{GaAs} was the growth rate. It is clearly seen that the dependence of y on C_{SOURCE} is linear. Thus, C_{SOURCE} is an universal parameter responsible for N content in the growing film.

Figure 4.6 shows the dependence of PL intensity of 0.2 μm-thick GaAsN layers on the PL peak energy and nitrogen composition. All samples were grown under the same growth conditions. N_2 flow rate was tuned to obtain the lowest RF power at a given plasma intensity. One can see that we can obtain the required nitrogen composition for any aperture. However, the optical quality of the samples is quite different. By using a 50-hole aperture allowed us to improve several orders the PL intensity of GaAsN layers. Since the better material quality was obtained with the

50-hole aperture of GaAsN bulk layer, all following growth experiments were been carried out by using the 50-hole aperture.

4.4 MBE growth conditions of GaAsN

We have investigated the effect of nitrogen incorporation mechanisms in dilute nitride GaAsN alloys grown by plasma-assisted molecular-beam epitaxy. In the traditional III-V systems, the band-gap energy is reduced as the nitrogen composition increases. For example, for 1% N added to GaAs, the band gap is reduced by 200 meV [21]. The resulting dilute nitride semiconductors are promising for a wide range of application in optical and electronic device such as long wavelength light emitters or lasers. For GaAsN alloys, the electron mobility and optical intensity decrease as the nitrogen incorporation increases.

Figure 4.7(a), and (b) show the optical properties of the nitrogen content and the crystal quality determine by double crystal x-ray rock curve. While the higher nitrogen incorporation, it shows the red shift of the wavelength and PL line-width broadening. For instance, the InGaAs alloy is common sense grown around 450^0C, growth temperatures in which affect the In sticking coefficient. Higher growth temperature can be easily produce better material quality. On the other hand in the dilute nitride GaAsN growth, a high growth temperature will degrade the material quality and rough the surface morphology. At high substrate temperatures, surface diffusion is fast and easily separated into two phases. The wafer grown at a high substrate temperature has very poor optical quality with almost no PL luminescence. Figure 4.8 shows a window for the substrate temperatures versus the optical quality and the material quality. There are two different surface morphologies demonstrate the rough surface growth at a too high temperature and mirror like surface is grown with low temperature as shown in Fig 4.9. As we know a low substrate temperatures can

prevent the nitrogen phase separation but it also damage the material due to impurity or non-radiatively centers incorporated. GaAsN growth is very different than other III-V compound alloys, and so it`s growth condition need to be optimized.

4.41 Effect of growth temperature and growth rate

It is found that the temperature independent of the sticking coefficient of nitrogen over the range of 400-530 ^{0}C and decreases at higher temperatures in our study. This fact is in agreement with other data and the predictions of thermodynamic calculations [22]. While the growth temperatures below 550 ^{0}C the 2x4 reconstruction of the pattern of reflection high-energy electron diffraction (RHEED) was observed both for GaAs and GaAsN. When the substrate temperature was more than 550 ^{0}C, a 3x3 RHEED pattern was clearly observed for the GaAsN growth. It was shown that such a RHEED pattern corresponds to the formation of N-rich surface [23]. A higher growth temperature can easily obtain better quality of the GaAsN layers, it was found to be strongly dependent on the growth rate. When the growth rate is lower than a certain value, the growth mode will change from two-dimensional to three-dimensional. There is a sharp degradation in optical and structural properties when this transition occurs. The value of minimum growth rate for obtaining a high PL intensity depends on the growth temperature. These data are presented in Figs 4.10(a), and (b),illustrating the growth temperature versus growth rate. The upper region corresponds to normal GaAs-like growth mode characterized by high PL intensity. The two bottom regions of lower growth rate correspond to the growth modes characteristic of a strong interaction between N atoms that leads to either formation of N-rich clusters or N segregation. There is some region of high “growth rate/growth temperature” that is free of the effects related to phase separation because in this

region the interaction between N atoms is suppressed. GaAsN layers grown in this growth window avoid the phase separation and show better optical properties.

4.42 Effect of annealing

It is well known that defects or non-radiative impurities related to low temperature growth, such as arsenic anti-site or interstitial defects, can be removed by post-growth annealing. We have investigated the effect by in situ annealing on our GaAsN layers in the growth chamber. The maximum increase in PL intensity for a given sample varied from 3 to 50 times depending on its initial quality in our study. The dependence of integrated PL intensity of the GaAsN and GaAs layers on different growth temperatures is shown in Fig 4.11. The solid line shows PL intensity of GaAs layers grown at 600 ^{0}C, which is considered to be an optimal growth temperature for GaAs. That PL intensity depends on growth temperature without Nitrogen content in the layers. The PL intensity of samples after annealing is shown as open circles. It is clearly seen that number of times we can improve PL intensity by annealing depends on the growth temperature rather than N presence in the layers. Samples grown at 520 ^{0}C and annealed for 1 hour at 750 ^{0}C under arsenic overpressure we can reach the same PL intensity as GaAs grown at 600 ^{0}C in Fig 4.11. However, samples growth at a lower temperature than 480^{0}C with a few percentage of nitrogen content or pure GaAs bulk could not achieved the same optical quality after thermal annealing. Compared to the GaAs growth at 600^{0}C, the optical intensity was 50% higher than the GaAsN growth it at 480^{0}C after thermal annealing. In this section, we studied the low temperature growth of the GaAsN material and the effect of in suit thermal annealing.

There are some universal parameters which connect plasma cell characteristics and growth rate with N composition in GaAsN layers. Plasma cell conductance affects the properties of structures grown. The quality of GaAsN layers is very

sensitive to the plasma source operation conditions and growth temperature and growth rate. Detailed optimization of these parameters and annealing regime allowed us to achieve very high optical quality GaAsN layers. It is possibility of avoiding the decrease in PL intensity of GaAsN layers with nitrogen content is demonstrated.

4.5 MBE growth of InGaAsN/GaAs quantum well

Molecular beam epitaxy (MBE) and Metal organic vapor deposition (MOCVD) are common methods to grow InGaAsN and GaAsN alloys [24-26]. In this section we are going to describe how to growth the InGaAsN quaternary alloys by solid source MBE. Adding the indium to the GaAsN is fairly straightforward. For the growth of InGaAsN QWs, indium is assumed to have unity sticking coefficient at the growth temperature and is not affected by the nitrogen incorporation. The nitrogen addition to GaAs is limited thermodynamically. In order to approach the longer wavelength, indium atom is added to the strain limit of the material. The thermodynamics and kinetics of the growth process are complex one and are still not fully understood for the semiconductor alloys. Based on the experiments of the growth GaAsN alloys, the sticking coefficient of indium is below at temperature 520^0C. The growth temperature of GaAsN is between 420^0C and 520^0C. In order to emit at 1.3μm, the InGaAsN material is predicted to be grown at around 420^0C or even lower to avoid phase separation. The growth conditions and parameters must follow the consequences.

(a) The MBE chamber must be very clean: In order to obtain high quality materials, because the growth at low temperature the impurities tend to more easily incorporated more easily in the material.

(b) The in-suit annealing technology needs to be study as a standard procedure: In order to avoid the phase separation, low temperature growth is used to obtain high

crystal quality and it need to be recovered the crystal quality through thermal annealing: samples are typically thermal treatment at 750^0C 30mins, we can modify the same annealing condition during growth of the $Al_{0.3}GaAs$ cladding layer at 700^0C in the laser devices.

More detailed parameters for growing the InGaAsN quantum well will be discussed in the following sections.

4.6 Improving the photoluminescence of InGaAsN quaternary alloy by thermal annealing

The influence of the thermal annealing on the PL properties of the InGaAsN samples is studied in this section. The PL system used for the room temperature PL measurement is shown in Fig 4.4. A solid state laser with a wavelength of 532nm was used as the excitation pumping source. Stand lock-in amplifier were used to improve the signal noise ratio. A deep level transmit spectrum (DLTS) measurement technology was used to identify the impurities level of samples as shown in Fig 4.12. Samples structure for the optical measurements consist of InGaAsN QWs and 60nm-thick GaAs barrier layers and covered by 30nm $Al_{0.3}GaAs$ carrier confinement layers as shown in Fig 4.13. The TEM images were used to give the further information about the effect of thermal annealing in InGaAsN/GaAs quantum well.

The wafer was cleaved into many pieces for the RTA annealing at different temperatures, for 5mins as shown in Fig 4.13(a), (b). Figure 4.13(a) shows that, after thermal annealing with an improvement, the PL peak intensity increases with increasing the annealing temperature ratio is more than one hundred time higher than the as grown samples. (b)The blue shifts of the emission wavelength depend on the

annealing temperature. The full width half maximum (FWHM) narrowed with increasing annealing temperature. It is quite clear that the material quality is improving with thermal annealing due to the reduction of non-radiative centers, and deep level defects as shown in the DLTS results in Fig 4.14.

Two samples were chosen for the TEM images study, one of them was thermal annealing at 750^0C for 5 mins another was without thermal annealing. The TEM studied can provided the information about the influence of thermal annealing on the structure properties of InGaAsN QWs. In Fig 4.15, TEM images indicate a change in the nitrogen and indium profiles in the quantum well after 750^0C thermal annealing. Many published paper were mention about the indium-profile becomes well define; the nitrogen diffusion out of the QW. Such a small model can explain the behaviors which we observed in the samples after thermal annealing in Fig 4.13(a). Comparing the TEM images and optical properties that indicted a blue shift of PL spectrum due to the potential energy fluctuation in the interface of the QW, which reduced after thermal annealing. The concentration of nitrogen is limited by the miscibility gap and indium composition which limited by the critical thickness. The blue-shift on thermal anneal increases difficult in obtaining the InGaAsN with a long wavelength.

4.7 Optimizing the photoluminescence of GaInAsN quantum well

The best long wavelength devices made with InGaAsN/GaAs active region still worse to compare with short InGaAs/GaAs devices. The growth process of deposition the nitrogen or inherent in the alloy or the material contains a high density of non-radiative recombination centers. Although many steps were taken in MBE growth and subsequent annealing to improve the material quality, here is still a long way to

go before high quality GaAsN layers can be obtain. The PL intensity greatly affected by post annealing procedure, the annealing temperature and times. It was found that growth conditions such as substrate temperature, growth rate, indium and nitrogen composition and thickness of quantum well also inference the material quality. Many factors were considered with regarding to improve PL intensity in our study, they are substrate temperature, plasma condition, growth rate, alloy composition, structure design, annealing procedure.

As we know the substrate temperature is the most important issue in the growth of quaternary InGaAsN/GaAs quantum wells. In Figure 4.16 shows the TEM images of InGaAsN/GaAs quantum well growth at different substrate temperatures. Low temperature growth was used for suppressing phase separation of indium and nitrogen atoms and smooth surface morphology. With the growth temperature is too low, the material incorporate too many un-removable defects or impurities which decrease PL intensity. The suitable growth temperature was the first key point to grow high quality quaternary InGaAsN/GaAs quantum wells.

Plasma conditions were optimized to improve PL efficiency. Accelerated species from the plasma, like ions, are well know to damage compound material and increase the defects density. In the present work we have carefully optimized both conductance and operation of nitrogen plasma source as well as growth parameters of InGaAsN layers. In order to stabilize the plasma conditions without affecting the conditions growth chamber, we install the plasma cell on a separate pumping system isolated the growth chamber by an HUV gate value. Incorporated an isolated value on the N source no only improved the nitrogen material uniformity but also reducing the negative effect on plasma ion damage. The proper plasma cell operation parameters of the plasma cell, such as RF power, aperture count, and N flow rate have an effect on the PL intensity. At this stage a limited range of RF power and nitrogen flow rate

were investigated with one suitable aperture (50 holes) in order to optimal the plasma with respect to the PL intensity.

The parameters for growing high quality InGaAsN/GaAs quantum well were obtained from the growth experiments of GaAsN and InGaAs materials. Growing the InGaAsN/GaAs quantum well, the total growth rate was an important parameters to be achieved. Three level growth rate were be used with keeping the same indium and nitrogen composition of the InGaAsN/GaAs QW. The optical characteristics in the total growth rate of 4.2A/s and 2.78A/s were the same. The PL intensity and the emission wavelength were the same. While the growth rate is below than 0.506 A/s, the pattern of reflection high energy electron diffraction turns to spotty and the growth proceeds through three-dimensional mode. The RT-PL in Fig 4.1 shows the optical properties of InGaAsN/GaAs QWs with high and low growth rates. Total Growth rate leads to steep decrease in luminescence efficiency of the grown layer. The minimum value of growth rate depends on nitrogen content and growth temperature. Defects caused by low temperature growth are removed by post-growth annealing. It showed that the impurity could be fully removed by thermal annealing demonstrated in the DLTS spectrum signal showing in Fig 4.18.

To achieve the long emitting wavelength, the ratio of indium and nitrogen concentration in the alloy material needs to vary. It is assumed that adding of nitrogen contributes most of defects, a higher indium to nitrogen content ratio is desired to be less defects in the QWs. The more strain in the QWs if there is higher indium to nitrogen ratio, the more dislocation density may be happened. This is a theory problem between In and N ratio if a long wavelength need to be achieved. A longest wavelength of 1.56μm can be achieved with poor PL intensity after post annealing as shown in Fig 4.18. While the nitrogen increase in the QW, the peak emission wavelength red-shifts but it drops the peak intensity at the same time. Comparing with

the peak intensity of InGaAsN/GaAs quantum well of 4.1% and 5.3% nitrogen content, the peak intensity of 5.3% nitrogen content was thirty times weaker than that of 4.1% nitrogen content. In order to push longer wavelengths, a strain compensating structure or a new alloy material needs to be developed. The structure of strain compensating design was considered with the GaAsN as the barrier layer between the InGaAsN/GaAs quantum well. The active region of the GaAsN /InGaAsN/GaAsN quantum well shows the more opportunity to shift the emission wavelength to 1.55μm without too much strain in the active region as show in Fig 4.19. The detailed growth conditions of GaAsN/InGaAsN/GaAsN quantum well were in Table 4.1. The peak intensity ratio was five times less than before. The reason of this behavior seems too much indium and Nitrogen in the quantum well, although it reduces the total stain in the active region by GaAsN strain compensation layer. Maybe the other solution for extending the longer wavelength is by Sb surfactant material.

4.8 The effect of Sb in InGaAs(N)(Sb) multiple quantum wells

Due to the limit of indium and nitrogen content in the InGaAsN/GaAs quantum well at wavelength beyond 1.3μm, the PL intensity decays generally and rapidly. The alloy system grown under unsuitable growth conditions, surfactants have been shown the improved incorporation and sticking of deposition species [27,28]. Recently, more and more research have been showing that antimony (Sb) can improve the threshold current density and the characteristic temperature in laser performance by it's surfactant effect in QWs[29,30]. In this section, the effecting of Sb was studied on InGaAs, InGaAsN multiple quantum wells grown by solid source molecular beam epitaxy (SSMBE). The structures of InGaAsSb/GaAs, InGaAsNSb/GaAs multiple quantum wells (MQWs) were investigated by room temperature photoluminescence (RT-PL) and high resolution X-ray rocking diffraction (HRXRD). The RT-PL intensity

significantly increased and narrowing line width by adding the dilute Sb on the highly strained InGaAs and InGaAsN MQWs compare with the Sb free growth samples. Our study elucidates the role of Sb as a surfactant effect in the growth of quaternary and pentanary alloys and reduce the impurity incorporation into the QWs during thermal annealing. In-suit Rheed pattern, RT-PL measurements and X-ray study clearly showed that the Sb acts keep the flat interfaces between the highly strained InGaAsSb, InGaAsNSb wells and GaAs barriers.

Our study elucidates the role of Sb as a surfactant effect in the growth of quaternary and pentanary alloy. Structures for this study were grown by Riber Epineat machine on N^{+}-GaAs (100) substrates. An As overpressure of 15 times group III flux has been chosen for the growth of the QWs. Thermal cracked cell of arsenic and antimony were used as the group V sources. A Sb valve cracked cell temperature was set at 470^{0}C with Sb beam flux as $1.8x10^{-8}$ torr measured by high vacuum gauge which corresponding to the Sb composition of 0.9% measurement by GaAsSb bulk. Radio-frequency (RF) plasma was used as the nitrogen radical source in the QWs. Five samples were grown with an active region consisting of 6nm InGaAs/GaAs or InGaAsN/GaAs triple quantum wells sandwiched between 60nm undoped GaAs waveguide layer three of them doped three levels of Sb content in the QWs [31]. A 30nm thick AlAs carrier confine layer inserted between the GaAs buffer and waveguide layer as shown in Fig 4.20. The growth temperature of the QWs, the GaAs waveguide layer and AlAs layers were set at 420^{0}C, 600^{0}C and 620^{0}C, respectively. Indium and nitrogen composition were estimated by pre-calibrated PL and X-ray diffraction as 38% and 1%, respectively. Fig 4.21 shows the structure properties of InGaAs/GaAs, InGaAs(Sb)/GaAs , InGaAsN/GaAs and InGaAsN(Sb)/GaAs highly strained MQWs by using HRXRD. The (004) diffraction pattern of a typical three period MQW is displayed. The observed sharp and well defined satellite peaks imply

a coherent periodicity of the QWs, suggesting the abrupt interfaces with Sb doping into the QWs. Figure 4.22 shows the PL spectrum of the as grown samples of InGaAs/GaAs and InGaAsSb QWs. The behavior of PL spectrum seems very similar with each other on two samples. Because of low temperature growth, the background impurities incorporating into the quantum well were clearly observed at 1eV emitting wavelength. Post annealing was applied to improve the material quality and reduce the nonradiative center in the QWs. Figure 4.22 shows the RT-PL spectrum of InGaAsSb/GaAs MQWs, it shows more than 30 times brightness than Sb free structures and narrowing the line width from 199nm to 73nm. The optical characteristics of InGaAs/GaAs quantum well were not improved after RTA thermal treatment as shown in Fig 4.23. The great improvement of optical characteristics indicated the Sb surfactant effect, shown in the Fig 4.24. A significant improvement of optical characteristics on the InGaAsSb/GaAs quantum well was observed after thermal treatment. This is quite interesting behavior of Sb incorporation into the InGaAs quantum well, which reduces the impurity level after thermal treatment. Thus, we suppose that the Sb materials not only provide the surfactant effects but also reduce the impurity incorporation in the quantum well during thermal treatment. In order to understand more details of this phenomenon, second ion mass spectrometer (SIMS) measurement will be applied.

Figure 4.25 shows the RT-PL spectrum of InGaAsN/GaAs and InGaAsNSb/GaAs MQWs with different Sb doping level after RTA annealing. The RT-PL intensity increased 4.7 times and narrowing line width from 71nm to 51nm comparing with Sb free structures. Three levels of Sb flux were used to find out the optimal doping window for the excellent optical quality. With increasing the Sb flux from 1.8×10^{-8} to 3.1×10^{-8} torr, RT-PL intensity maintains the same order. While the Sb fluxes increase to 6.02×10^{-8} torr, RT-PL intensity drops 3.3 times lower than others. The optimal Sb

beam flux was obtained in the InGaAsNSb QWs samples. The influence of Sb material doping in the InGaAsN MQWs has been proved to have improved the optical characteristics.

In summary, the highly strained InGaAs(Sb) and InGaAsN(Sb) MQWs structures were grown by SSMBE. The improvement of PL characteristics was obtained from InGaAsSb and InGaAsNSb structures. The X-ray investigation also clearly showed that the Sb acts to keep the flat interfaces between the highly strained InGaAsSb, InGaAsNSb wells and GaAs barriers. The addition Sb in the active layer is useful for the long wavelength laser.

Reference

[1] Y. Qui, S. A. Nikishin, H. Temkin, V. A. Elyukhin, and Y. A. Kudriavtsev, "Thermodynamic considerations in epitaxial growth of GaAsB1-xBNBxB solid solutions," *Appl. Phys. Lett.*, vol. 70, pp. 2831-2833, 1997.

[2] S. Wei and A. Zunger, "Giant and Composition-Dependent Optical Bowing Coefficient in GaAsN Alloys," *Phys. Rev. Lett.*, vol. 76, no. 4, pp. 664-667, Jan. 22, 1996.

[3] A. Mascarenhas and Y. Zhang, "Dilute nitride based III-V alloys for laser and solar cell applications," *Current Opinion in Solid State & Materials Science*, vol. 5, pp. 253-259, 2001.

[4] W. Orellana and A. C. Ferrax, "*Ab initio* study of substitutional nitrogen in GaAs," *Appl. Phys. Lett.*, vol. 78, no. 9, pp. 1231-1233, Feb. 26, 2001.

[5] J. D. Perkins, A. Mascarenhas, Y. Zhang, J. F. Geisz, D. J. Friedman, J. M. Olson, and S. R. Kurtz, "Nitrogen-Activated Transitions, Level Repulsion, and Band Gap Reduction in GaAsB1-xBNBxB with x<0.03," *Phys. Rev. Lett.*, vol. 82, no. 16, pp. 3312-3315, Apr. 19, 1999.

[6] W. Shan, W. Walukiewicz, J. W. Ager III, E. E. Haller, J. F. Geisz, D. J. Friedman, J. M. Olson, and S. R. Kurtz, "Band Anticrossing in GaInNAs Alloys," *Phys. Rev. Lett.*, vol. 82, no. 6, pp. 1221-1224, Feb. 9, 1999.

[7] Y. Zhang and W. Ge, "Behavior of nitrogen impurities in III-V semiconductors," *J. Lumin.*, vol. 85, pp. 247-260, 2000.

[8] Y. Zhang, A. Mascarenhas, H. P. Xin, and C. W. Tu, "Formation of an impurity band and its quantum confinement in heavily doped GaAs:N," *Phys. Rev. B*, vol. 61, no. 11, pp. 7479-7482, Mar. 15, 2000.

[9] Y. Zhang and A. Mascarenhas, "Isoelectronic impurity states in GaAs:N," *Phys. Rev. B*, vol. 61, no. 23, pp. 15562-15564, June 15, 2000.

[10] Y. Zhang, A. Mascarenhas, H. P. Xin, and C. W. Tu, "Scaling of band-gap reduction in heavily nitrogen doped GaAs," *Phys. Rev. B*, vol. 63, no. 161303-1, pp. 161303-4, 2001.

[11] Y. Zhang, A. Mascarenhas, J. F. Geisz, H. P. Xin, and C. W. Tu, "Discrete and continuous spectrum of nitrogen-induced bound states in heavily doped GaAsB1-xBNBxB," *Phys. Rev. B*, vol. 62, no. 085205-1, pp. 085205-8, 2001.

[12] H. M. Cheong, Y. Zhang, A. Mascarenhas, and J. F. Geisz, "Nitrogen-induced levels in GaAsB1-xBNBxB studied with resonant Raman scattering," *Phys. Rev. B*, vol. 61, no. 20, pp. 13687-13690, May 15, 2000.

[13] E. D. Jones, A. A. Allerman, S. R. Kurtz, N. A. Modine, K. K. Bajaj, S. T. Tozer, and X. Wei, "Photoluminescence-linewidth-derived reduced exciton mass for InByBGaB1-yBAsB1-xBNBxB alloys," *Phys. Rev. B*, vol. 62, no. 11, pp. 7144-7148, Sept. 15, 2000.

[14] M. Kozhevnikov, V. Narayanamurti, C. V. Reddy, H. P. Xin, C. W. Tu, A. Mascarenhas, and Y. Zhang, "Evolution of GaAsB1-xBNBxB conduction states and giant Au/GaAsB1-xBNBxB Schottky barrier reduction studied by ballistic electron emission spectroscopy," *Phys. Rev. B*, vol. 61, no. 12, pp. 7861-7863, Mar. 15, 2000.

[15] S. Sato, N.Nishiyama, T. Miyamoto, T. Takahashi, N. Jikutani, M. Arai, A. Matsutani, F. Kogayama, and K. Iga, ”Continuous wave operation of 1.26 μm GaInNAs/GaAs vertical-cavity surface-emitting lasers grown by metalorganic chemical vapour deposition,” *Electron. Lett.*, **36**(24), 2018, 2000.

[16] A. W. Jackson, R. L. Naone, M. J. Dalberth, J. M. Smith, K. J. Malone, D. W. Kisker, J. F. Klem, K. D. Choquette, D. K. Serkland, K. M. Geib, “OC-48 capable InGaAsN vertical cavity lasers,” *Electron. Lett.*, **37**(6), 355, 2001.

[17] G. Steinle, F. Mederer, M. Kicherer, R. Michalzik, G. Kristen. A. Yu. Egorov, H. Riechert, H. D. Wolf, K. J. Ebeling, “Data transmission up to 10 Gbit/s with 1.3 μm wavelength InGaAsN VCSELs,” *Electron. Lett.*, **37**(10), 632, 2001.

[18] B. Borchert, A. Yu. Egorov, S. Illek, M. Komainda, H. Riechert, “1.29 μm GaInNAs multiple quantum-well ridge-waveguide laser diodes with improved performance,” *Electron. Lett.*, **35**(25), 2204., 1999.

[19] T. Kitatani, K. Nakahara, M. Kondow, K. Uomi, and T. Tanara, “A 1.3-μm GaInNAs/GaAs Single-Quantum-Well Laser Diode with a High Characteristic Temperature over 200 K,” *Jpn. J. Appl. Phys.*, **39**(2A), L86 , 2000.

[20] M. Fischer, D. Gollub, M. Reinhard, A. Forchel, *13th International Conferences in Indium Phosphide and Related Materials*, Nara, Japan, 14-18, WA1-1, Conference Proceedings *pp*.101-104., May, 2001.

[21] V. A. Odnoblyudov, A. R. Kovsh, A. E. Zhukov, N. A. Maleev, E. S. Semenova, V. M. Ustinov, “Thermodynamic Analysis of the Growth of GaAsN Ternary Compounds by Molecular Beam Epitaxy,” *Semiconductors*, **35**(5), 533 .2001.

[22] R. J. Hauenstein, D. A. Collins, X. P. Cai, M. L. O’Steen, T. C. McGill, “Reflection high energy electron diffraction study of nitrogen plasma interactions with a GaAs (100) surface,” *Appl. Phys. Lett.*, **66**(21), 2861., 1995.

[23] A. R. Kovsh, J. S. Wang, L. Wei, R. S. Shiao, J. Y. Chi, B. V. Volovik, A. F. Tsatsul' nikov, and V. M. Ustinov "Molecular beam epitaxy growth of GaAsN layers with high luminescence efficiency" *J. Vac. Sci. Technol. B,* Vol.20, pp.1158-1162, 2002.

[24] A. Kaschner, T. Luttgert, H. Born, A. Hoffmann, A. Yu. Egorov, H. Riechert, “Recombination mechanisms in GaInNAs/GaAs multiple quantum wells,” *Appl.*

Phys. Lett., **78**(10), 1391, 2001.

[25] M. Kondow, K. Uomi, A. Niwa, T. Kitatani, S. Watahiki, and Y. Yazawa, "GaInNAs: A Novel Material for Long-Wavelength-Range Laser Diodes with Excellent High-Temperature Performance," *Jpn. J. Appl. Phys.*, **35**(2B), 1273 .1996.

[26] H. Riechert, A. Yu. Egorov, B. Bochert, S. Illek, *Compound Semiconductor*, **6**(5), 71 .2000

[27] X. Yang, J. B. Herous, M. J. Jurkovic and W. I. Wang, "High-temperature characteristics of 1.3 μm InGaAsN:Sb/GaAs multiple-quantum-well lasers grown by molecular-beam epitaxy," *Appl. Phys. Lett.*, Vol. 76, No 7, 795,.2000.

[28] Kerstin Volz, Vincent Gambin, Wonill Ha, Mark A.Wistey, Homan Yuen, Seth Bank, James S.Harris, "The role of Sb in the MBE growth of (GaIn)(NAsSb), " *Journal of Crystal Growth*, Vol. 251, 360, 2003.

[29]Takeo Kageyama, Tomoyuki Miyamoto, Masataka Ohta, Tetsuya Matsuura, Yasutaka Matsui and Fumio Koyama, "Sb surfactant effect on GaInAs/GaAs highly strained quantum well lasers emitting at 1200 nm range grown by molecular beam epitaxy," *Journal of Applied Physics*, Vol 96, No1 44 .2004.

[30] W. Li, J. B. Heroux and W. I. Wang, "InGaAsSbN: A dilute nitride compound for midinfrared optoelectronic devices," *Journal of Applied Physics*, Vol. 94, No.7, 4248, 2003.

[31] J. S. Wang, R. S. Hsiao, G. Lin, K. F. Lin, J. Y. Chi, J. F. Chen, H. C. Yu, and V. M. Ustinov, "Molecular-beam-epitaxy growth of high-quality InGaAsN/GaAs quantum well lasers emitting at 1.3 μ m," *Journal Vacuum Science Technology(B)*, Vol. 22, No6, 2663, 2004.

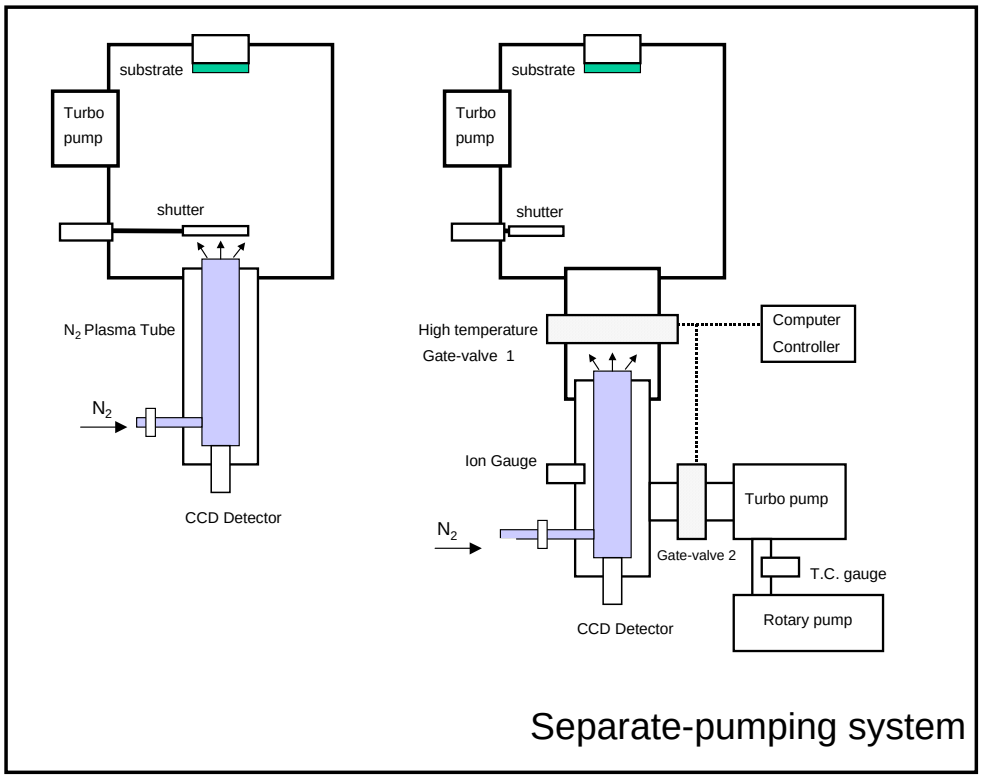

Fig 4.1 The schematic of the N-plasma system and N_2 gas injection system.

Fig 4.2 The front views of plasma source with mounted PBN plate.

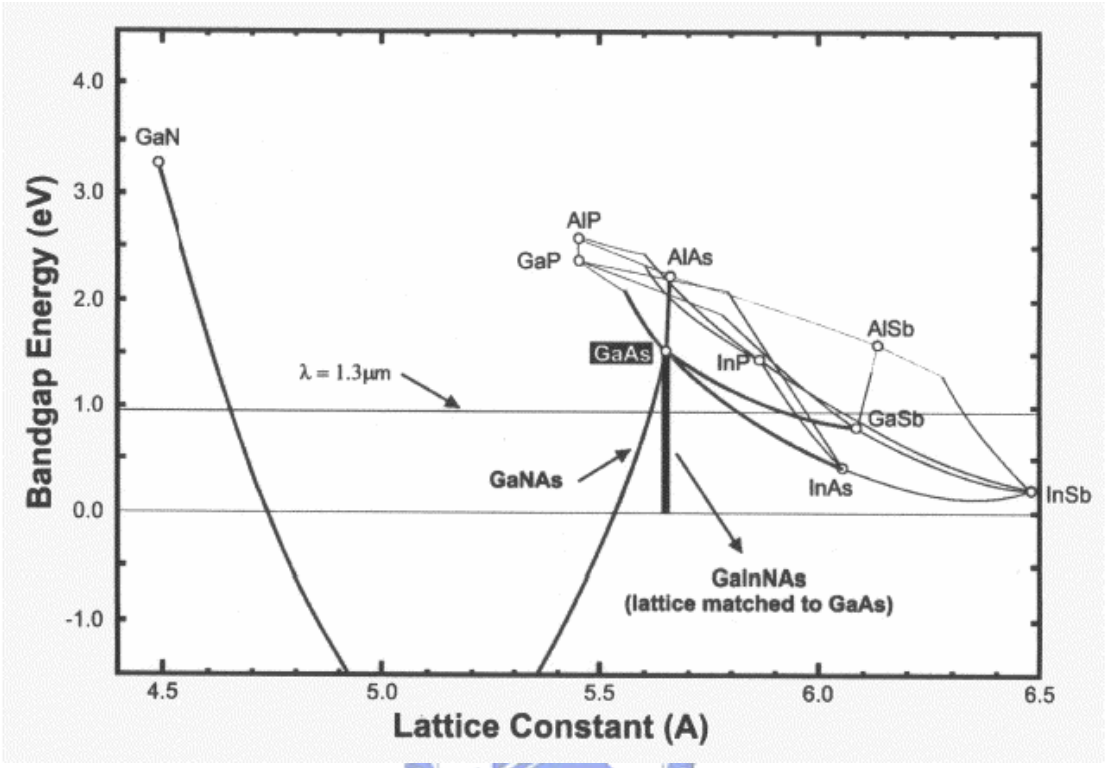

Fig 4.3 Bandgap versus lattice constant graph for III–V alloys showing lines of lattice match to GaAs for nitride–arsenide alloys and to InP for arsenide–phosphide alloys in the region applicable to long-wavelength fiber systems.

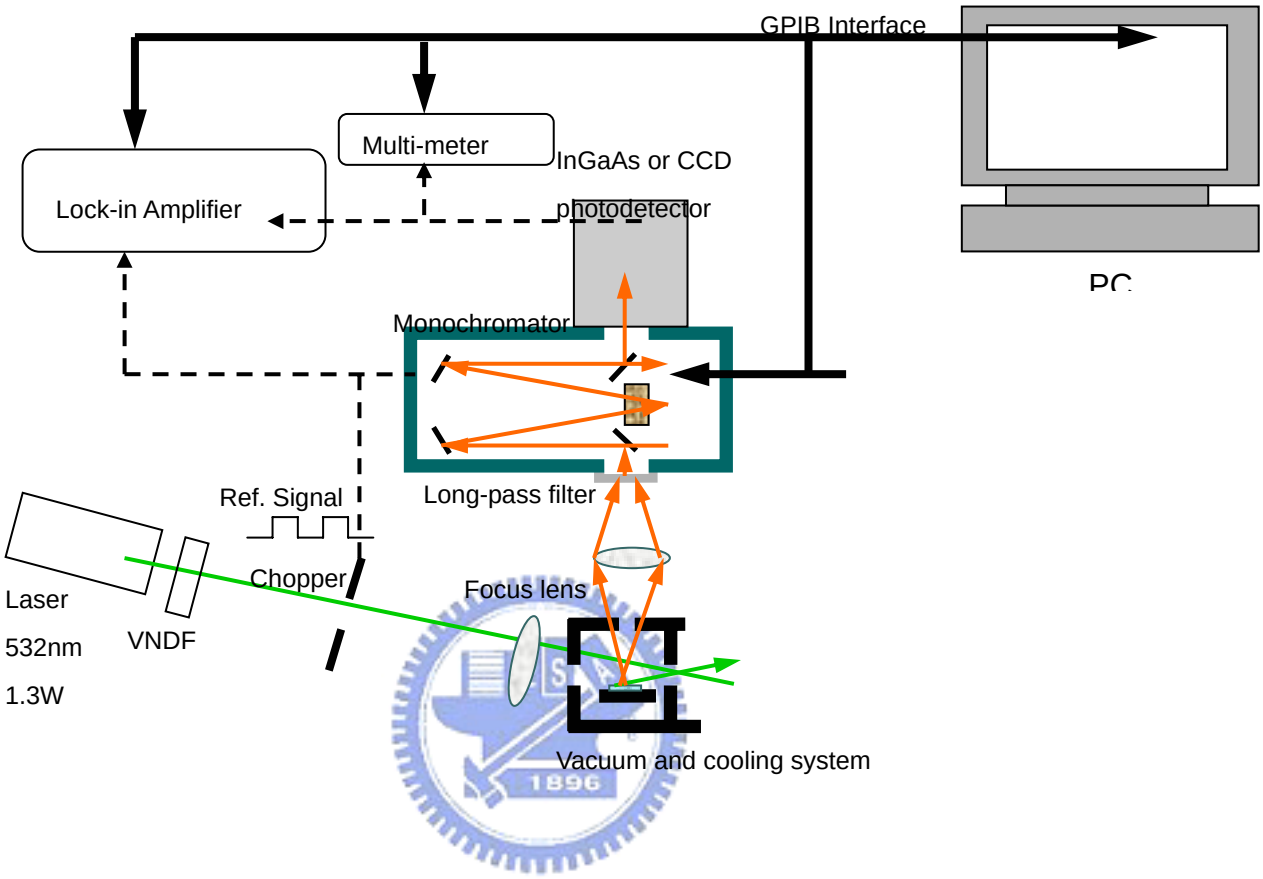

Fig 4.4 The Photoluminescence (PL) setup designed for the optical properties measurements.

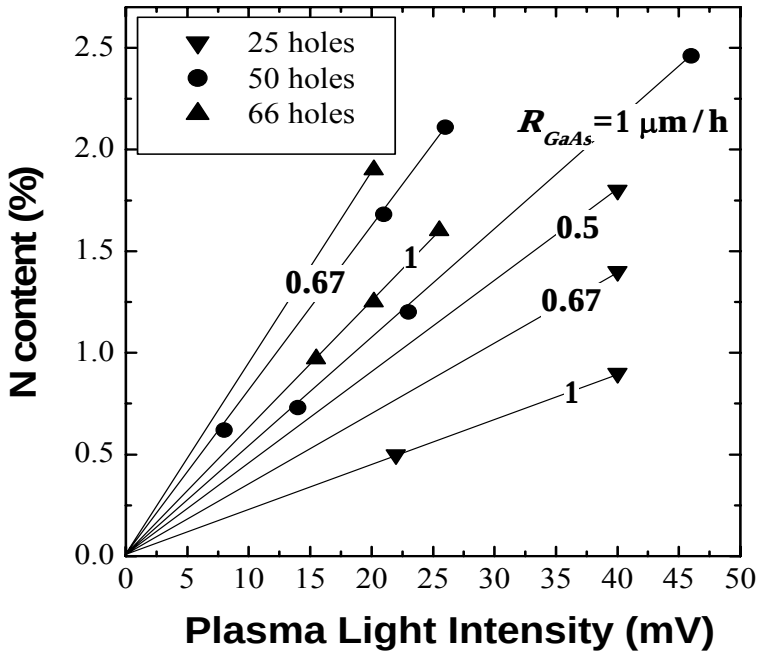

Fig 4.5 Dependence of N composition of GaAsN layers on plasma condition **(a)** plasma light intensity at different GaAs growth rates and different aperture layouts. Growth rates are shown as numbers on corresponding curve.

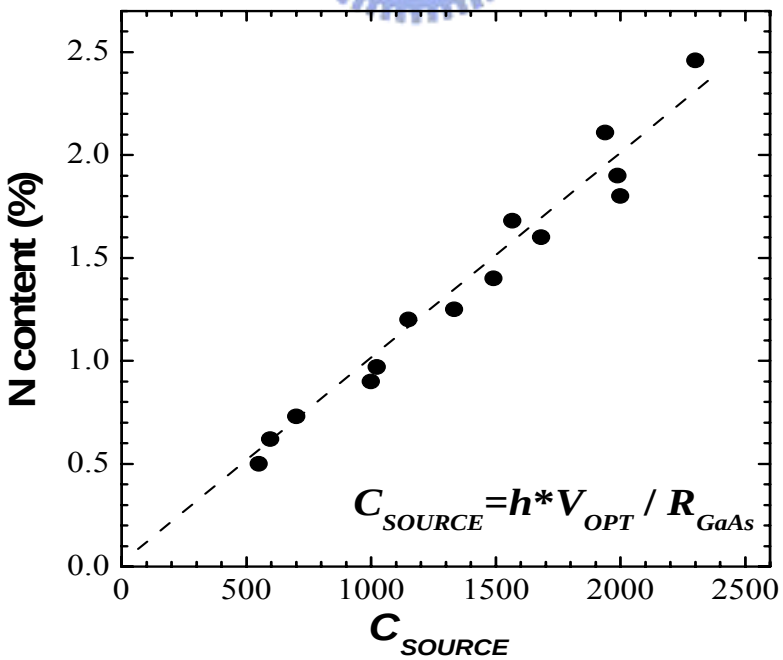

Fig 4.5 (b) N content vs parameter C_{SOURCE}

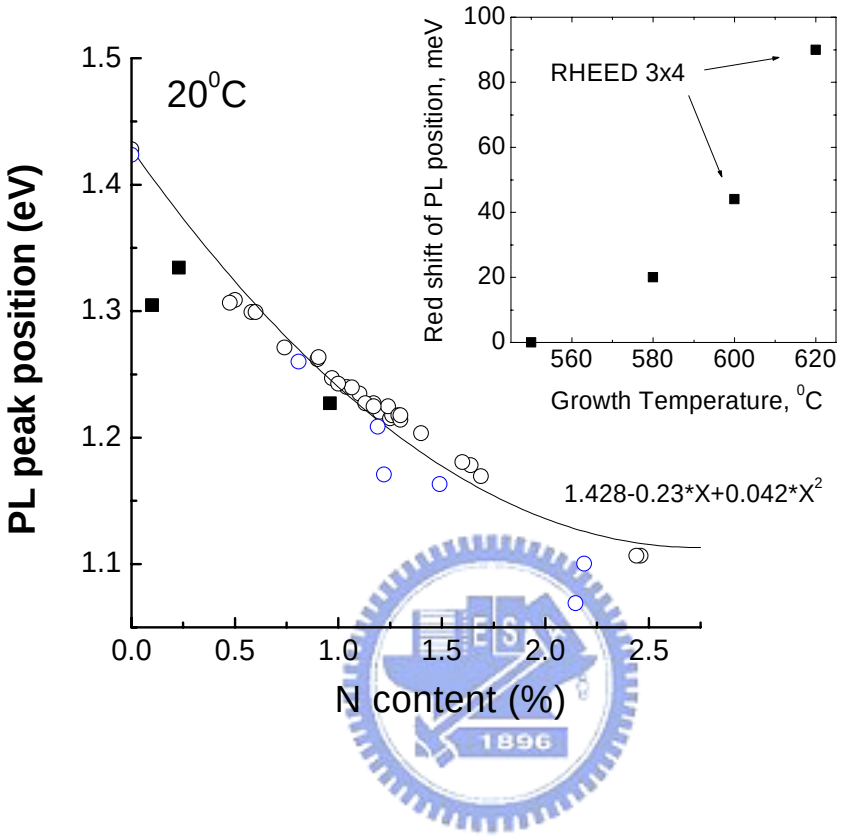

Fig 4.6 Dependence of RT-PL position on nitrogen content, with 0.2 μm-thick GaAsN layers. Insert shows the substrate temperature dependence on the emission wavelength red shift.

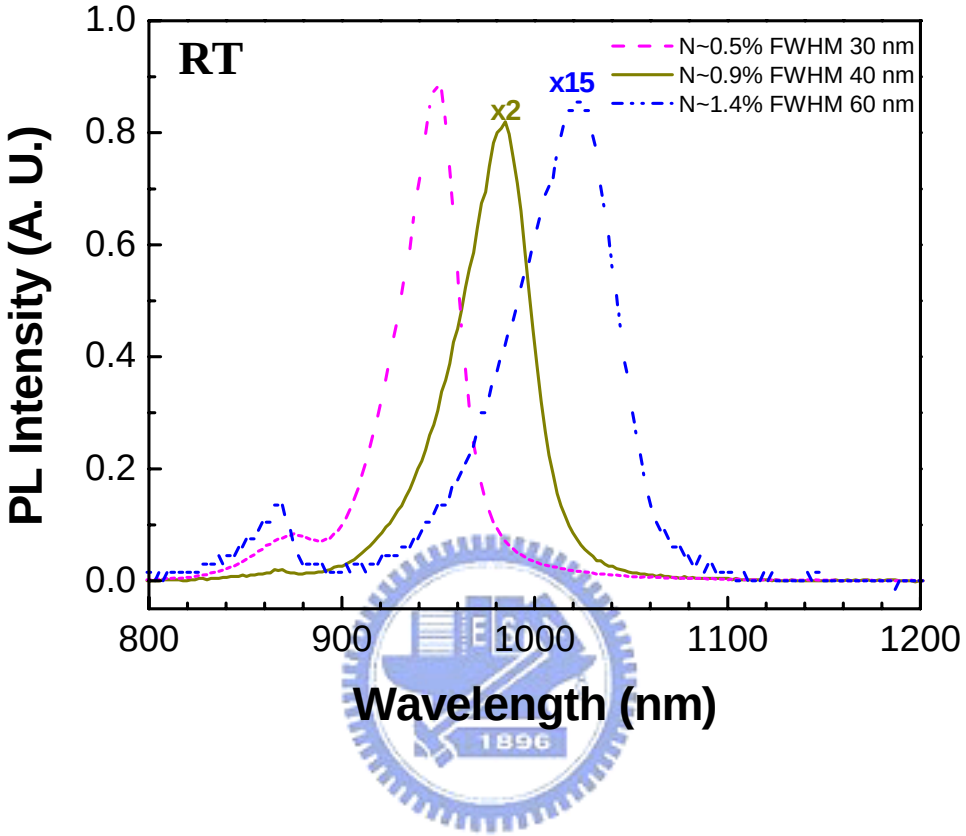

Fig 4.7 (a) The RT-PL emission wavelength and PL intensity of GaAsN bulk material dependence on the nitrogen composition.

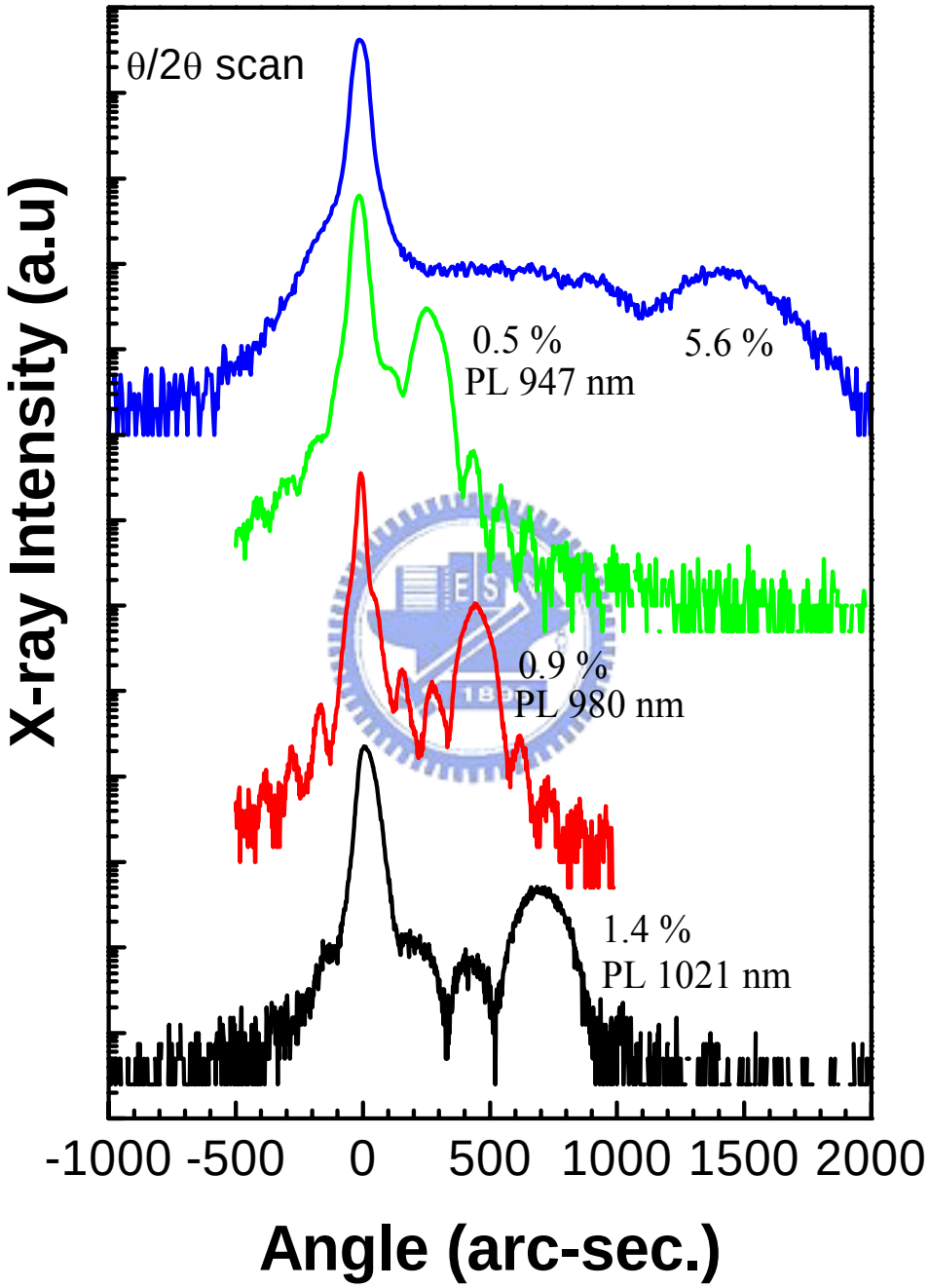

Fig 4.7 (b) Plot of XRD spectra and the corresponding PL emission wavelength of the GaAsN bulk material with nitrogen content of 0.5%,0.9%,1.4% and 5.6%.

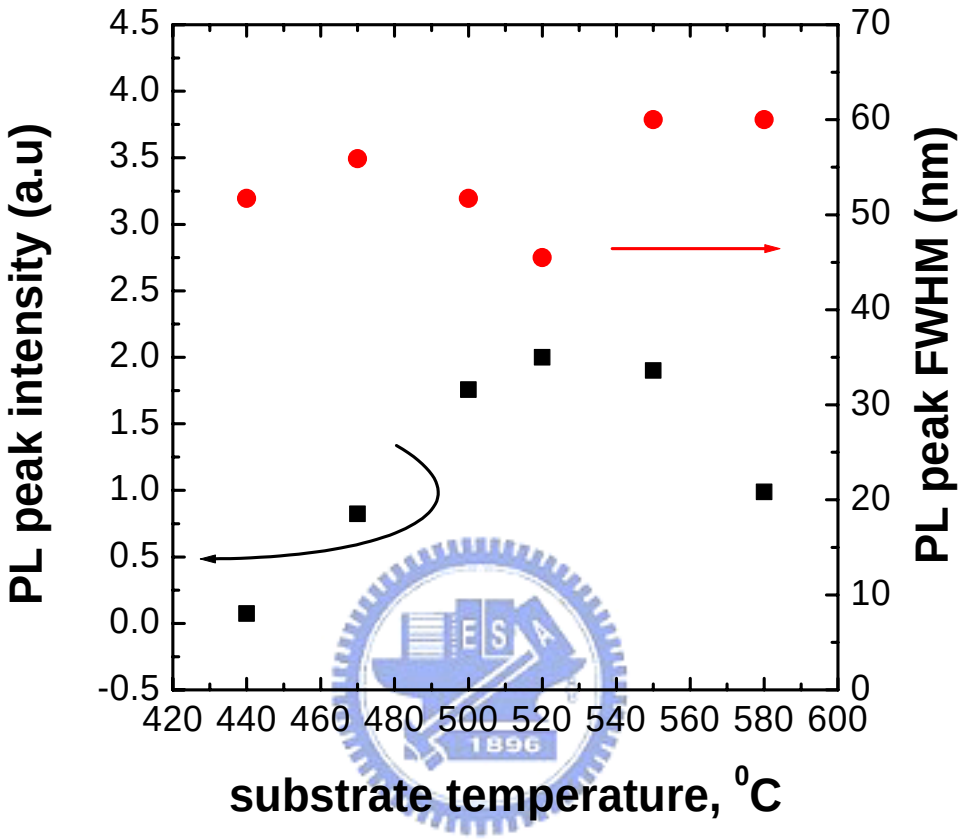

Fig 4.8 PL peak intensity and peak FWHM versus substrate temperature of the grown GaAsN layer. A window between the growth substrate temperatures with optical quality affects the material quality.

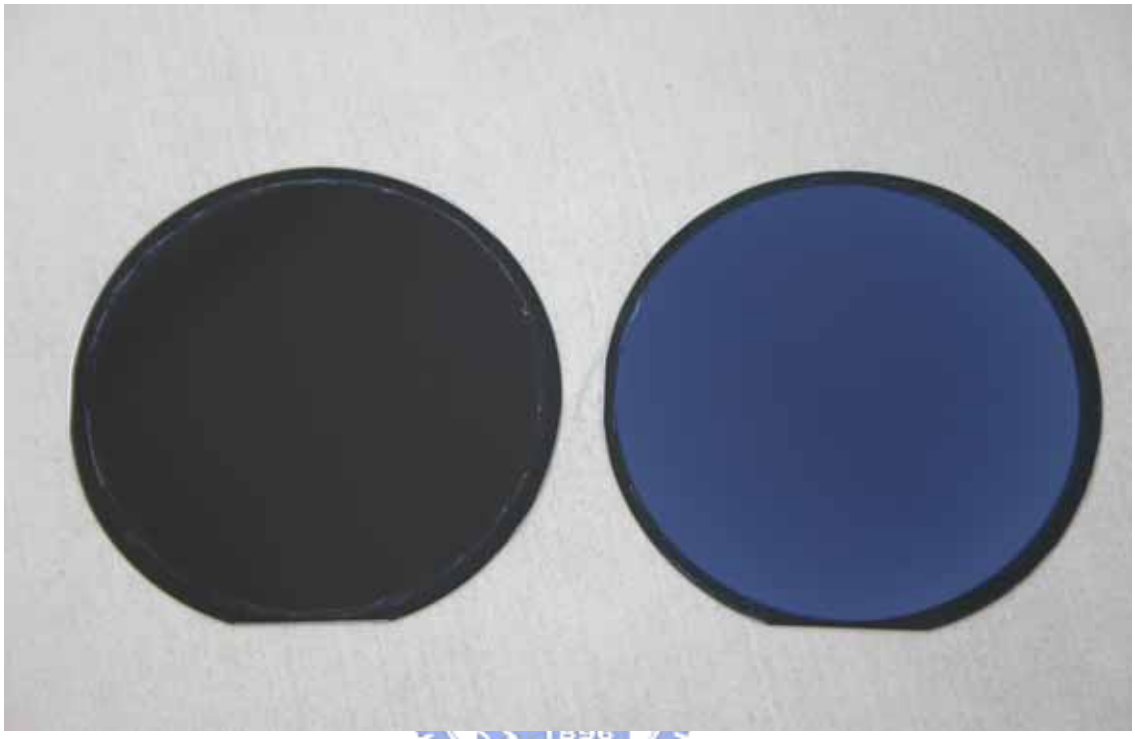

Fig 4.9 Photograph of wafers with GaAsN bulk material deposited on GaAs substrate. The wafer on the right side was grown with too high substrate temperature, the wafer on the left side was grown in the correct region temperature.

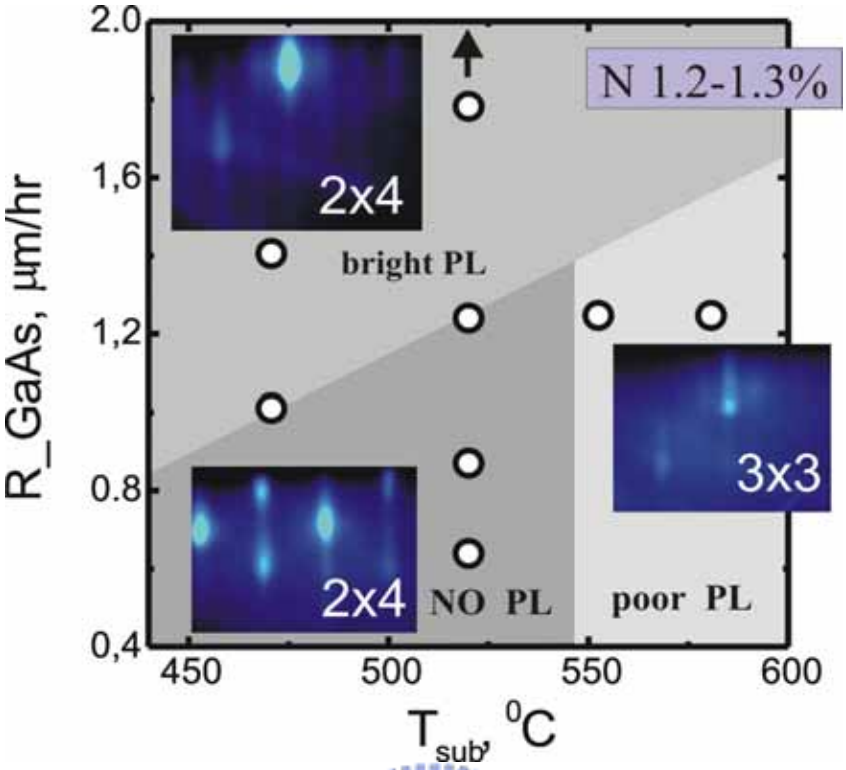

Fig 4.10 (a) RHEED images of GaAsN thin film, grown with too high and suitable temperature.

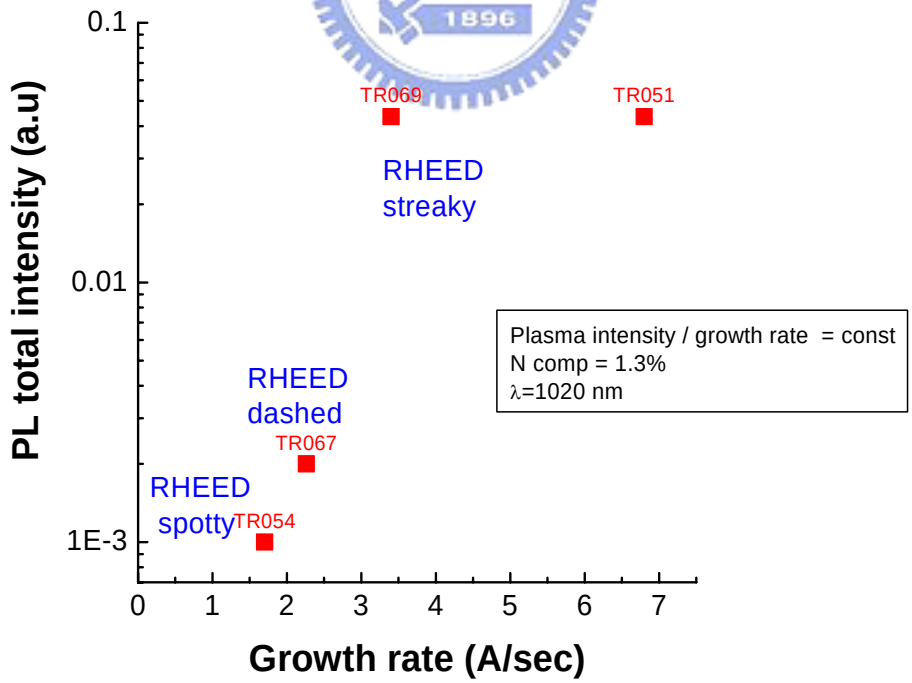

Fig 4.10 (b) Dependence of Growth rate and PL intensity. Plasma condition was kept constant for all samples.

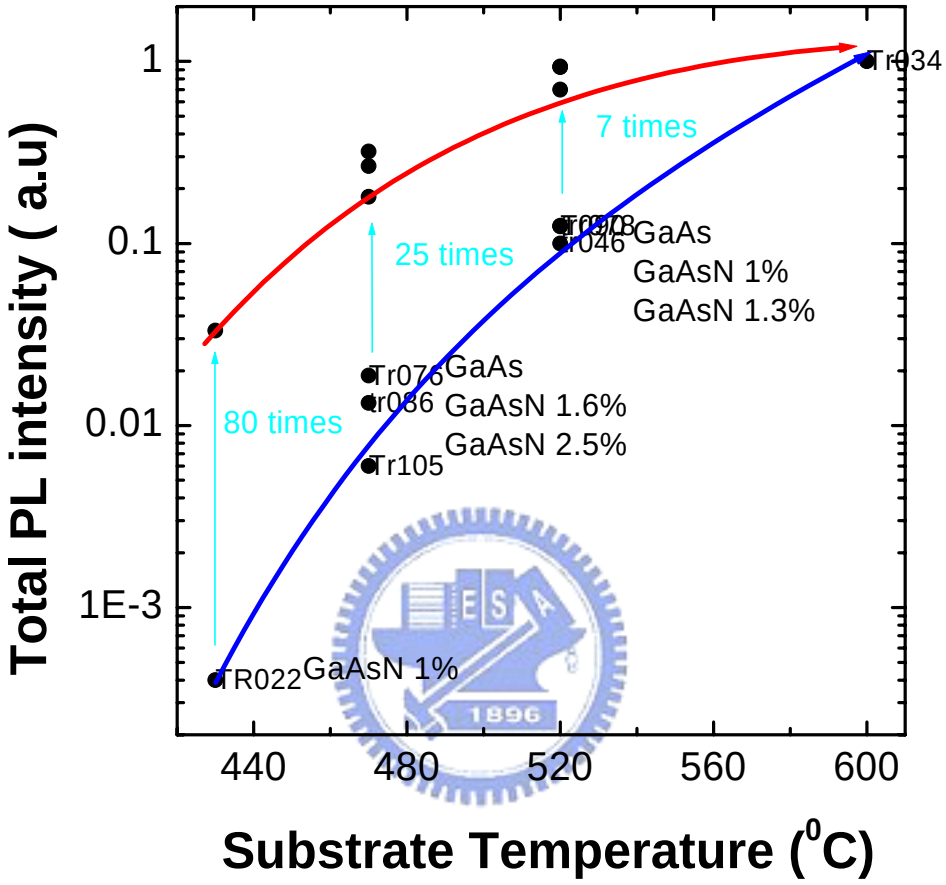

Fig 4.11 Dependence of integrated PL intensity of the GaAsN and GaAs layers on the growth temperature.

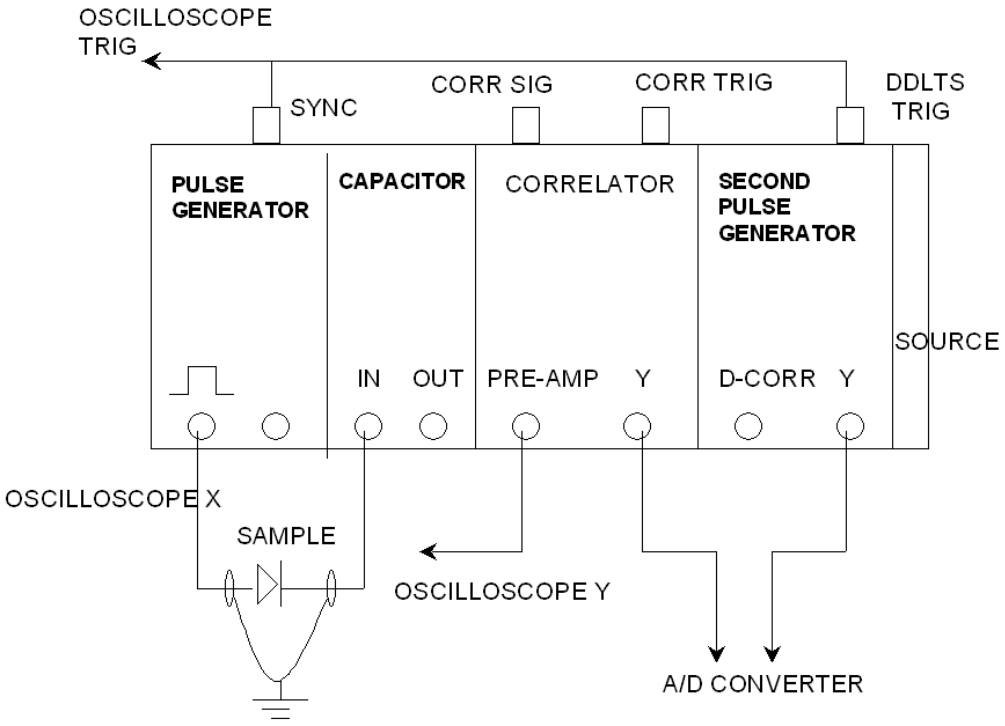

Fig 4.12 (a) Schematic diagram of DLTS and CV electrical measurement.

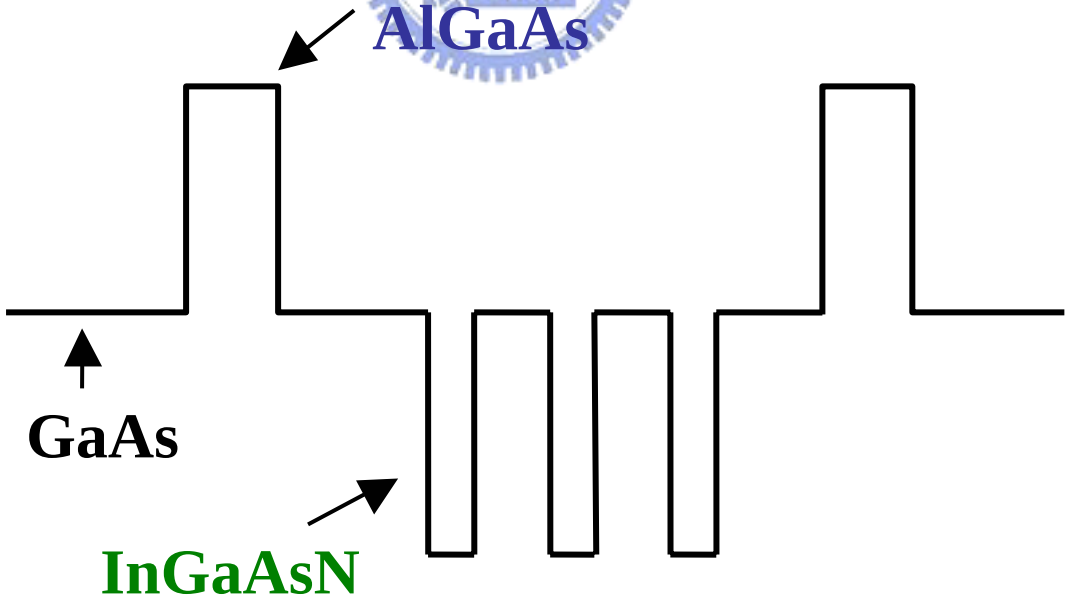

Fig 4.12 (b) Schematic of MBE growth structure for optical measurements.

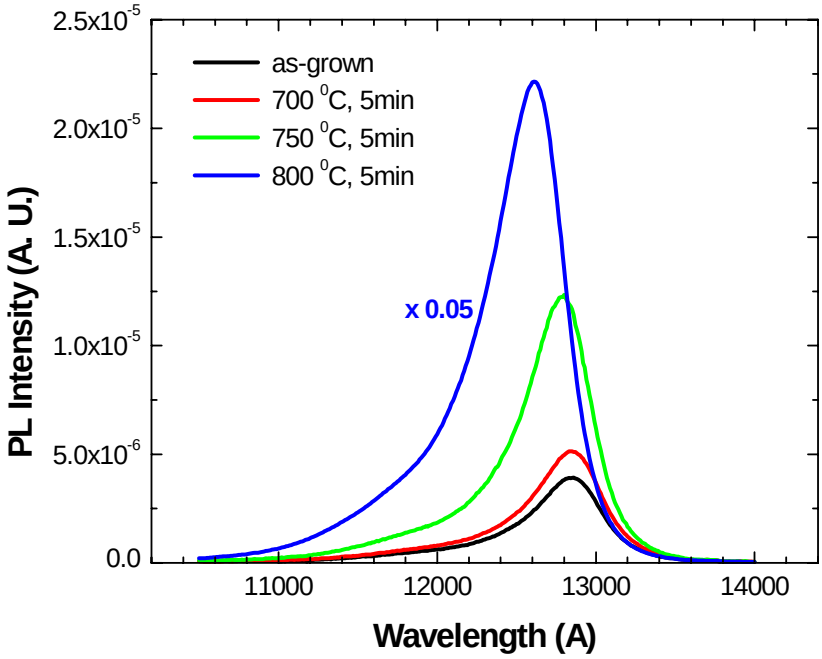

Fig 4.13 (a) Dependence of PL intensity on the annealing temperature

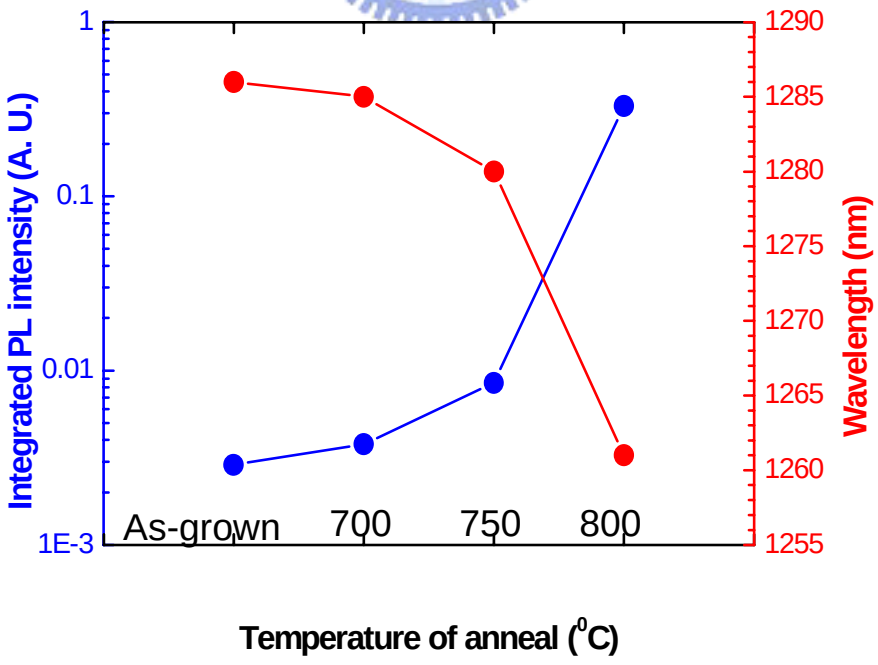

Fig 4.13 (b) The emission wavelength dependence on the annealing temperature

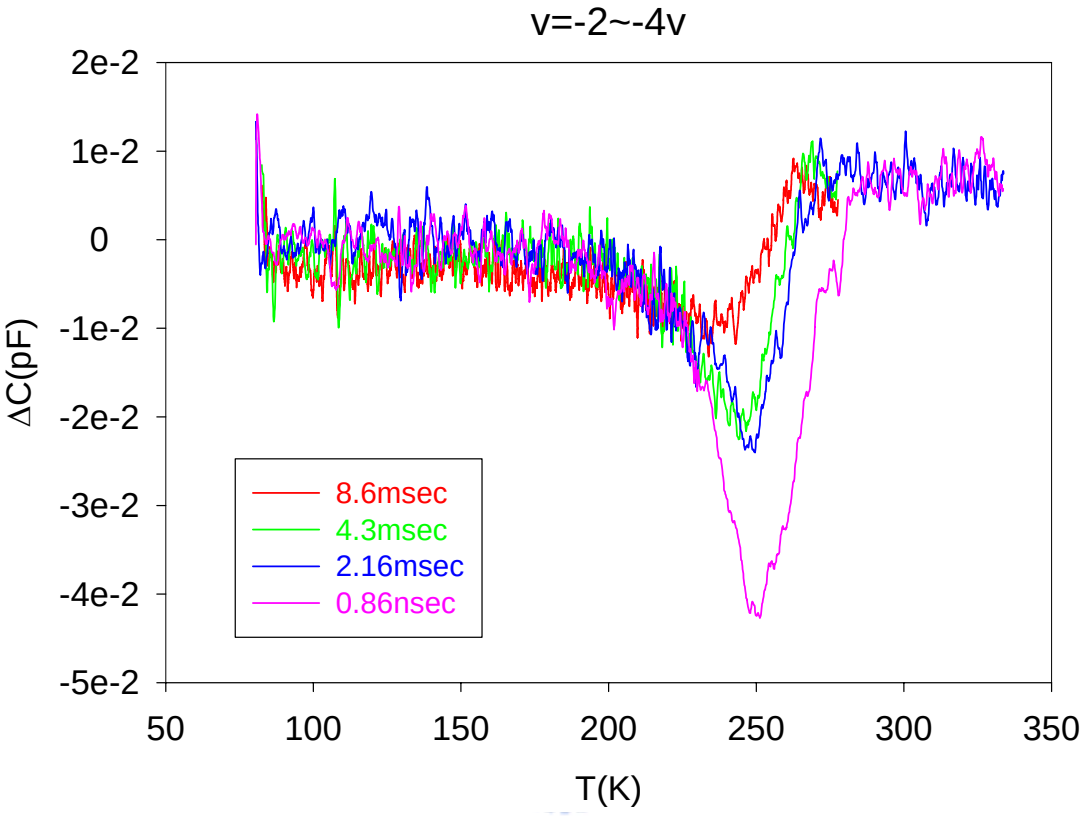

Fig 4.14 The DLTS spectra of as-grown InGaAsN/GaAs quantum well.

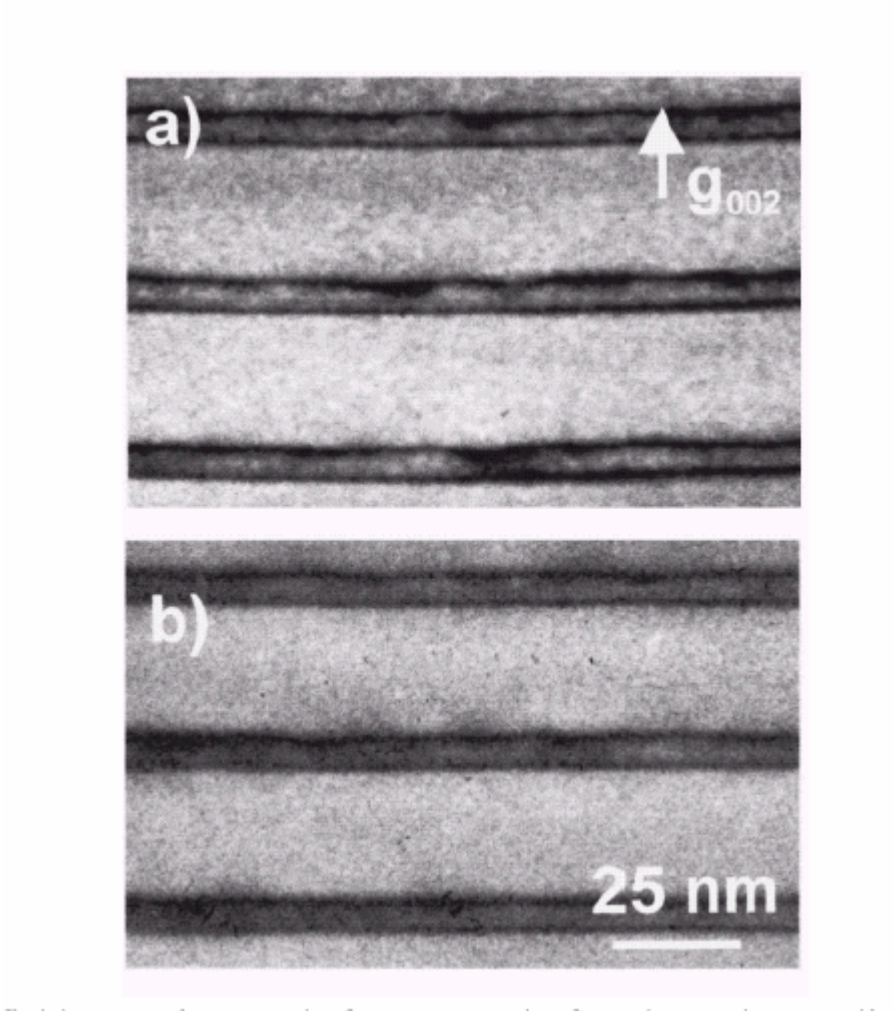

Fig 4.15 The TEM images of InGaAsN/GaAs quantum well with as grown and at 750^0C after 30 mins thermal treatment. Dark-field TEM-images before **(a)** and after thermal annealing **(b)**, which show contrast-fluctuations of a length-scale.

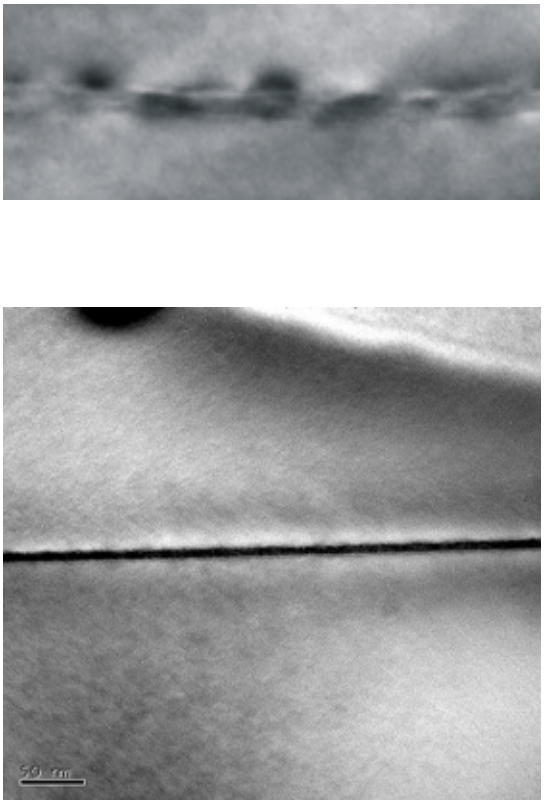

Fig 4.16 TEM images of InGaAsN/GaAs quantum well grown at substrate temperature of 450^0C and 420^0C.

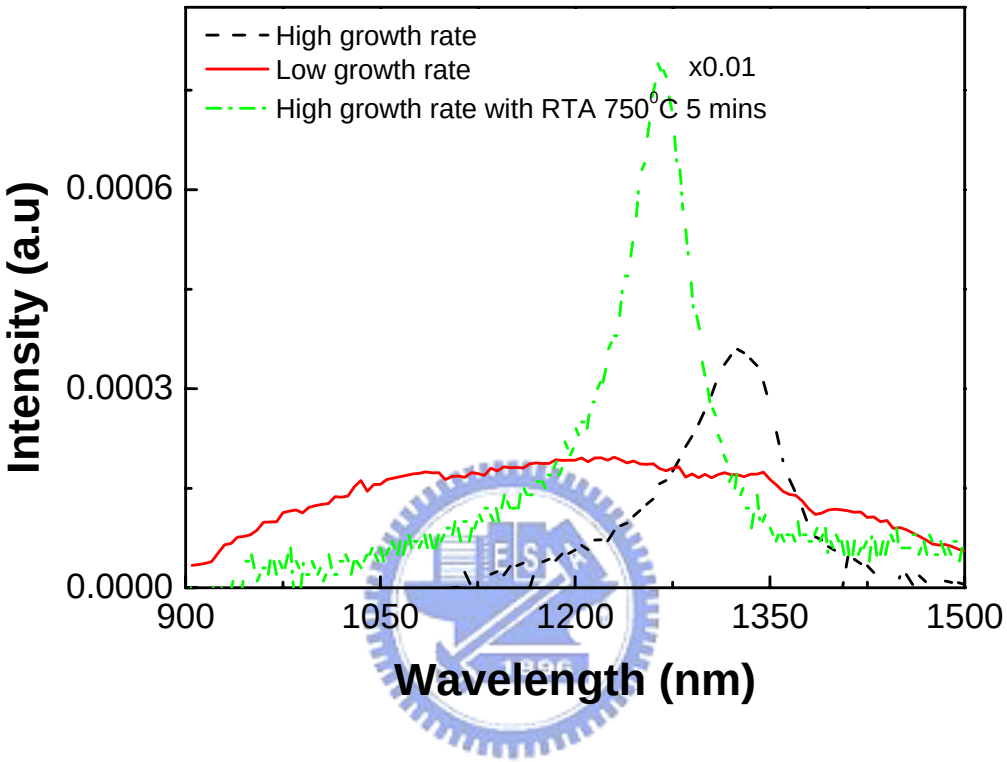

Fig 4.17 RT-PL spectra of InGaAsN/GaAs QWs grown at high and low growth rates.

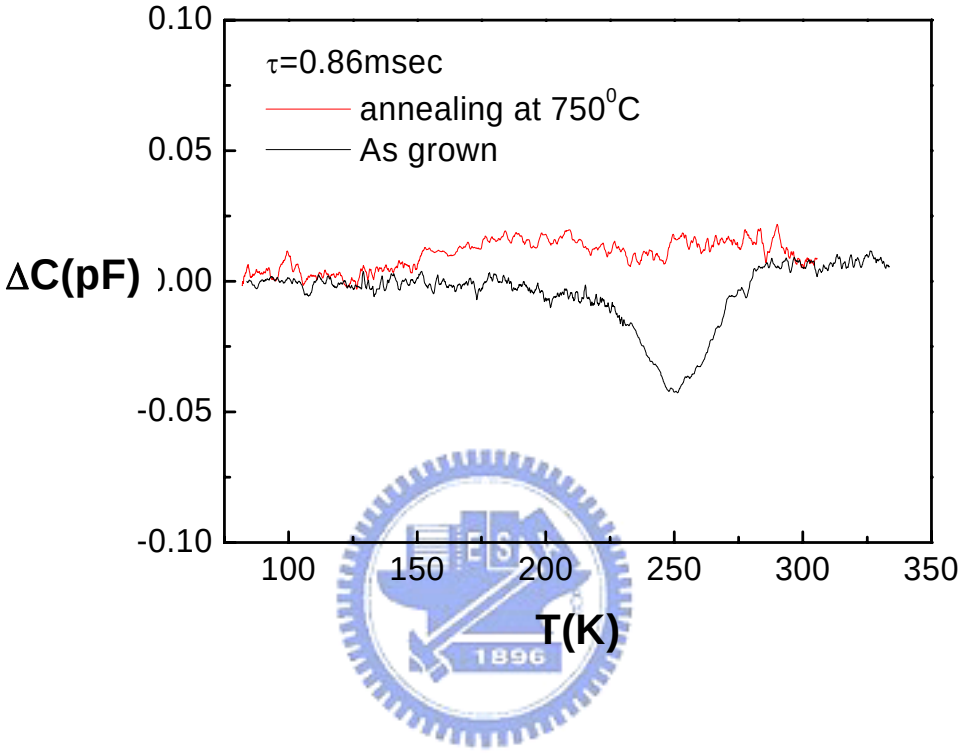

Fig 4.18 DLTS spectra present the impurities level of as grown sample of InGaAsN/GaAs QWs and after 750^0C 10mins thermal annealing.

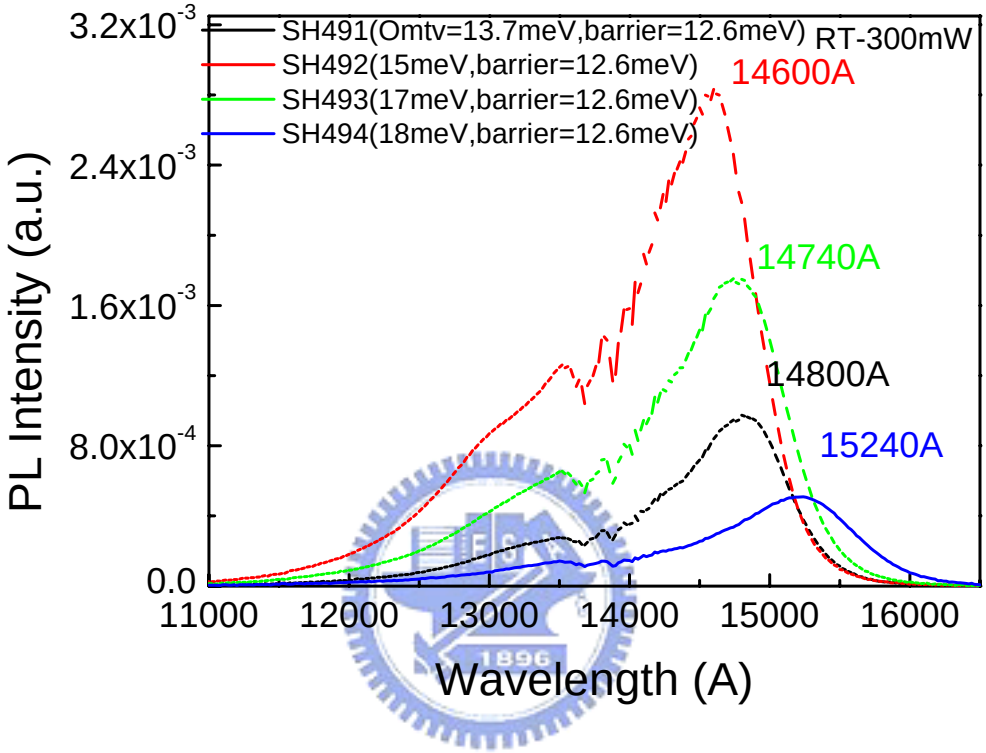

Fig 4.19 The RT-PL spectra of GaAsN/InGaAsN/GaAsN QWs with GaAsN strain-compensation layer.

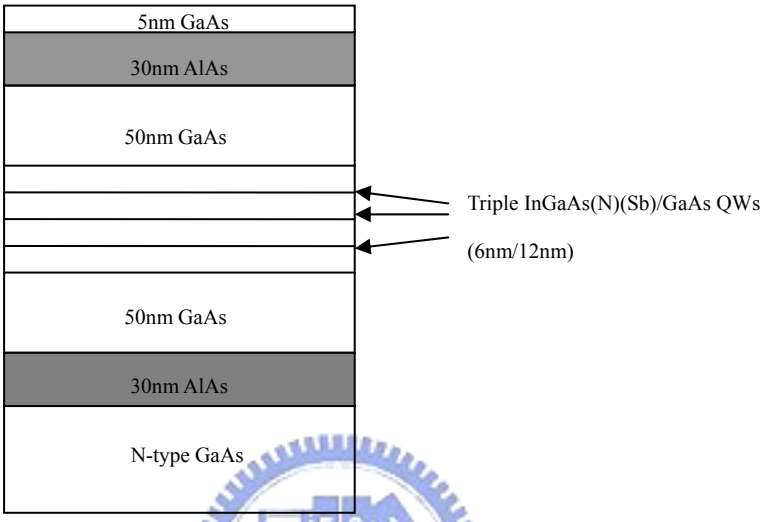

Fig 4.20 The schematic structure of PL measured sample with InGaAsN(sb)/GaAs QW

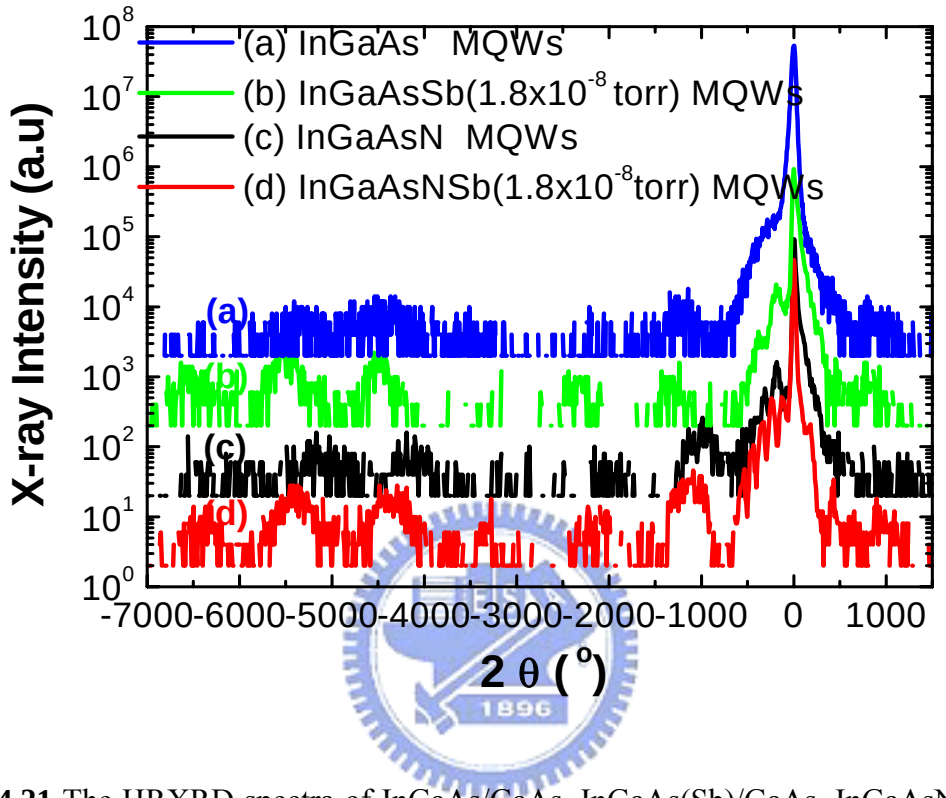

Fig 4.21 The HRXRD spectra of InGaAs/GaAs, InGaAs(Sb)/GaAs, InGaAsN/ GaAs and InGaAsN(Sb)/GaAs highly strained MQWs.

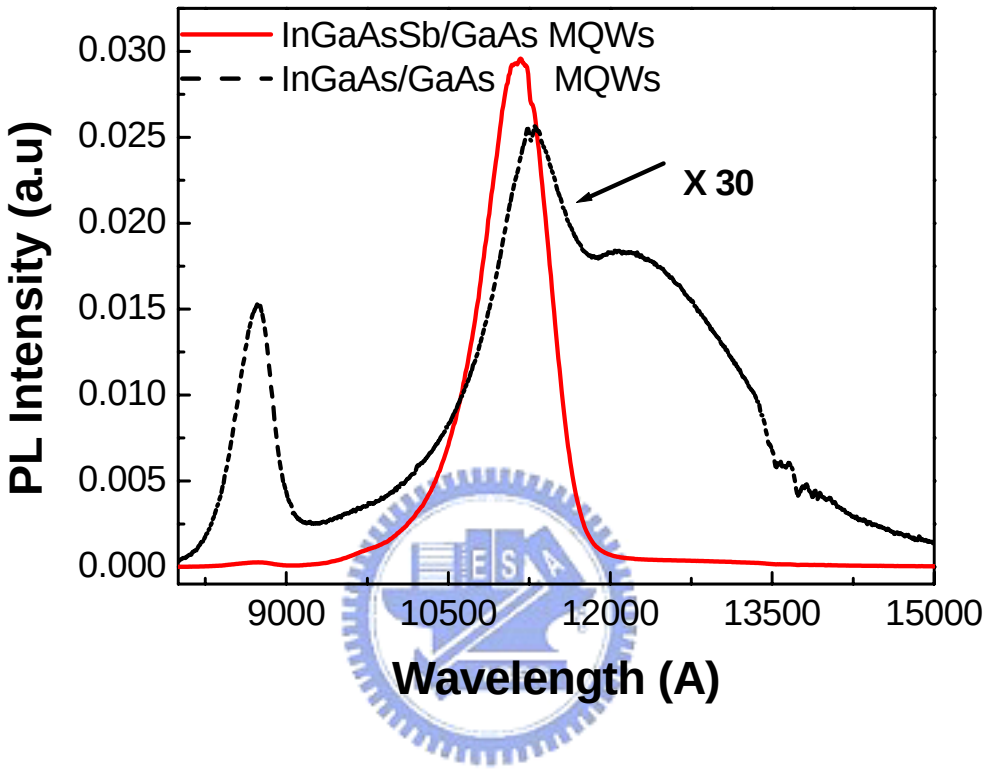

Fig 4.22 The PL spectra of the as grown samples with InGaAs/GaAs and InGaAsSb QWs active region.

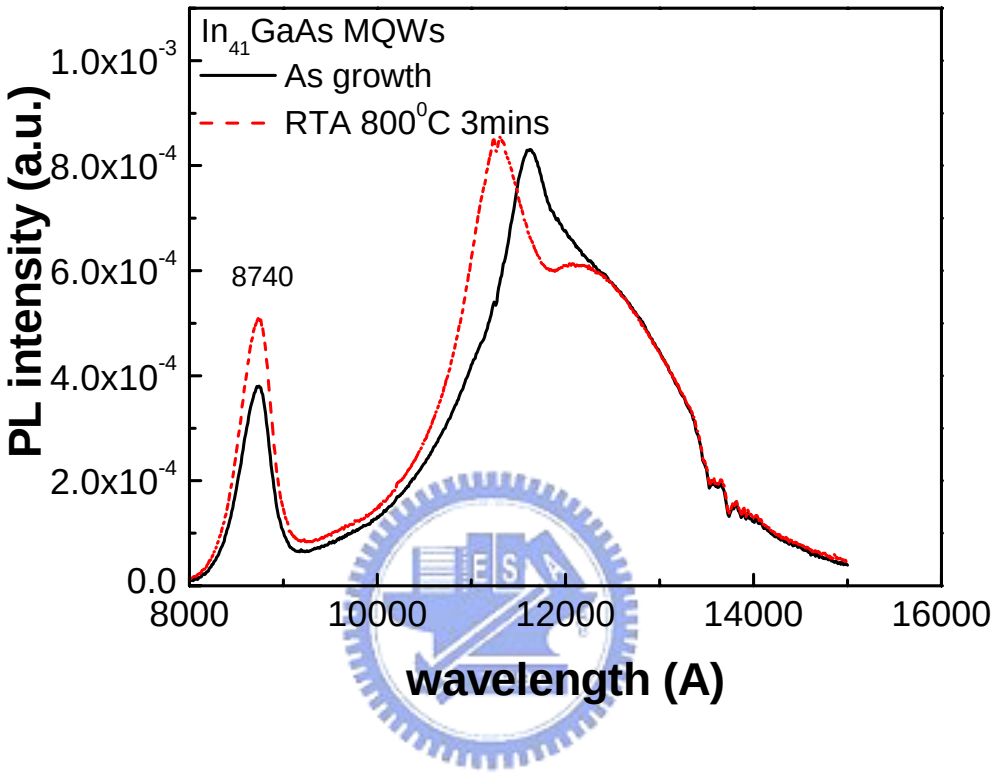

Fig 4.23 RT-PL spectra of as grown and InGaAs/GaAs MQWs of RTA treatment at 800^0C 3 mins.

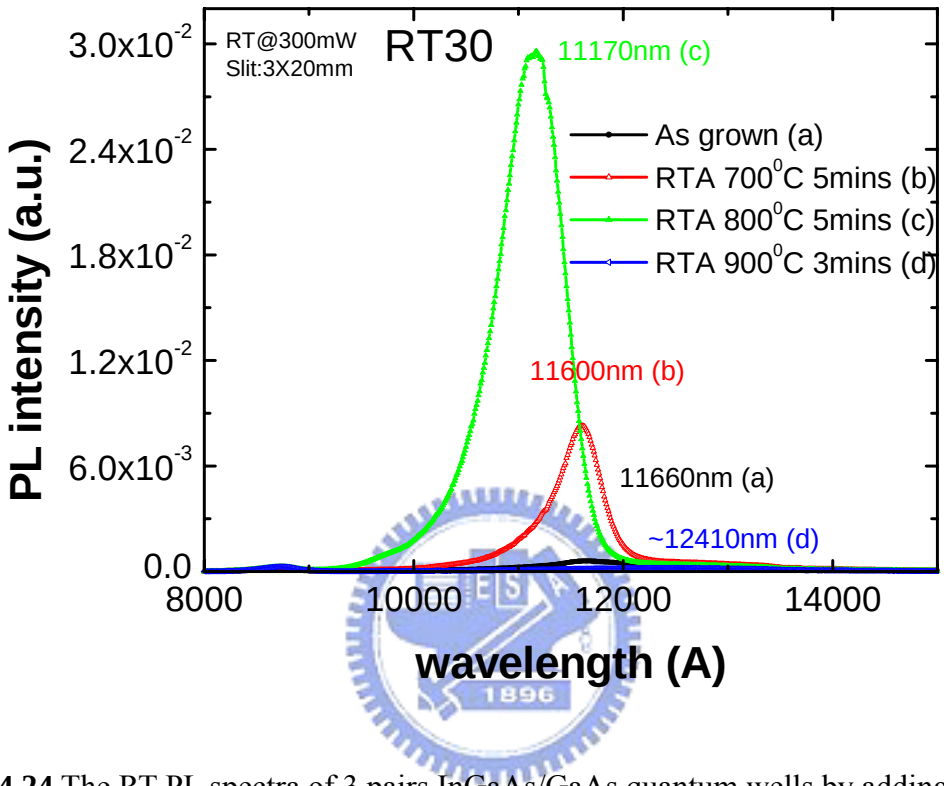

Fig 4.24 The RT-PL spectra of 3 pairs InGaAs/GaAs quantum wells by adding the Sb material into.

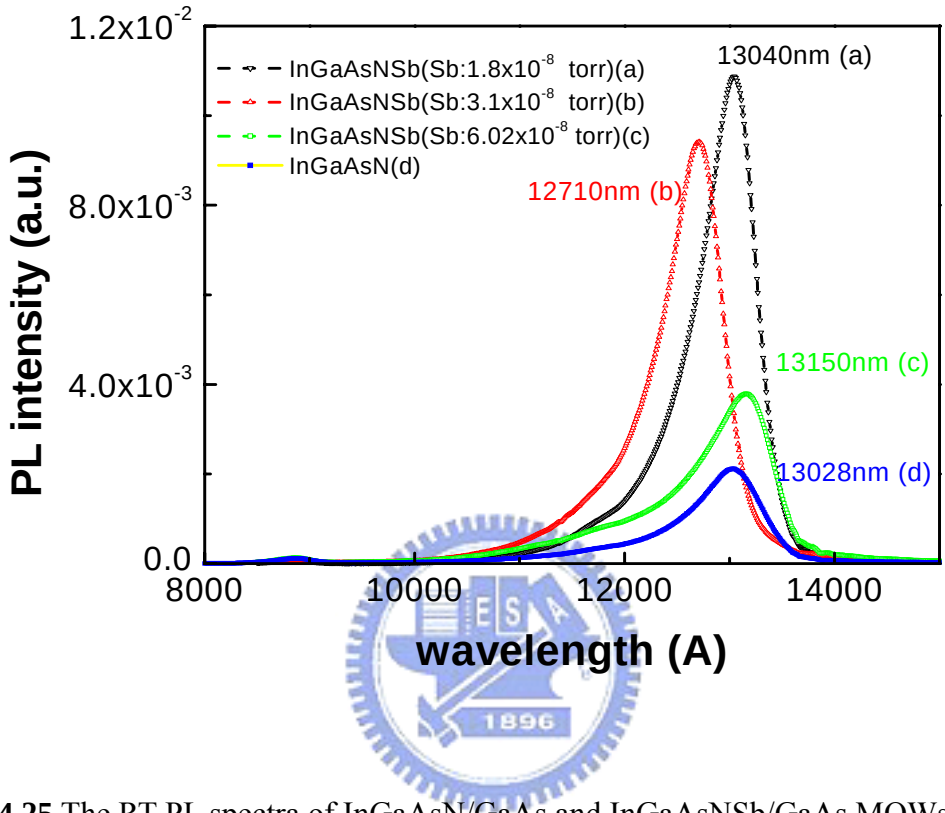

Fig 4.25 The RT-PL spectra of InGaAsN/GaAs and InGaAsNSb/GaAs MQWs with different Sb doping level after RTA annealing.

Chapter 5: InGaAsN lasers

1.3μm vertical cavity surface emitting lasers (VCSELs) are promising transmitter for short and midrange optical networks because these lasers can be used for standard single mode and multimode silica fiber. The primary challenge in making a 1.3μm VCSEL has been the integration of high reflectivity DBRs with a suitable active region. Jayataman et al [1] reported a single mode VCSEL emitting power more than 2 mW around 1.3μm by using the wafer-fused structure consisting of an InP-based active region combined with AlGaAs DBR mirrors. Recently the develop of active region can be grown directly on a GaAs substrate resulted in room temperature CW operation of monolithically grown 1.3μm VCSELs using either InGaAsN or GaAsSb quantum well (QWs) or InAs quantum dots[2-5]. Temperature stability of InGaAsN lasers has been shown to be superior to that of InP based lasers but other characteristics were not good enough due to low material quality [5-7]. In the following articles we report our recent results in the development of an InGaAsN/GaAs based approach to long wavelength lasers grown by molecular beam epitaxy (MBE) under low temperature growth technology.

Chapter 5.1 High power InGaAsN edge emitting lasers

High power single mode lasers are highly desirable as pumps for Raman fiber amplifers and many non-linear channel switching applications in optical networks. VCSELs at 1.3μm emitting wavelength range will be extremely useful for MANs and LANs, pump lasers must work at 1.45μm to be useful in combination with EDFAs at 1.55μm. In order to provide fiber applications over entire low loss fiber region, lasers must provide high power over the entire at 1.2~1.5μm range.

The main propose of this section is to report on laser results with InGaAsN active region growth by RF plasma assist solid source MBE. Most of the works are supported by my colleagues who are responsible for the laser fabrication and testing. The fabrication of InGaAsN edge emitting laser is categorized into two kinds of processes, they are broad area (BA) process and ridge-waveguide (RWG) processes.

The structures used in this work are grown by solid source molecular beam epitaxy (MBE) with a Riber Epineat machine. Atomic nitrogen is produced by Applied Epi Unibulb nitrogen plasma cell. A radio-frequency (RF) coupled plasma source is employed to generate reactive nitrogen radicals from high-purity N_2. The laser structure consists of cladding layers of 1.5-μm-thick n- and p-type $Al_{0.3}Ga_{0.7}As$ doped with Si and Be, respectively and GaAs waveguide of 0.35 μm thickness. 30% Al content is used for the cladding layer to obtain narrow beam divergence. We use single InGaAsN QW of 6.5 nm width placed between GaAs barriers for active regions. The In and N contents are 36% and 2.2%, respectively. The growth temperature of cladding layers is 700^0C to provide in situ annealing of the active region during growth of the top cladding layer. According to the data of other groups and our own study, we founded that substrate temperature is the key parameter for the growth of high quality InGaAsN QW with 1.3 μm emitting wavelength. It has to be low enough to avoid 3D transition of the growth mode. On the other hand, too low a growth temperature of the growth enhances absorption of impurities. It has to be just low enough to avoid 3D transition of the growth mode [8].

Broad area process is a simplified process for fast evaluation of LD or the equivalent MBE system quality. Broad-area negative stripe pattern of 50 μm is defined by photolithography at first. After HCl/H_2O dip to remove the native oxide of GaAs contact layer, p-type metal of Ti/Pt/Au (~ 30/30/100 nm) or AuBe (~ 200 nm) is then deposited by E-gun or thermal coater. The substrate is then thinned down to

around 100 μm. Before n-metallization, simultaneous removing of non-metallized p-contact layer and cleaning of the wafer backside is done by wet etching in H_2SO_4:H_2O_2:H_2O (1:8:40), followed by DI water rinse. The n-type metal deposited is Ni/Ge/Au (~ 30/70/300 nm) or AuGe (> 300 nm). The fabricated devices are then cleaved into laser bars for direct-probed measurement. The RWG process is a standard process for high performance and reliable LD fabrication. First, the positive stripe pattern is defined by photolithography. The photoresist (PR) stripe is used as a mask for ridge definition. Stripe etching down to the cladding layers with controlled cladding remaining adjacent to the separate confined- heterostructure (SCH) region is done by wet etching in H_2SO_4:H_2O_2:H_2O (1:8:40), followed by DI water rinse. Low temperature (~ 100^0C) PECVD Si_3N_4 or SiO_2 is then deposited. The dielectric deposited on PR is then lift-off. Before p-metallization, positive 100-μm PR stripe is defined between ridges for subsequent metal lift-off. This process of metal isolation is facilitated for the measurement of laser bars at the final stage. The residual process steps of p-metallization, wafer thin down, and n-metallization are the same for BA process.

The L-I curve shows the fundamental characteristics of laser diode. Fig 5.1 shows the schematic diagram of L-I characteristic measurement system. From the L-I curve one can immediately determine the experimental threshold current, *Ith*, from the intercept of the above-threshold curve with the abscissa. The differential (or external) quantum efficiency (*hd*), defined as the number of photons out per electron in, can be calculated from the slope of the above threshold curve, provided the wavelength (λ) is known, i.e.

$$\eta_d = \frac{d(\frac{L}{h\nu})}{d(\frac{I - I_{th}}{q})} = \frac{1.24}{\lambda(\mu m)} \frac{dL}{d(I - I_{th})}$$

where L is the light power at current I, hn is the photon energy, q is electron charge, and Ith is the threshold current. HP-8114A pulse generator and/or ILX-light wave LDP-3811 continuous wave or pulse current source is used for current injection. The light output is detected by a calibrated InGaAs PD reverse-biased at 9 volts. The injection current and the detection current is then gated and integrated by the Standford Research System SR250 gated integrator and averager. The whole measurements are GPIB-interfaced and controlled by the personal computer as shown in Fig 5.2.

Broad area laser were fabricated with 50μm ridge width and 0.4mm, 0.5mm, 1mm, and 2mm cavity length. In Fig 5.3, we show the L-I-V characteristics of broad area lasers with different cavity length and the insert showing the lasing spectrum of different driving current. From the broad area results can be exacted the material quality and the loss of waveguide design. It shows that the threshold current increase while increase the cavity length and the lasing wavelength around 1.29μm. Calculation form the threshold current density with reverse of different cavity length as shown in Fig. 5.4. The transverse current density is in a value of 410A/cm^2 and compares with other group's results is shown in Fig 5.5. The material quality of InGaAsN/ GaAs lasers seems among the world best with other groups. Figure 5.6 shows an internal quantum efficiency of 96% with an internal loss of 4.5cm^{-1} and a slope efficiency of 0.67W/A for a cavity length of L=1 mm.

The exact dimensions for the fabricated narrow ridge structures were examined with SEM images. Figure 5.7 shows the SEM micrographs of the structures of the

crossing view. The ridge width is determined to be 2.7 μm. In the first set the residual thickness of the top cladding layer was 0.2μm. In the SEM image, the upper cladding layer, the SCH waveguide layer, the QW active regions can penetrate about 0.4 μm into the bottom cladding layer.

Fig 5.8 shows dependence of total output power recorded in pulse regime for RW stripe. The L-I-V curve and conversion efficiency are also shown in Fig 5.8. The lasing wavelength is 1.285 μm at the threshold. The threshold current is 20.6 mA. The differential efficiency is as high as 69% (0.67 W/A). To the best of our knowledge this is the highest value reported for InGaAsN-based lasers. The output power higher than 400 mW is achieved. This value is limited by experiment condition (drive current supply). Ideal I-V characteristic and high differential efficiency provides level of total wall-plug efficiency higher than 30% at 100 mW [9].

Fig 5.9 shows CW operation of RW diode after facet coating, bonding, and packaging in TO46 can. Far field patterns shown in Fig 5.10(a) prove single mode operation up to the highest power recorded. Lasing spectra shown in Fig 5.10(b) are getting wider with drive current and shifts to 1.31 μm at high power. Threshold current and differential efficiency are 22 mA and 62%, respectively. The maximum value of 210 mW of single mode output power is limited by thermal rollover. To the best of our knowledge this is the highest value ever reported for single mode 1.3 μm range lasers based on GaAs. Low internal loss (3 cm^{-1}) of this laser structure ensures high differential efficiency in longer diodes. It means that considerably higher output power can be achieved for longer cavity diodes due to better thermal dissipation. Characteristic temperature of this diode is 85 K in 20 – 80 ^{0}C temperature range.

Ridge waveguide lasers based on single $In_{0.36}GaAsN_{0.022}$ QW in GaAs matrix have been fabricated and measured. 3 and 10um wide ridge with different cavity length had been demonstrated high crystal quality by laser characteristics. The

Temperature characteristics achieved 121K in 10um ridge with 1 mm cavity length. The differential efficiency of 62% and the single mode output power of 210 mW, limited by thermal rollover, were achieved at lasing wavelength around 1300nm in 3um narrow ridge lasers. The present approach utilize GaAs substrates advantages of high thermal conductivity and high quality and large size opens new possibilities for high power application of laser diodes in the wavelength range of 1300nm.

Ch 5.2 InGaAsN Intra-cavity contacted VCSEL

Kondow *et al.* [10] first reported that the material of the InGaAsN/GaAs system can be used as an alternative to the currently used InP-based material system for emitting at 1.3 μm. Furthermore, the possibility to monolithically combining the active regions of the InGaAsN/GaAs quantum wells (QWs) with the AlGaAs/GaAs semiconductor distributed Bragg reflectors (DBRs) makes this material system highly attractive for GaAs-based long wavelength vertical cavity surface emitting lasers (VCSELs). It has been employed successfully in 1.3 μm edge emitting lasers and VCSELs by both molecular beam epitaxy (MBE) [11-14] and metal-organic chemical vapor deposition (MOCVD) [15-17]. In this section, we presents the characteristics of a monolithic intra-cavity contacted VCSEL with an InGaAsN/GaAs QWs active region, emitting at 1304 nm, as grown by MBE under low-temperature growth conditions.

The samples were grown by Riber-epineat solid source MBE on GaAs substrates. Low temperatures have been used to grow InGaAsN/GaAs QWs to suppress the phase separation caused by nitrogen incorporation. The optimal growth temperature for the InGaAsN layer was set to as low as 400-420 ℃ [18-20], which is lower than that of GaAsN alloys [21].

The intra-cavity contacted design has been used to achieve high-frequency

operation and prevent free-carrier absorption in p-doped materials, and thus to provide high output power [13, 14]. The active region consisted of two 6-nm-thick InGaAsN quantum wells separated by 12-nm- thick GaAs spacers. Point defects formed during growth at such low temperatures were removed by annealing at 750 ^{0}C for 10 minutes, following the deposition of a 55-nm-thick $Al_{0.98}Ga_{0.02}As$ current-confinement aperture layer. The In and nitrogen contents of the quantum wells were 35% and 1.7%, respectively. The top and bottom DBR mirrors consisted of 25 and 33 pairs of undoped $Al_{0.9}GaAs/GaAs$, respectively. The contact layers were 1.75λ thick GaAs, doped with silicon and beryllium, respectively. Following epitaxial growth, the VCSELs were fabricated in electrically injected intra-cavity contacted devices as shown in Fig 5.11(a). Fig 5.11(b) pilots the experiment and simulation results of 10 pairs $Al_{0.9}Ga_{0.1}As/GaAs$ DBRs with half λ cavity before the fully structure fabricated. Two-step mesa patterns, with diameters of 20 and 46 μm respectively was defined on the wafer surface by dry etching. Then, the $Al_{0.98}Ga_{0.02}As$ aperture layer was selectively oxidized at 420 °C. Finally, intra-cavity metal contacts were deposited by e-beam evaporation using a lift-off process.

Figure 5.12(a) shows the reflection spectra of VCSELs that include the normalized PL spectrum of InGaAsN/GaAs QWs active region. Fig 5.12(b) show two step etched sidewall of Intra cavity contacted VCSELs. A few pairs of top DBR mirrors were removed in making the reflection spectra measurements, to observe the wavelength of the cavity resonance. The detuning between the PL peak wavelength (1276 nm) and the position of the cavity resonance (1296 nm) was approximately 20 nm detuning.

Two aperture size were been fabricated in the intra cavity contacted VCSEL, which are 18um and 7um. The L-I-V curve of the intra cavity VCSEL with 18 um aperture size shows in Fig 5.13. The threshold current is 3.8 mA and 3.6 mA at 20℃

under CW and pulse operation respectively. The oxide aperture is approximately 18μm in diameter, which implies a threshold current density of 1.9KA/cm^2. This is the lowest value ever reported for 1.3 μm range InGaAsN/GaAs QW VCSELs. Under pulse operation, the output power is more than 10 mW with an initial slope efficiency of 0.20 W/A, while the CW maximum output power exceeds 1 mW with an initial slope efficiency of 0.15 W/A.

Figure 5.14 presents the RT-CW L-I-V curves of the single mode intra-cavity contacted InGaAsN/GaAs QW VCSELs with a current aperture of 7 μm. A threshold current of 1.6 mA and an output power of 0.7 mW with an initial slope efficiency of 0.17 W/A were obtained under RT-CW operation. The insert reveals that a side mode suppression rate of 40 dB with a lasing wavelength as long as 1304 nm was achieved at a driving current of 6.5 mA. Figure 5.15 plots the threshold current under CW operation and lasing wavelength under pulse operation as a function of the operation temperature. The wavelength shifted with temperature at a rate of 0.077 nm/K. CW operation was achieved up to 85^{0}C. The threshold current was minimum at below room temperature, indicating a non-optimized detuning between the gain peak and the cavity resonance. The calculated thermal impedance of 2.06 K/mW is obtained from the wavelength shifted rate with the dissipated power and the operation temperature. This value is roughly two times higher than the InGaAsN QW VCSELs with fully doped DBRs structures [24]. We think this is may be because of the relatively less heat dissipation for the intra-cavity contacted structures. Therefore, optimizing the detuning between the gain peak and the cavity resonance can result in increases the maximum output power and improves the over-temperature performance.

This work demonstrated the successful MBE growth of high-quality InGaAsN/GaAs intra-cavity contacted VCSEL under low-temperature growth conditions. A RT-CW single mode output power of 0.75 mW with an initial slope

efficiency of 0.17 W/A and a side mode suppression ratio of 40 dB was achieved at a lasing wavelength as long as 1304nm.

Reference

[1] V. Jayaraman, M. Mehta, A. W. Jackson, S. Wu, Y. Okuno, J. Piprek, and J. E. Bowers, "High-power 1320-nm wafer-bonded VCSELs with tunnel junctions," IEEE Photonics. Lett., 15.,1495, 2003.

[2] G. Steinle. H. Riechert, and A. Yu. Egorov, "Monolithic VCSEL with InGaAsN active region emitting at 1.28 μm and CW output power exceeding 500 μW at room temperature," Electron. Lett., 37., 93, 2001.

[3] A. Ramakrishnan, G. Steinle, D. Supper, C. Degen, and Ebbinghaus, "Electrically pumped 10 Gbit/s MOVPE-grown monolithic 1.3 μm VCSEL with GaInNAs active region," Electron. Lett., 38., 322, 2002.

[4] M. Yamada, T. Anan, K. Kurihara, K. Nishi, K. Tokutome, A. Kamei, and S. Sugou, "Room temperature low-threshold CW operation of 1.23 μm GaAsSb VCSELs on GaAs substrates," Electron. Lett., 36., 637, 1384, 2000.

[5] J. A. Lott, N. N. Ledentsov, V. M. Ustinov, N. A. Maleev, A. E.ukov, A. R. Kovsh, M. V. Maximov, B. V. Volovik, Zh. I. Alferov, and D. Bember, "InAs-InGaAs quantum dot VCSELs on GaAs substrates emitting at 1.3 μm," Electron Lett., 36, 637, 1384, 2000.

[6] S. iiiEK, A. Ultsch, B. Borchert, A. Yu. Egorov, and H. Riechert, "Low threshold lasing operation of narrow stripe oxide-confined GaInNAs/GaAs multi quantum well lasers at 1.28 μm," Electronic .Lett, 36, 725, 2000.

[7] B. Borchert, A. Yu. Egrov, S. IIIeks, M. Komainda, and H.Riechert, "1.29 μm GaInNAs multiple quantum-well ridge-waveguide laserdiodes with improved

performance," Electron .lett., 35, 2204, 1999.

[8] A. J. Ptak, S.W. Johnston, Sarah Kurtz, D. J. Friedman, W. K. Metzger, "A comparison of MBE- and MOCVD-grown GaInNAs," Journal of Crystal Growth, 251, 392–398, 2003.

[9] Kovsh, A. R., Wang, J. S., Wei, L., Shiao, R. S., Chi, J. Y., Volovik, B. V., Tsatsul'nikov, A. F. and Ustinov V. M., "Molecular beam epitaxy growth of GaAsN layers with high luminescence efficiency," J. Vac. Sci. Technol. B, 20(3), pp.1158-1161, 2002.

[10] M. Kondow, K. Uomi, A. NiWa, T. Kitatani, S. Watahiki, Y. Yazawa, "GaInNAs: A Novel Material for Long-Wavelength-Range Laser Diodes with Excellent High-Temperature Performance," Jpn. J. Appl. Phys., 35, 1273, 1996.

[11] A. Egorov, D. Bernklau, D. Livshits, V. Ustinov, Z. Alferov, and H. Riechert, "High power CW operation of InGaAsN lasers at 1.3 μm," Electron. Lett., 35, 1643, 1999.

[12] M. Reinhardt, M. Fischer, M. Kamp, J. Hofmann, and A. Forchel, "1.3-μm GaInNAs-AlGaAs distributed feedback lasers," IEEE Photon. Technol. Lett., 12,. 239, 2000.

[13] H. C. Schneider, A. J. Fischer, W. W. Chow, "Temperature dependence of laser threshold in an InGaAsN vertical-cavity surface-emitting laser," Appl. Phys. Lett., Vol. 78, No. 22, 28, May 2001.

[14] A. W. Jackson, R. L. Naone, M. J. Dalberth, J. M. Smith, K. J. Malone, D. W. Kisker, J. F. Klem, K. D. Choquette, D. K. Serkland, and K. M. Geib, "OC-48 capable InGaAsN vertical cavity lasers," Electron. Lett., 37, 355, 2001.

[15] G. Steinle, F. Mederer, M. Kicherer, R. Michalzik, G. Kristen, A. Y. Egorov, H. Riechert, H. D. Wolf, and K. J. Ebeling, "Data transmission up to 10 Gbit/s with

1.3 μm wavelength InGaAsN VCSELs," Electron. Lett., 37, 632, 2001.

[16] N. Tansu and L. J. Mawst, "Low-threshold strain-compensated InGaAs(N) (λ = 1.19-1.31μm) quantum-well lasers," IEEE Photon. Technol. Lett., 14, 444, 2002.

[17] T. Takeuchi, Y.-L. Chang, M. Leary, A. Tandon, H.-C. Luan, D. Bour, S. Corzine, R. Twist, and M. Tan, "1.3 μm InGaAsN vertical cavity surface emitting lasers grown by MOCVD," Electron. Lett., 38, 1438, 2002.

[18] A. Ramakrishnan, G. Steinle, D. Supper, C. Degen, and G. Ebbinghaus, "Electrically pumped 10 Gbit/s MOVPE-grown monolithic 1.3 μm VCSEL with GaInNAs active region," Electron. Lett., 38, 322, 2002.

[19] A. Yu. Egorov, D. Bernklau, B. Borchert, S. IlleK, D. Livshits, A. Rucki, M. Schuster, A. Kaschner, A. Hoffmann, Gh. Dumitras, M. C. Amann, and H. Riechert, "Growth of high quality InGaAsN heterostructures and their laser application," J. Crystal Growth, 545, 227-228, 2001.

[20] J. S. Wang, A. R. Kovsh, R. S. Hsiao, L. P. Chen, J. F. Chen, T. S. Lay, and J. Y. Chi, "High nitrogen content InGaAsN/GaAs single quantum well for 1.55 μm applications grown by molecular beam epitaxy," J. Crystal. Growth, .262, 84, 2004.

[21] A. R. Kovsh, J. S. wang, L. Wei, R. S. Shiao, J. Y. Chi, B. V. Volovik, A. F. Tsatsul'nikov, and V. M. Ustinov, "Molecular beam epitaxy growth of GaAsN layers with high luminescence efficiency," J. Vac. Sci. Technol. B, 20, 1158, 2002.

[22] P. Sitarek, K. Ryczko, G. Sek, J. Misiewicz, M. Fischer, M. Reinhardt, and A. Forchel, "Optical investigations of InGaAsN/GaAs single quantum well structures Solid-State," Electronics, 47, 489, 2003.

[23] A. Polimeni, M. Capizzi, M. Geddo, M. Fischer, M. Reinhardt, and A. Forchel, "Effect of temperature on the optical properties of (InGa)(AsN)/GaAs single quantum wells," Appl. Phys. Lett., 77, 2870, 2000.

[24] M. C. Larson, C. W. Coldren, S. G. Spruytte, H. E. Petersen, and J. S. Harris, "Low-threshold oxide-confined GaInNAs long wavelength vertical cavity lasers," IEEE Photon. Technol. Lett., 12, 1598, 2000.

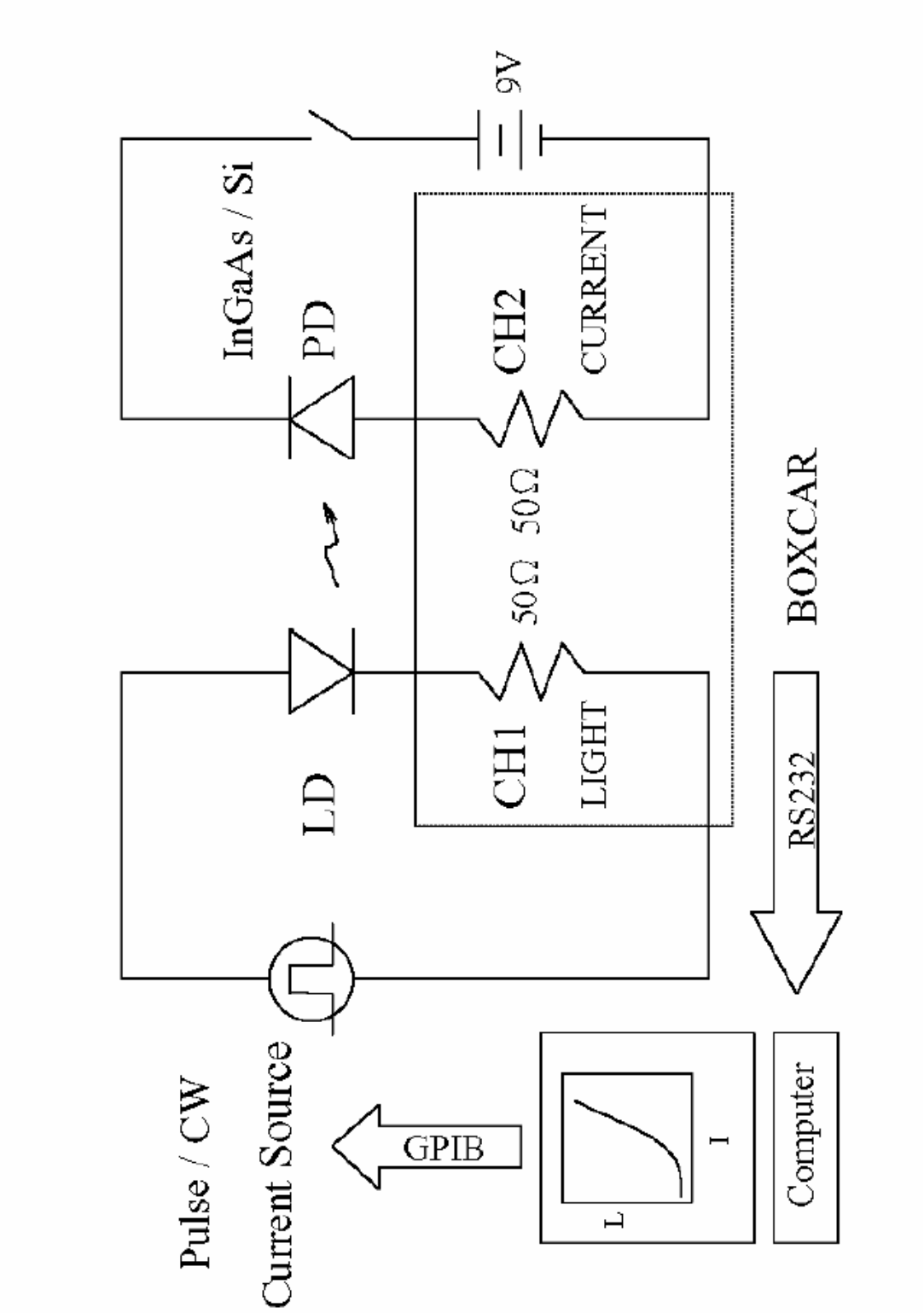

Fig 5.1 The schematic diagram of L-I measurement system.

Fig 5.2 The image of laser measurement system.

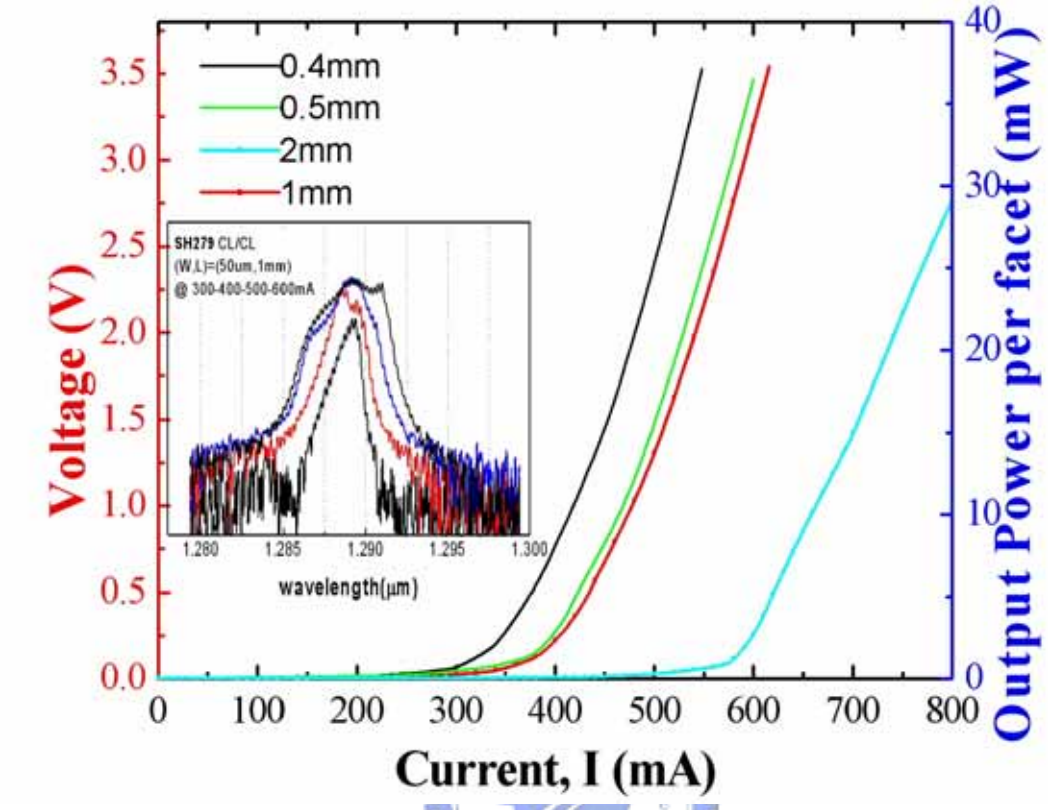

Fig 5.3 The L-I-V curve of 50μm-ridge broad area lasers. The insert shows the lasing spectra.

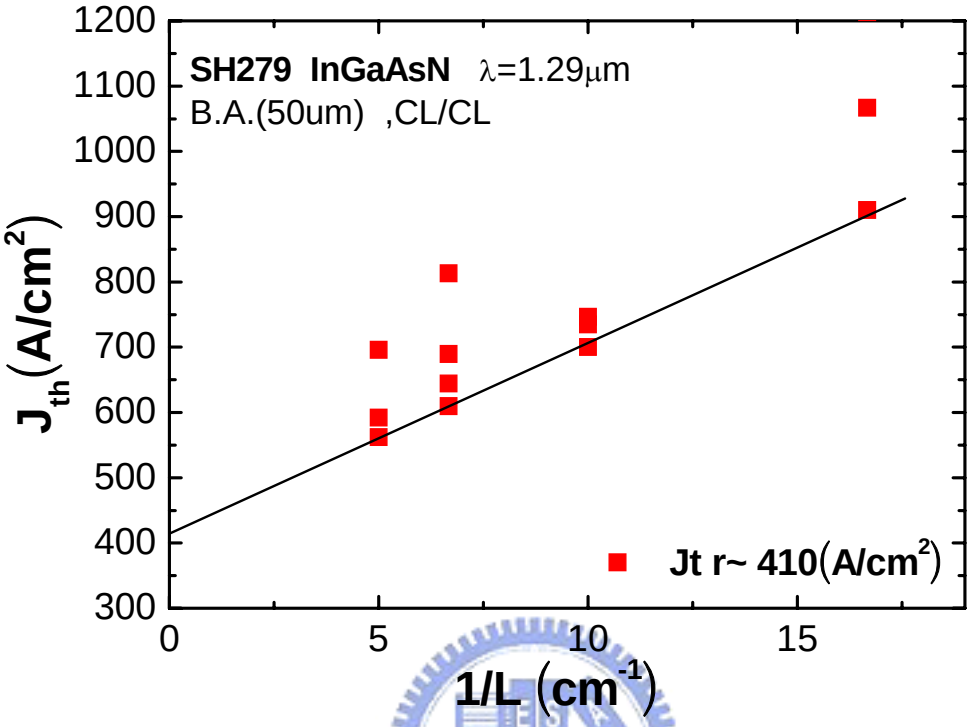

Fig 5.4 Dependence of threshold current density and reverse cavity length of InGaAsN/GaAs broad are edge emitting lasers.

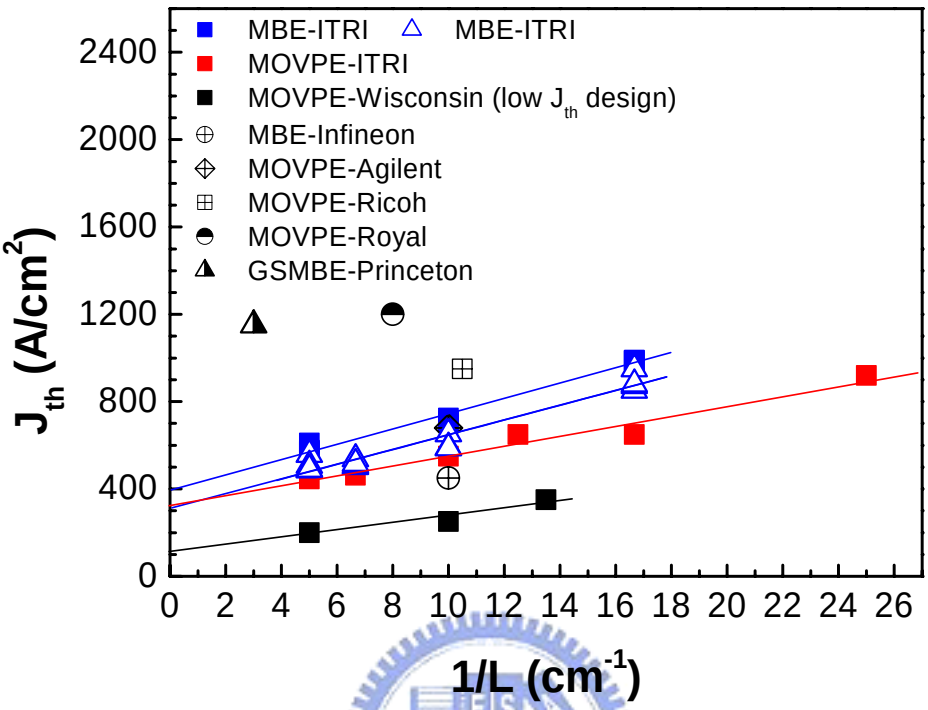

Fig 5.5 The threshold current density versus the reciprocal cavity length for 1.3μm InGaAsN ridge waveguide lasers with 3μm width under pulsed operation at room temperature.

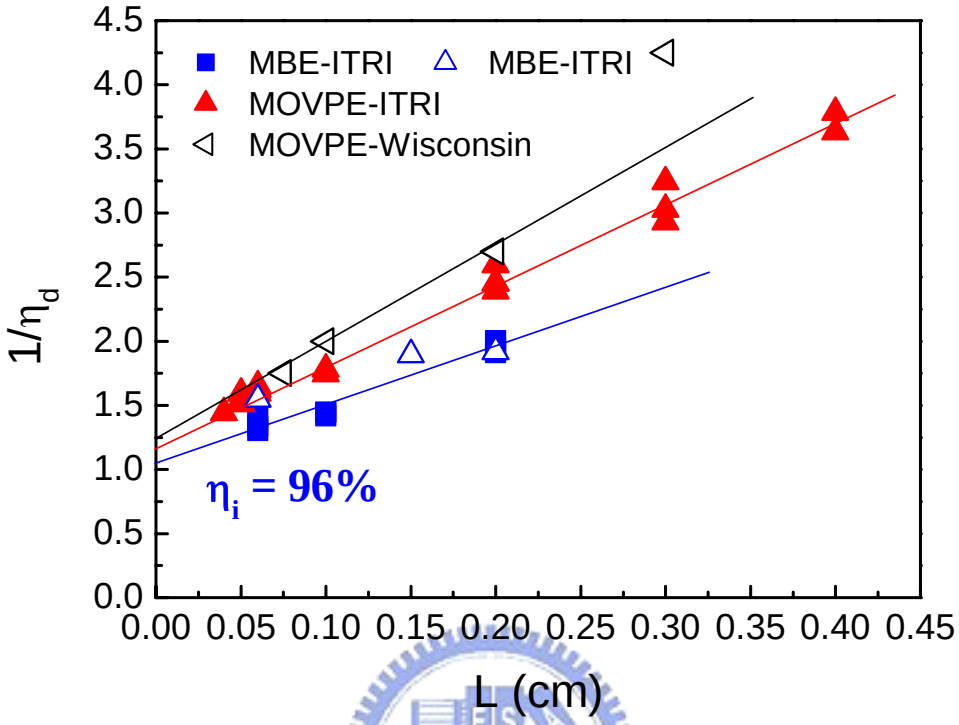

Fig 5.6 An internal quantum efficiency with an internal loss exacted from a 50μm with 1 mm cavity length laser.

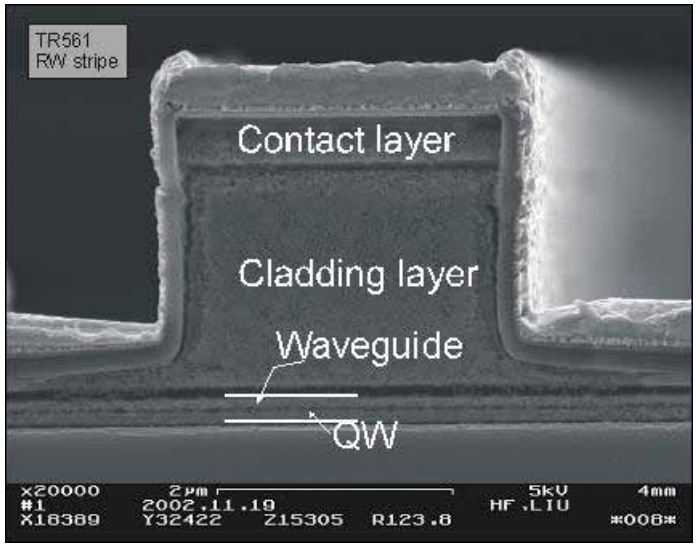

Fig 5.7 Cross sectional SEM image of the InGaAsN/GaAs laser structure.

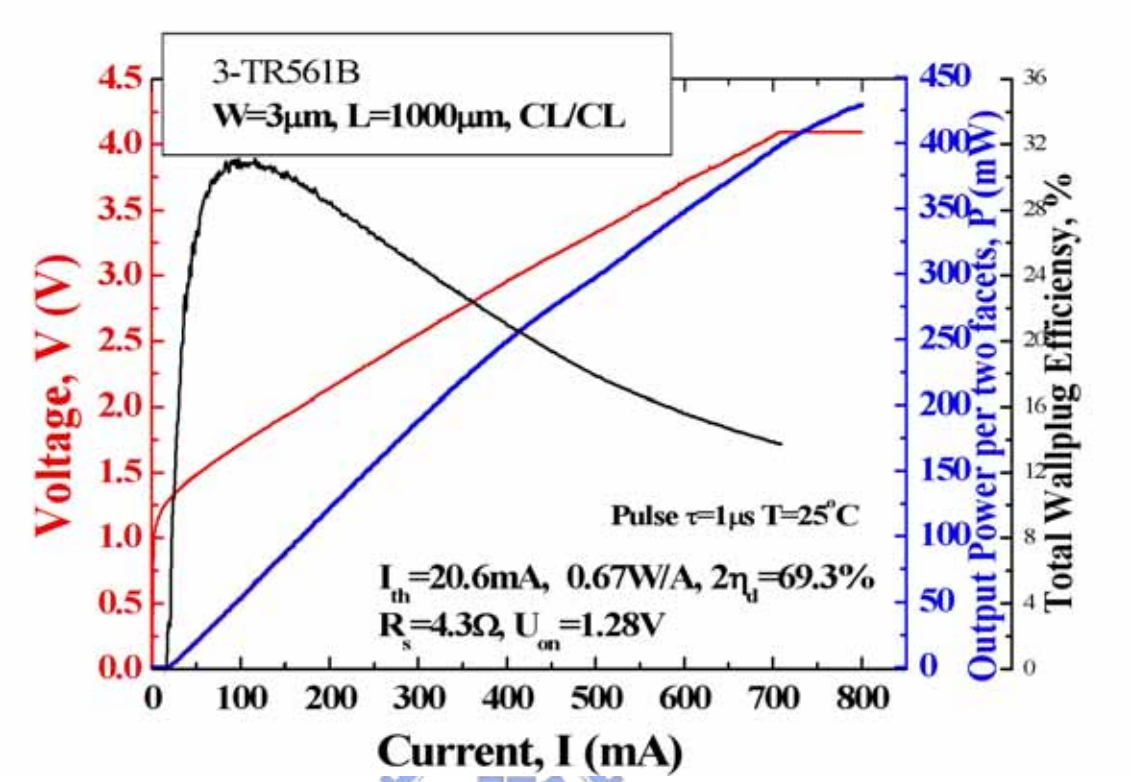

Fig 5.8 Dependence of total output power recorded on threshold current in pulsed regime for RW stripe. *I-V* curve and conversion efficiency are also shown.

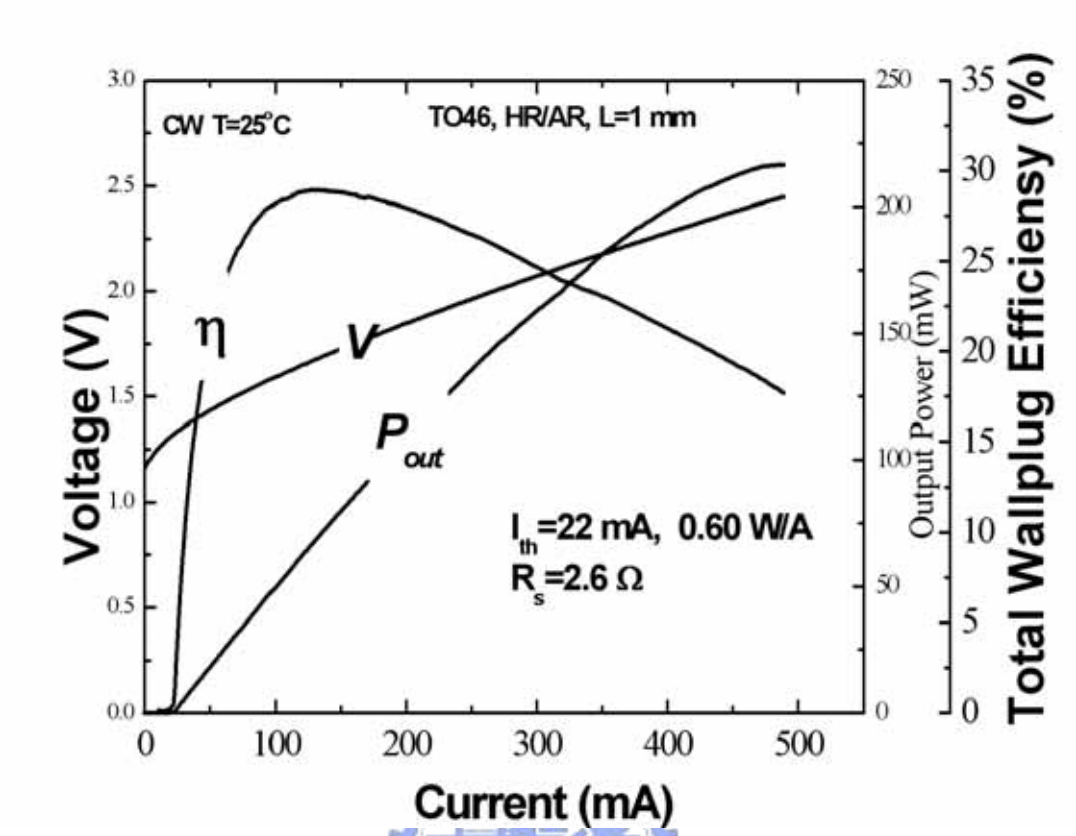

Fig 5.9 L-I-V characteristics of the InGaAsN laser under CW operation of RW diode after facet coating, bonding, and packaging in TO46 can.

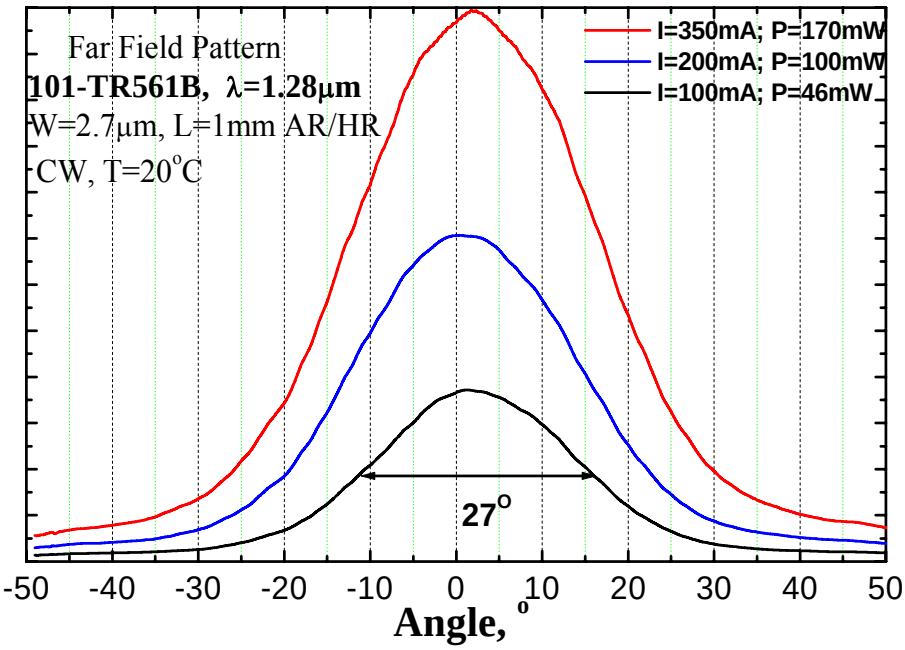

Fig 5.10 (a) Far field patterns of the InGaAsN under single mode operation up to the highest power recorded.

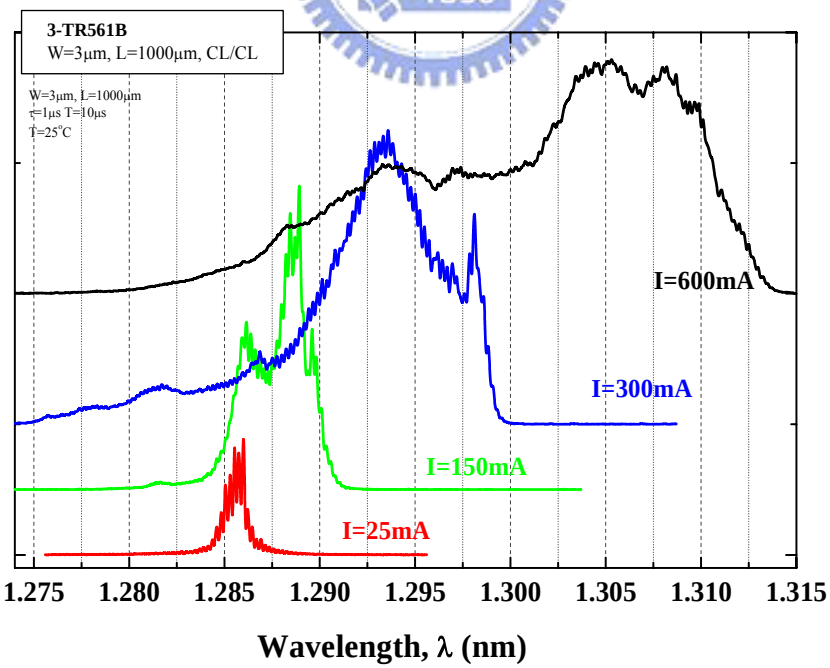

Fig 5.10 (b) Measured lasing spectra of the InGaAsN laser, the lasing spectra are getting wider with drive current and shifts to 1.31 μm at high power.

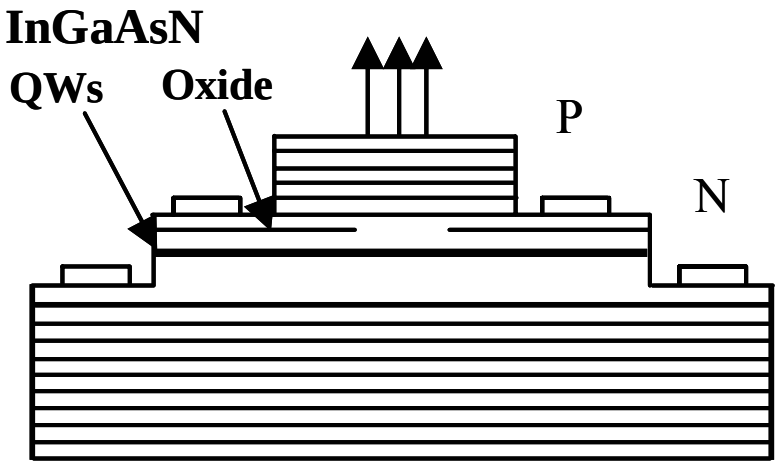

Fig 5.11 (a) The schematic of intra cavity contacted InGaAsN/GaAS VCSELs.

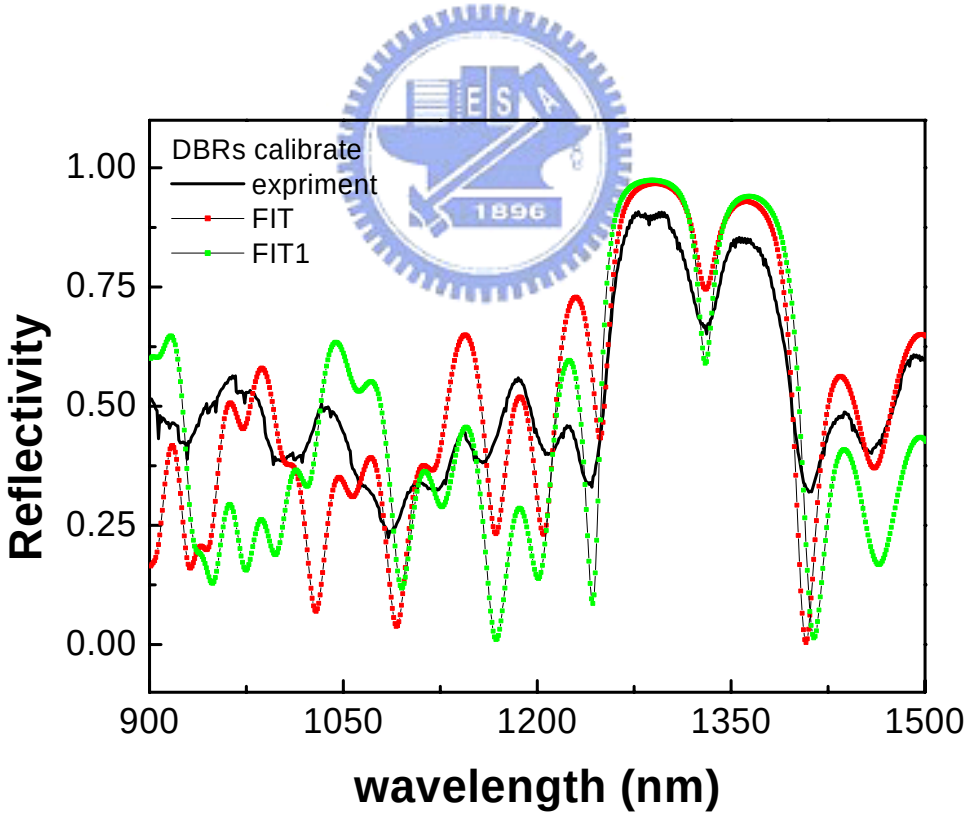

Fig 5.11 (b) The spectra of measured and simulated reflectance of the VCSELs sample.

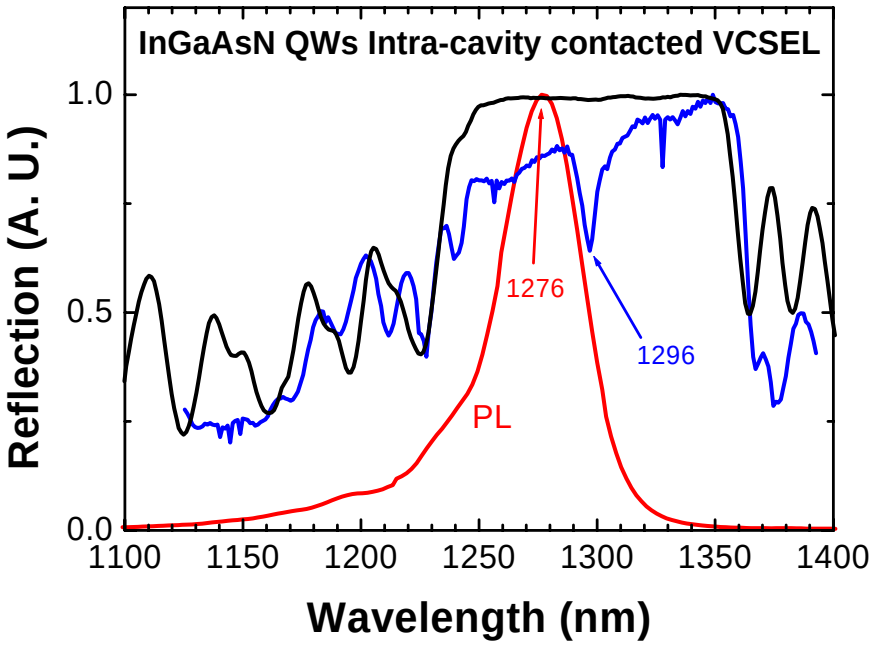

Fig 5.12 (a) The reflection spectra of VCSELs that included the normalized PL spectrum of InGaAsN/GaAs QWs active region.

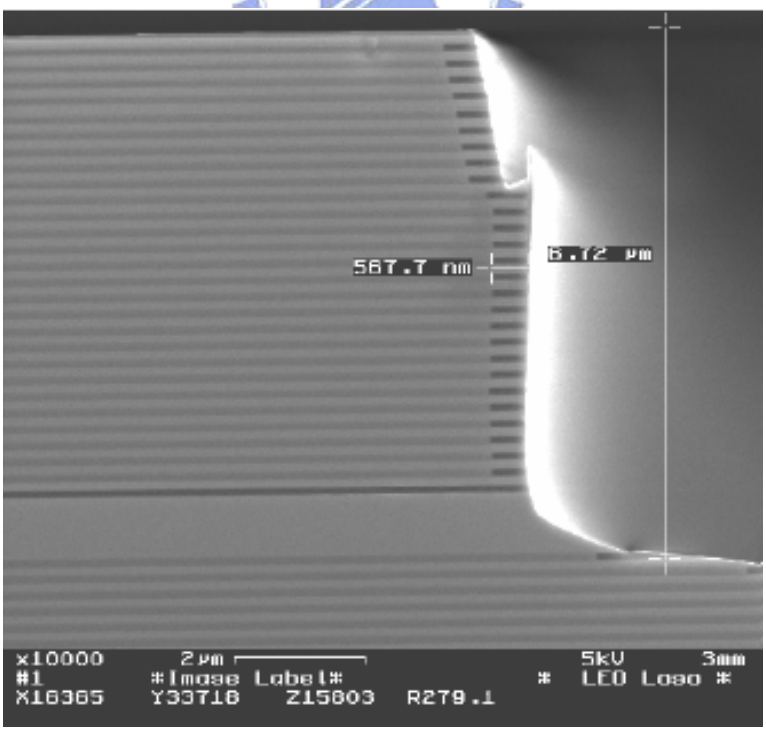

Fig 5.12 (b) Cross-sectional SEM photographs show the two steps etched sidewall of 1.3µm InGaAsN Intra cavity contacted VCSEL grown by MBE.

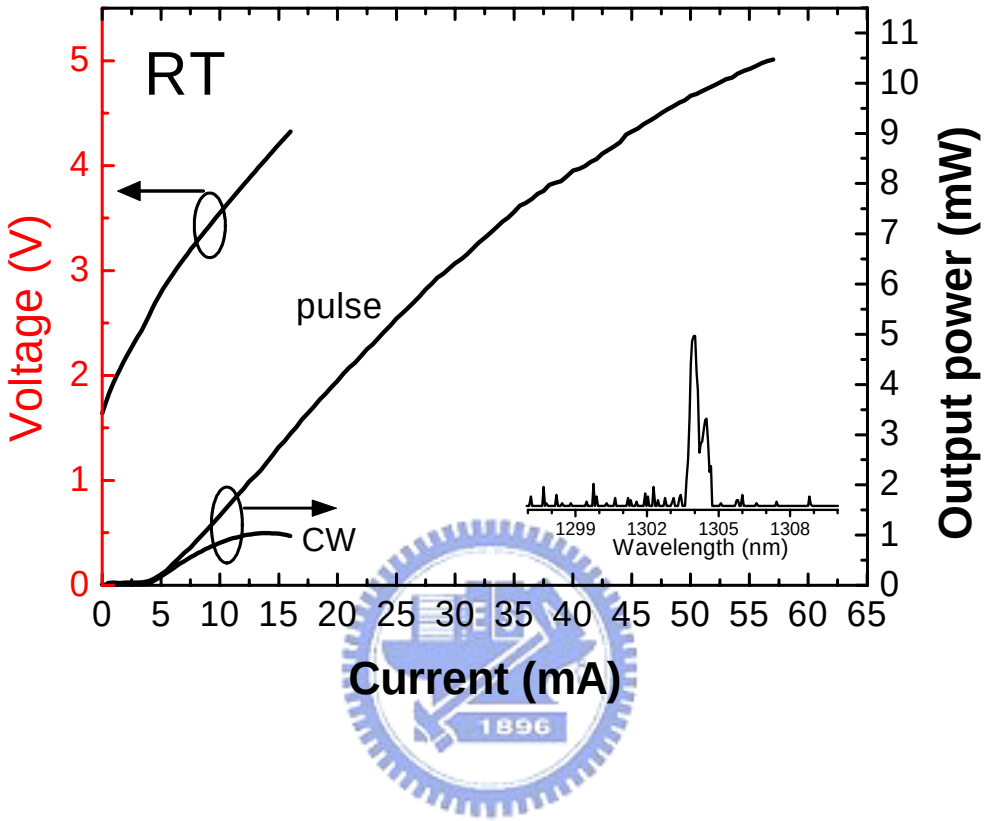

Fig 5.13 The L-I-V curve of the intra cavity VCSEL with 18 μm oxided aperture size.

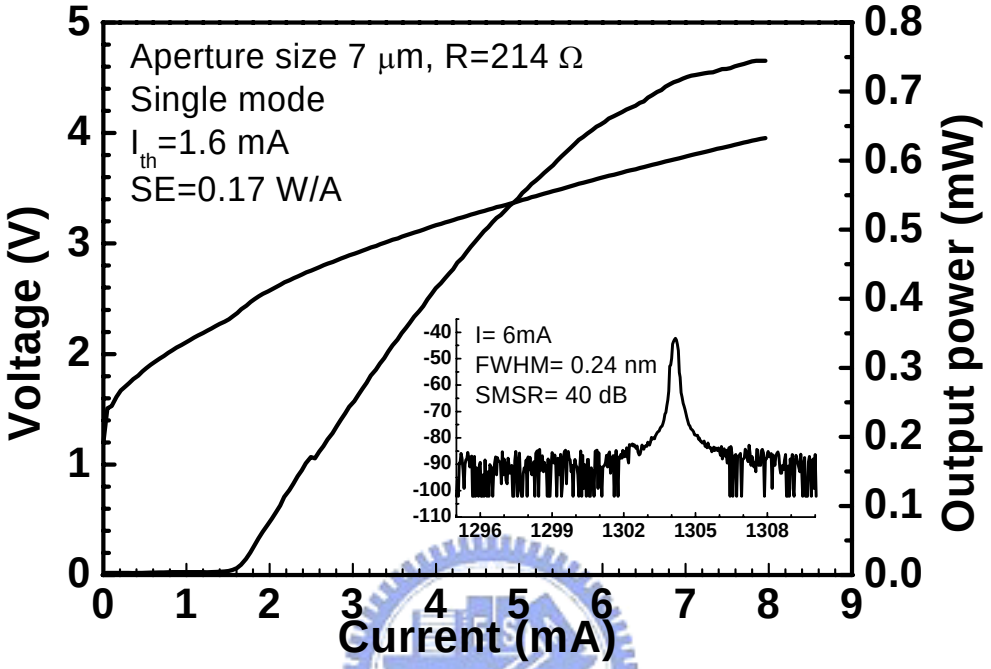

Fig 5.14 The RT-CW L-I-V curves of the single mode intra-cavity contacted InGaAsN/GaAs QW VCSELs with a current aperture of 7 μm.

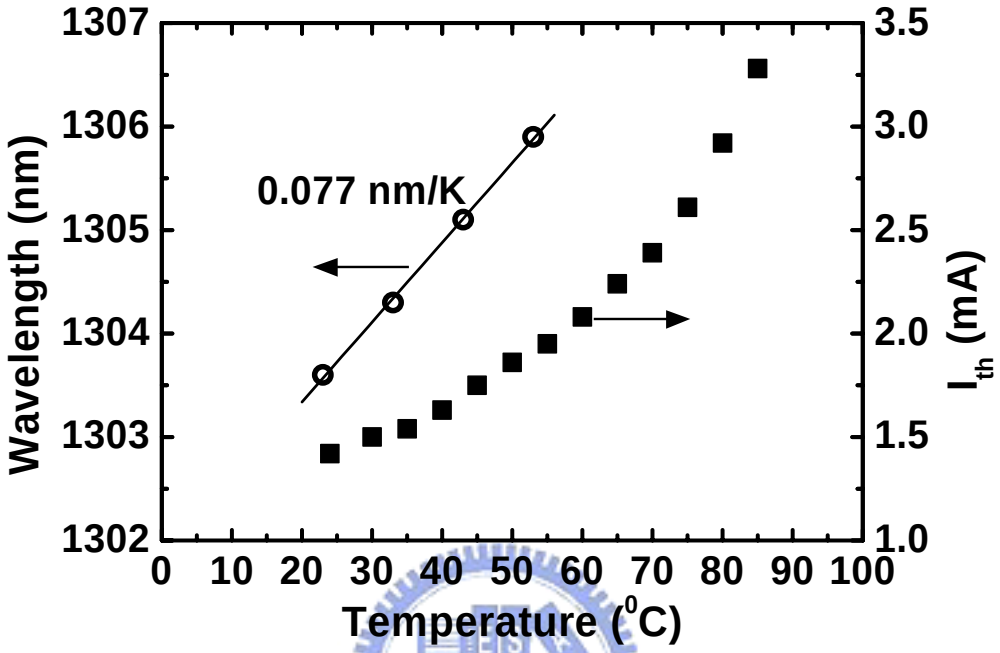

Fig 5.15 The threshold current under CW operation and lasing wavelength under pulsed operation as a function of the operation temperature.

Chapter 6: Summary

To realize InAs QD VCSEL at 1.3μm is a challenging task, several problems must be overcome to realize this device. The challenges lie in the precise controls over DBR reflectivity, detuning range, and resistance of the devices. One of the accomplishments in this dissertation is the successful realization of this device. On the other hand, another new type material structure InGaAsN/GaAs QW achieved high gain VCSEL. Using RF plasma assisted-MBE, we demonstrated the successful operation of InGaAsN/GaAs QW VCSEL at 1.3μm. The materials grown mechanisms and RF effects have been addressed and investigated in details here. In this work, tremendous efforts have been made regarding material growth, laser design, and characterization. We study the growth mechanism of QDs and QW at 1.3μm by plasma–assisted MBE. It is also demonstrated that InAs/GaAs QDs and InGaAsN/GaAs QWs can work effectively as ideal VCSEL lasing media. As to InAs/GaAs QD study, InAs/GaAs QDs were grown layer by layer such that these QDs are coupled vertically. The vertically coupled QDs can be utilized in the VCSEL design. This approach offers us many advantages such as high efficiency, high power, and narrow lasing line width.

As to InGaAsN/GaAs QW study, by low temperature plasma –assisted MBE growth and a highly reactive atomic nitrogen plasma source, a high crystalline, homogeneous InGaAsN/GaAs film was thus grown on GaAs. Although low temperature growth can suppressed the phase separation, it may incorporate certain impurity. Hence thermal annealing process was then applied following the material growth to reduce defects and improve the PL intensity.

Thermal annealing can dramatically increase the PL intensity by a factor of two but PL emitting peak blue shifts the wavelength, which leads to atom rearrangement

and bandgap change. Beside the above approaches, the highly strain InGaAs/GaAs and InGaAsN/GaAs multiple stack QWs were grown assisted by dilute Sb surfactant. As a result, our RT-PL, X-ray diffraction, and other measurements indicants significant impurity reduction, high crystalline quality, and better QW interface results.

In chapter 3, the laser fabrication and characterization are presented. InAs/GaAs QDs as lasing medium for three types of laser are fully investigated. These lasers are 1.3μm InAs/GaAs QD edge emitting laser, vertical coupled InAs/GaAs QD VCSEL, and fully doped InAs/GaAs VCSEL. In particular, our fully doped InAs/GaAs VCSEL exhibited superior performance with J_{th} ~1mA, output power 0.28mW, and characteristic temperature of 427K.

Chapter 5 deals with laser characterization of the ridge waveguide laser and the intra cavity contacted InGaAsN/GaAs QW VCSEL. InGaAsN/GaAs QW intra-cavity contacted VCSEL with a low J_{th} of 2kA/cm^2 at room temperature was achieved. Moreover, this device, with a 7μm oxide aperture layer with output power 0.7mW, incorporated, exhibited a impressive performance, such as a CW single mode suppression rate of 40dB and slope efficiency 0.17W/A. On the other hand, the device with 18μm oxide aperture layer incorporated, operated in the CW multiple mode with output power 1mW and slope efficiency 0.15W/A.

In conclusion, InGaAsN/GaAs QW or InAs/GaAs QDs as a laser medium is very likely to be a promising solution to future long wavelength VCSEL commercialization.

Curriculum Vita

***Name*:** Mr. Ru-Shang Hsiao

***Place of Birth*:** Hsin -Chu, Taiwan

***Date of Birth*:** June 12, 1975

***Electronic Mail*:** rshsiao@itri.org.tw

Education:

Ph.D. Electrophysics , National Chiao Tung University, Taiwan

M.S. Electronics, Chung Yuan Christian University Taiwan.

B.S. Electronics, Chung Yuan Christian University Taiwan.

***Areas of Special Interest*:**

MBE, MOCVD growth, RF plasma dilute Nitrogen, high vacuum epitaxy.

Optical / RF photonics measurement

Low dimensional QDs and QW material

Optical microscopy and micro-photoluminescence

C-V, DLTS measurements.

Title of Ph.D. Thesis: GaAs based 1.3μm lasers grown by MBE

Publication List

Refereed Papers:

1. **Ru-Shang Hsiao**, Wen-Di huang, Wei-I Lee, Chi-Ling Lee, Jenn-Fang Chen, Ming-Ta Hsieh, P-S. Guo, Shin-Chang Lee ”Thickness dependence of Current Conduction and Carrier Distribution of GaAsN Grown on GaAs”*Japan Journal of Applied Physics 2005 Vol44, No 10 pp*
2. J. F. Chen, **R. S. Hsiao**, Y. P. Chen, J. S. Wang and J. Y. Chi ”Strain relaxation in InAs/InGaAs quantum dots investigated by photoluminescence and C-V profiling” *Applied Physics Letter 2005 Vol87 page141911-3*
3. J. F. Chen, **R. S. Hsiao**, C. K. Wang, J. S. Wang, and J. Y. Chi “Characterization of electron emission from relaxed InAs quantum dot capped with InGaAs” *Journal of applied physics 2005 Vol 98 page 013716~1-5*
4. Jenn-Fang Chen, **Ru-Shang Hsiao**, Yu-Chih Chen, Yi-Ping Chen, Ming-Ta Hsieh Jyh. Shyang Wang and Jim.Y.Chi “Effect of Nitrogen Incorporation into InAs layer in InAs/InGaAs Self-Assembled Quantum dots” *Japan Journal of Applied Physics 2005 Vol44, No 9A pp6395~6399*
5. H-P D Yang, CLu, **R Hsiao**, C Chiou, C Lee, C Huang, H Yu, C Wang, K Lin, N A Malee, A.R Kovsh, C Sung, C Lai, J Wang, J Chen and J Y Chi **“**Characteristics of MOCVD and MBE grown InGaAsN VCSEL” *Semicond Sci. Technol 20(2005) 1-6*
6. Jyh-Shyang Wang, **Ru-Shang Hsiao**, Jenn-Fang Chen, Chu-Shou Yang Gray Lin, Chiu-Yueh Liang, Chih-Ming Lai, Hui-Yu Liu, Tung-Wei Chi, and Jim-Y Chi “Engineering laser gain spectrum using electronic vertically coupled InAs/GaAs quantum dots” *IEEE photonic technology letter 2005 Vol 17 No 8 pp:1590-1592*
7. K. P. Chang, S. L. Yang, D. S. Chuu, **R. S. Hsiao,** J. F. Chen L. Wei, J. S. Wang, and J. Y. Chi Characterization of self-assembled InAs quantum dots with InAlAs/InGaAs strain-reduced layers by photoluminescence spectroscopy ``*Journal of Applied Physics ‘’ 97, 083511-1 2005*
8. **Ru-Shang Hsiao**, Jyh-Shyang Wang, Kun-Feng Lin, Li Wei, Hui-Yu Liu, Chiu-Yueh Liang, Chih-Ming Lai, Alexey R. Kovsh, Nikolay A. Maleev, Jim-Y Chi, and Jenn-Fang Chen ``Single Mode 1.3 μm InGaAsN/GaAs Quantum Well Vertical Cavity Surface Emitting Lasers Grown by Molecular Beam Epitaxy ‘’*Japanese. Journal of Applied Physic* Vol 43, 12A, L1555~1557, 2004
9. J .F. Chen, **R. S. Hsiao**, S. H. Shih, P. Y. Wang, J. S. Wang, J. Y. Chi "Properties of Defect Traps in Triple-Stack InAs/GaAs Quantum Dots and effect of Annealing" *Japanese. Journal of Applied Physic* Vol 43, 9AB, L1150~1153 2004

10. J. S. Wang, **R. S. Hsiao**, G. Lin, K. F. Lin, H. Y. Liu, C. M. Lai, L. Wei, C. Y. Liang, and J. Y. Chi ‘’Molecular-beam-epitaxy growth of high-quality InGaAsN/GaAs quantum well lasers emitting at 1.3 μm’’ *Journal of Vacuum Science & Technology B:* Vol. 22, No. 6, pp. 2663–2667, 2004
11. J. S. Wang, A. R. Kovsh, **R. S. Hsiao**, L. P. Chen, J. F. Chen, T. S. Lay, and J. Y. Chi "High nitrogen content InGaAsN/GaAs single quantum well for 1.55 μm applications grown by molecular beam epitaxy" *J. Crystal Growth* Vol. 262, pp. 84-88, (2004).
12. S. T. Chou, S. Y. Lin, **R. S. Hsiao**, L. C. Wei, J. S. Wang, J. Y. Chi. "The Influence of Quantum-Dot 30-Period on High-Performance InAs/GaAs Quantum-Dot Infrared Photodetectors : *Journal of Vacuum Science & Technology B Vol23, Issue 3 ,page 1129-1131* 2005
13. L. Ya. Karachinsky, N. Yu. Gordeev, I. I. Novikov, M. V. Maximov, A. R. Kovsh, J. S. Wang, **R. S. Hsiao**, J. Y. Chi, V. M. Ustinov, and N. N. Ledentsov "Electroluminescent Studies of Emission Characteristics of InGaAsN/GaAs Injection Lasers in a Wide Temperature Range" *Semiconductors*, Vol. 38, No. 6, pp. 727–731, (2004).
14. A. R. Kovsh, J. S. Wang**, R. S. Hsiao**, L. P. Chen, D. A. Livshits, G. Lin, V. M. Ustinov, J. Y. Chi " High power (200 mW) Single Mode Operation of GaAs based InGaAsN/GaAs Ridge Waveguide Lasers with Wavelength around 1300 nm" *Electron. Lett.* Vol. 39, No. 24, pp. 1726-1728, (2003).
15. J. S. Wang, **R. S. Hsiao**, G. Lin, L. Wei, Y. T. Wu, A. R. Kovsh, N. A. Maleev, A. V. Sakharov, D. A. Livshits, J. F. Chen, and J. Y. Chi "Ridge waveguide 1310 nm lasers based on multiple stacks of InAs/GaAs quantum dots" *phys. stat. sol. C* Vol. 0, No. 4, pp. 1339–1342, (2003).
16. A. R. Kovsh, J. S. Wang, L. Wei, **R. S. Shiao**, J. Y. Chi,B. V. Volovik, A. F. Tsatsul'nikov, and V. M. Ustinov "Molecular beam epitaxy growth of GaAsN layers with high luminescence efficiency" *J. Vac. Sci. Technol. B* Vol.20, pp. 1158-1162, (2002).

International Conference Papers:

1. **R. S. Hsiao**, J.S. Wang, G. Lin, C.Y. Liang, H.Y. Liu, T.W. Chi, J. F. Chen, and J.Y. Chi MBE growth of high quality vertically coupled InAs/GaAs quantum dots laser emitting around 1.3μm *Physics and Technology, St Petersburg, Russia, June 21–25, 2005*

2. **Ru-Shang Hsiao**, Shih-Yen Lin, Chiu-Yueh Liang , Jyh-Shyang Wang, Jim-Yong Chi and Jenn-Fang Chen "The Observation of Photoluminescence Decay for MBE

Grown 1.3 μm InGaAsN/GaAs Quantum Well Structure" *North American Conference on Molecular Beam Epitaxy (NAMBE) 2004*

3. S. T. Chou, M . C. Wu, S. Y. Lin, **R. S. Hsiao**, L. C. Wei, J. S. Wang, J. Y. Chi. "The Influence of Quantum-Dot Period on High-Performance InAs/GaAs Quantum-Dot Infrared Photodetectors : *North American Conference on Molecular Beam Epitaxy (NAMBE) 2004*
4. **R. S. Hsiao**, J. S. Wang, L. C. Wei, C. M. Lai, K. F. Lin, H.Y. Liu, A. R. Kovsh, N. A. Maleev, J. F. Chen, J.Y. Chi, and V. M. Ustinov "1.3 μm InGaAsN intra-cavity contacted VCSELs with low threshold current density grown by MBE" 12th Int. Symp. Nanostructures: *Physics and Technology, St Petersburg, Russia, pp. 71-72, June 21–25, 2004.*
5. C. M. Lai, J. S. Wang**, R. S. Hsiao**, L. Wei, K. F. Lin, H. Y. Liu, A. R. Kovsh, N. A. Maleev, J. F. Chen, and J. Y. Chi "MBE grown 1.3-um InGaAsN/GaAs double QW VCSELs with low threshold current density of 1.6 KA/cm^2 under room temperature CW operation" *Photonics Europe 2004, Strasbourg, France, Apr. 26-30, 2004. (invited paper)*
6. Hung-Pin D. Yang, Chen-Ming Lu, **Ru-Shang Hsiao**, Chih-Hung Chiou, Cheng-Hung Lee, Chun-Yuan Huang, Hsin-Chieh Yu, Chin-May Wang, Kuen-Fong Lin, Chih-Ming Lai, Li-Chung Wei, Nikolai A. Maleev, Alexey R. Kovsh, Chia-Pin Sung, Jyh-Shyang Wang, Jenn-Fang Chen, Tsin-Dong Lee, and Jim Y. Chi "Characteristics of InGa(N)As VCSELs for fiber-optic applications" *Photonics West Optoelectronics 2004, San Jose, California, USA, Jan. 24-29, 2004.*
7. J. S. Wang, N. A. Maleev, A. R. Kovsh, **R. S. Hsiao**, C. M. Lai, L. Wei, J. F. Chen, J. A. Lott, N. N. Ledentsov, V. M. Ustinov, and J. Y. Chi "1.3 μm InAs-InGaAs quantum dot VCSELs on GaAs substrates with all-semiconductor DBRs" *5th Pacific Rim Conference on Lasers and Electro-Optics, Taipei, Taiwan, Dec. 15-19, 2003.*
8. J. S. Wang, A. R. Kovsh, **R. S. Hsiao**, G. Lin, D. A. Livshits, I. F. Chen, Y. T. Wu, L. P. Chen, J. F. Chen, and J. Y. Chi "Long-Wavelength Ridge-Waveguide InGaAsN/GaAs Single Quantum Well Lasers Grown by Molecular Beam Epitaxy" *5th Pacific Rim Conference on Lasers and Electro-Optics, Taipei, Taiwan, Dec. 15-19, 2003.*
9. G. Lin, I. F. Chen, J. S. Wang, **R. S. Hsiao**, L. Wei, J. Y. Chi, D. A. Livshits, A. R. Kovsh, and V. M. Ustinov "1.3 μm InGaAsN Edge Emitting Lasers with Near-Circular Beam Divergence" *5th Pacific Rim Conference on Lasers and Electro-Optics, Taipei, Taiwan, Dec. 15-19, 2003.*

10. A. R. Kovsh, J. S. Wang, **R. S. Hsiao**, L. P. Chen, D. A. Livshits, G. Lin, J. Y. Chi, and V. M. Ustinov "1.3 μm high power (180mW) single mode ridge waveguide lasers based on InGaAsN/GaAs quantum well" *12th EURO-MBE WORKSHOP, Austria, Feb. 16 - 19, 2003.*

11. A. R. Kovsh, D. A. Livshits, N .A. Maleev, A. E. Zhukov, V. M. Ustinov, J. S. Wang, **R. S. Hsiao**, G. Lin, J. Y. Chi, and N. N. Ledentsov "1.3 micron single lateral mode lasers based on InAs QDs and InGaAsN quantum wells" *2003 North American Conference on Molecular Beam Epitaxy, Colorado, USA, Sep. 28- Oct. 2, 2003.*

12. I. P. Soshnikov, A. R. Kovsh, V. M. Ustinov, N. V. Kryzhanovskaya, N. N. Ledentsov, D. Bimberg, H. Kirmse, W. Neumann, O. M. Gorbenko, J. S. Wang, **R. S. Hsiao**, and J. Chi "Structural and optical properties of Ga(As,N)/GaAs epilayers grown with continuous and pulsed deposition and nitridization" *11th Int. Symp. Nanostructures:Physics and Technology, St Petersburg, Russia, pp. 334-336, June 23–28, 2003.*

13. **R. S. Hsiao**, J. F. Chen, C. K. Wang, S. H. Shih, Y. J. Chen, P. Y. Wang, J. S. Wang, and A. R. kovsh "Defect properties of multiple-stack InAs/GaAs quantum dot structures and annealing effects" *International Electron Devices and Materials Symposium, Taipei, Taiwan, ROC, pp. 341-344, 2002.*

14. H. C. Yu, S. J. Chang, Y. K. Su, J. S. Wang, A. R. Kovsh, Y. T. Wu, K. F. Lin, **R. S. Shiao**, L. P. Chen, C. Y. Huang, W. J. Jiang, C. P. Sung, and J. Y. Chi "Investigation and fabrication of 1.3 um InAs quantum dot resonant cavity light emitting diodes" *International Electron Devices and Materials Symposium, Taipei, Taiwan, ROC, pp. 240-242, 2002.*

15. G. Lin, J. S. Wang, **R. S. Hsiao**, L. Wei, Y. T. Wu, J. Y. Chi, A. R. Kovsh, and D. A. Livshits "The spectral and temperature behavior of single mode InAs/InGaAs/GaAs quantum dot lasers lasing at 1.3 μm range" *International Electron Devices and Materials Symposium, Taipei, Taiwan, ROC, pp. 233-235, 2002.*

16. A. R. Kovsh, N. A. Maleev, A. E. Zhukov, S. S. Mikhrin, D. A. Livshits, Y. M. Shernyakov, A . V. Sakharov, M. V. Maximov, V. M. Ustinov, Zh. I. Alferov, J. S. Wang, **R. S. Shiao**, L. Wei, Y. T. Wu, G. Lin, J. Y. Chi, N. N. Ledentsov,and D. Bimberg "1.3 μm lasers based on InAs/GaAs quantum dots with high optical gain" *The Fourth International Conference on Low Dimensional Structures and Devices, Fortaleza - Ceara, Brazil, December 8-13, 2002.*

17. J. S. Wang, **R. S. Shiao**, G. R. Lin, L.C. Wei, Y. T. Wu, J. Y. Chi, A. R. Kovsh, N. A. Maleev, A.V. Sakharov, and D.A. Livshits "Narrow ridge waveguide 1310 nm lasers based on multiple stacks of InAs/GaAs quantum dots" *2nd International*

Conference on Semiconductor Quantum Dots, Tokyo, Japan, September 30-October 3, 2002.

Domestic Conference Papers:

1. **R. S. Hsiao**, J.S. Wang, G. Lin, C.Y. Liang, H.Y. Liu, T.W. Chi, J.F. Chen, J.Y. Chi MBE growth of high quality vertically coupled InAs/GaAs quantum dots laser emitting around 1.3μm *MBE Taiwan 2005*
2. **R. S. Hsiao**, T. W. Chi, G. Lin, J. S. Wang , C. Y. Liang , J. F. Chen, J. Y. Chi The Influence of Sb doping in the InGaAsN mutiple quantum wells growth by molecular beam epitaxy *MBE Taiwan 2005*
3. **R. S. Hsiao**, J. S. Wang, L. Wei, C. M. Lai, K. F. Lin, H. Y. Liu, A. R. Kovsh, N. A. Maleev, V. M. Ustinov, J. F. Chen, and J. Y. Chi "1.3μm InGaAsN intra-cavity contacted VCSEL with low thershold current density grown by MBE" *MBE Taiwan 2004.*
4. J. S. Wang, N. A. Maleev, A. R. Kovsh, **R. S. Hsiao**, C. M. Lai, L. Wei, J. F. Chen, J. A. Lott, N. N. Ledentsov, V. M. Ustinov, and J. Y. Chi "1.3 μm InAs-InGaAs Quantum Dot VCSELs With All-semiconductor DBRs Grown by Molecular Beam Epitaxy" *MBE Taiwan 2004 (invited paper).*
5. K. P. Chang, **R. S. Hsiao,** C. M. Lin Y. W. Lui, S. L. yang, L.Wei, J. S. Wang, J. Y. Chi Photoluminescence study on the self-assembled InAs/GaAs quantum dot with InAlAs/InGaAs composite stain reduced layers 中國物理年會 2004